

Rotation, activity, and lithium abundance in cool binary stars*

K. G. Strassmeier**, M. Weber, T. Granzer, and S. Järvinen

Leibniz-Institut für Astrophysik Potsdam (AIP), An der Sternwarte 16, D-14482 Potsdam, Germany

Received 2012, accepted 2012

Published online 2012

Key words Binaries: spectroscopic, stars: fundamental parameters, stars: late-type, stars: rotation, techniques: radial velocities, techniques: photometry, starspots

We have used two robotic telescopes to obtain time-series high-resolution optical echelle spectroscopy and VI and/or by photometry for a sample of 60 active stars, mostly binaries. Orbital solutions are presented for 26 double-lined systems and for 19 single-lined systems, seven of them for the first time but all of them with unprecedented phase coverage and accuracy. Eighteen systems turned out to be single stars. The total of 6,609 $R=55,000$ echelle spectra are also used to systematically determine effective temperatures, gravities, metallicities, rotational velocities, lithium abundances and absolute $H\alpha$ -core fluxes as a function of time. The photometry is used to infer unspotted brightness, $V - I$ and/or $b - y$ colors, spot-induced brightness amplitudes and precise rotation periods. An extra 22 radial-velocity standard stars were monitored throughout the science observations and yield a new barycentric zero point for our STELLA/SES robotic system. Our data are complemented by literature data and are used to determine rotation-temperature-activity relations for active binary components. We also relate lithium abundance to rotation and surface temperature. We find that 74% of all known rapidly-rotating active binary stars are synchronized and in circular orbits but 26% (61 systems) are rotating asynchronously of which half have $P_{\text{rot}} > P_{\text{orb}}$ and $e > 0$. Because rotational synchronization is predicted to occur before orbital circularization active binaries should undergo an extra spin-down besides tidal dissipation. We suspect this to be due to a magnetically channeled wind with its subsequent braking torque. We find a steep increase of rotation period with decreasing effective temperature for active stars, $P_{\text{rot}} \propto T_{\text{eff}}^{-7}$, for both single and binaries, main sequence and evolved. For inactive, single giants with $P_{\text{rot}} > 100$ d, the relation is much weaker, $P_{\text{rot}} \propto T_{\text{eff}}^{-1.12}$. Our data also indicate a period-activity relation for $H\alpha$ of the form $R_{H\alpha} \propto P_{\text{rot}}^{-0.24}$ for binaries and $R_{H\alpha} \propto P_{\text{rot}}^{-0.14}$ for singles. Its power-law difference is possibly significant. Lithium abundances in our (field-star) sample generally increase with effective temperature and are paralleled with an increase of the dispersion. The dispersion for binaries can be 1–2 orders of magnitude larger than for singles, peaking at an absolute spread of 3 orders of magnitude near $T_{\text{eff}} \approx 5000$ K. On average, binaries of comparable effective temperature appear to exhibit 0.25 dex less surface lithium than singles, as expected if the depletion mechanism is rotation dependent. We also find a trend of increased Li abundance with rotational period of form $\log n(\text{Li}) \propto -0.6 \log P_{\text{rot}}$ but again with a dispersion of as large as 3–4 orders of magnitude.

© 2012 WILEY-VCH Verlag GmbH & Co. KGaA, Weinheim

1 Introduction

In a previous paper (Strassmeier et al. 2000; paper I) we reported on radial and rotational velocities, chromospheric emission-line fluxes, lithium abundances, and rotation periods of a total sample of 1,058 G5–K2 dwarfs, subgiants, and giants based on 1,429 moderate-resolution KPNO coude spectra and 8,038 Strömgren y photometric data points. The aim of this survey was to detect new candidates for Doppler imaging but, besides the discovery of 170 new variable stars and 36 new spectroscopic binaries, the more intriguing result was that 74% of the G-K stars with Ca II H&K emission also showed significant lithium on their surface. However, G-K giants should have very few lithium on their surface because of convective mixing. Theoretical models predict that surface lithium has to be diluted by many factors once a

star arrives at the bottom of the red giant branch (Iben 1967, Charbonnel & Balachandran 2000). Out of the 21 Doppler imaging candidates found, just four stars were single stars, three of them evolved, the rest were spectroscopic binaries, but all four single stars had very strong lithium.

Despite that it is generally acknowledged that higher than normal lithium abundance is common among magnetically active stars, no unique correlation with rotation rate was found after Skumanich's (1972) original discovery. Recently, White et al. (2007) revisited this issue in their sample of solar-type dwarfs but no such correlation was found. Almost all surveys just revealed trends, if at all, and even these appear to be of different quality (e.g. Lébre et al. 2006; Böhm-Vitense 2004; do Nascimento et al. 2000, 2003; De Medeiros et al. 2000; De Laverny et al. 2003; Randich et al. 1993). The comprehensive survey of nearby giants by Luck & Heiter (2007) did not even show a trend. However, the line broadening in their stellar sample was just 3–7 km s^{-1} and likely too narrow a range to see a trend. Böhm-Vitense (2004) suggested that the steep decrease of

* Based on data obtained with the STELLA robotic telescopes in Tenerife, an AIP facility jointly operated with IAC, and the Automatic Photoelectric Telescopes in Arizona, jointly operated with Fairborn Observatory.

** Corresponding author. e-mail: kstrassmeier@aip.de

$v \sin i$ in early G giants as well as in Hyades F dwarfs at effective temperatures cooler than $\approx 6,450$ K, i.e. at their lithium dip at about the same temperature, are the result of deep mixing and related to the merging of the hydrogen and the helium convection zones. More recently, Takeda et al. (2010) announced evidence for a (positive) correlation of Li abundance with rotational velocity in a sample of solar-analog stars.

The spectroscopic survey of 390 solar-like dwarf stars by White et al. (2007) included 28 of the stars in our survey. Relating Ca II H&K radiative losses to stellar rotation, White et al. (2007) found a saturation of chromospheric emission for rotational velocities above approximately 30 km s^{-1} . In an earlier paper, Strassmeier et al. (1994) verified that evolved stars obey qualitatively the same scaling of Ca II-K-line flux with stellar rotational velocity or period as do main-sequence stars (see, e.g., Mamajek & Hillenbrand 2008, Pace & Pasquini 2004, or Pizzolato et al. 2003 for a summary). No qualitative difference was found between single evolved stars and their equally rapidly rotating counterparts in a spectroscopic binary. However, large scatter indicated that rotation might not be the only relevant parameter. Based on a sample of 22 intermediate-mass G and K giants in close binaries, Gondoin (2007) not only verified the rotational dependency of (coronal) X-ray surface flux but also found a dependency on surface gravity. Such a dependence could stem from the effect of gravity on coronal electron density and on the overall sizes of coronal loops.

Massarotti et al. (2008) reported rotational and radial velocities for 761 giants within 100 pc of the Sun. They found that all binaries in their sample with periods less than 20 days have circular orbits while about half the orbits with periods between 20–100 days still showed significant eccentricity. They also found evidence that the rotational velocity of horizontal branch stars is larger than that of first-ascend giants by a few km s^{-1} . Earlier, De Medeiros et al. (2002) presented a study of 134 late-type giants in spectroscopic binaries and found a considerable number of G-K giant stars with moderate to moderately-high rotation rates. These rotators have orbital periods shorter than 250 days and circular or nearly circular orbits and appear to be synchronized with the orbit.

The present paper follows up on the newly identified spectroscopic binaries with active components from our paper I. Its direct aim is to determine their orbits on the basis of high-precision radial velocities and to separate their component's rotation and activity tracers along with other absolute astrophysical parameters. Only with precise stellar parameters can we directly compare binary components with single stars and then be aware of the spectrum contamination from unknown secondaries or even tertiary stars. We recall that an unknown continuum contribution from a secondary star impacts on the determination of the effective temperature, gravity etc. and could together drastically alter the derived lithium abundances and thereby mask any relation

if present. In Sect. 2 we restate our sample selection criteria and give a summary of the target stars. In Sect. 3 we describe the new observations and in Sect. 4 we derive basic quantities from the spectra and the light curves. These include radial velocities, orbital parameters, rotational velocities and photometric periods, stellar atmospheric parameters like temperature, gravity and metallicity, lithium abundances, and absolute H α -core fluxes. Sect. 5 lists notes to individual stars. Sect. 6 presents the analysis in terms of rotation, temperature, activity, and lithium-abundance relations. Finally, Sect. 7 summarizes our findings and conclusions.

2 Sample selection

Our sample selection is based on the 1,058 stars from the KPNO Doppler-imaging candidate survey in paper I. It itself was drawn from a total of 6,440 stars from the Hipparcos catalog (ESA 1997, van Leeuwen 2007) for the brightness range $7^{\text{m}}0\text{--}9^{\text{m}}5$ and declination -30° through $+70^\circ$, $B - V$ colors between $0^{\text{m}}67$ and $1^{\text{m}}0$ for stars with parallaxes $\pi > 20 \text{ mas}$ (i.e. G5–K3 dwarfs) and between $0^{\text{m}}87$ and $1^{\text{m}}2$ for $3 < \pi < 20 \text{ mas}$ (i.e. G5–K2 giants and subgiants). These criteria were imposed to select stars with a significant outer convective envelope where the likelihood of detecting magnetic activity is highest. Out of the 1,058 stars, 371 (35%) were found with Ca II H&K emission but only 78 (7.3%) with $v \sin i \geq 10 \text{ km s}^{-1}$. On the contrary, a lithium line was detected in 283 (74%) of all stars that had Ca II emission (with 58% of the stars with lithium above $10 \text{ m}\text{\AA}$). Out of a subsample of 172 stars with moderate to strong Ca II emission, 168 (97.7%) turned out to be photometric variable and for 134 a photometric (rotational) period could be obtained. Finally, 36 targets were single-lined spectroscopic binaries (SB1), of which 17 were new detections. A further 16 targets were found “possible SB1s”. An additional 30 targets were double-lined spectroscopic binaries (SB2), of which 19 were new detections. Two targets were even triple lined (SB3) of which one was a new detection and another four were new candidates. All along, there were a few misidentifications and misinterpretations as well as unrecognized literature entries. Whenever recognized, we try to clarify these in the present paper.

We now present time-series observations of all those targets in the survey that were previously unknown or suspected spectroscopic binaries in 2000. This sample comprised 59 stars presented in this paper. One additional star was added because of its comparable uncertain orbit despite being a fourth magnitude star ($\epsilon \text{ UMi}$). During the final observational stages for the present paper we learned that Griffin (2009), Griffin (2010) and Griffin & Filiz Ak (2010) had picked up many of our original SB candidate stars from paper I that found their way into the new edition of the CABS catalog (Eker et al. 2008), and independently determined orbital elements. We compare our results whenever possible. Stellar identifications and some basic observable prop-

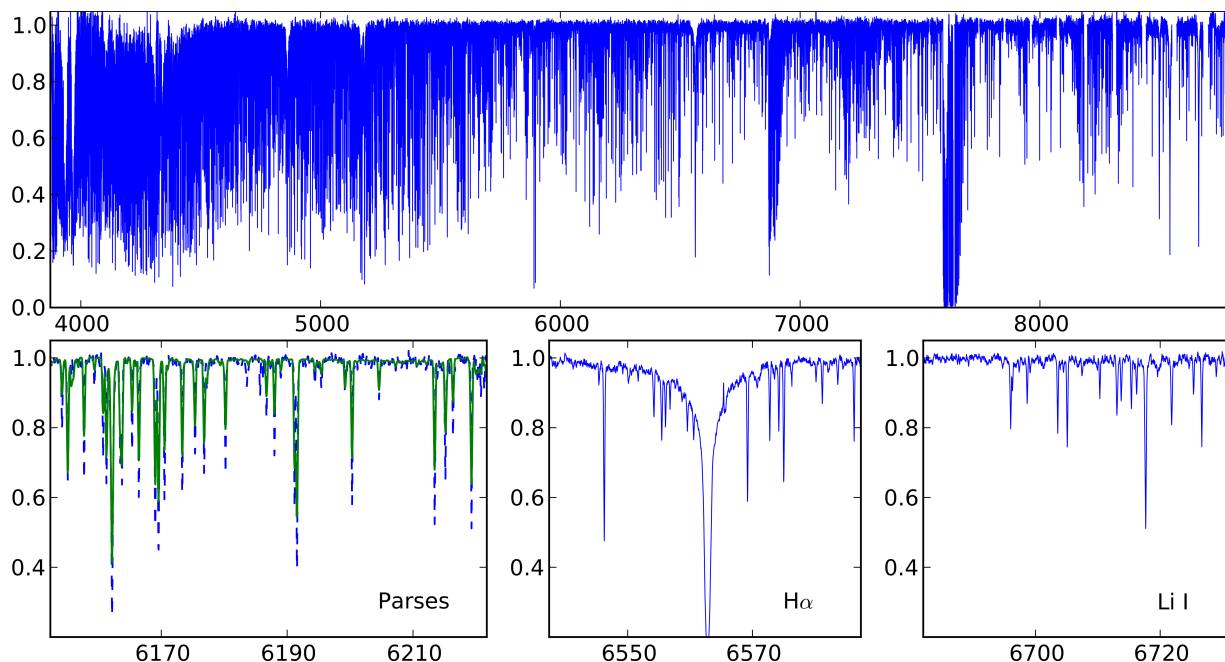


Fig. 1 HD 171067 as an example for a STELLA/SES spectrum. The top panel shows the entire wavelength coverage from 3880–8820 Å. Note the increasing inter-order gaps starting around 7340 Å. The lower panels zoom into three wavelength regions employed in this paper for analysis; from left to right, one of the five échelle orders that are used for the PARSES spectrum-synthesis fit (thick line), the Balmer H α line, and the region around the neutral lithium line at 6708 Å. HD 171067 ($V=7^m2$) is an inactive single, slightly evolved, G8 star with $v \sin i < 3 \text{ km s}^{-1}$. Exposure time was 1200 s.

erties for all our target stars are summarized in Table 1. Note that three of the stars actually do not show significant Ca II H&K emission and would not be dubbed magnetically active but are left in the sample because they were monitored initially in order to search for signs of binarity. All three turned out to be single stars though. Altogether, 18 of the SB1 candidates were found to be single with some of them still members of a visual-binary system. These stars are also in Table 1 but are summarized in a separate table later in the paper. In one case the two components of a wide visual binary (BD+11 2052AB = ADS 7406AB) were treated as separate stars throughout the paper. One double-lined binary (HD 16884) turned out to be actually a quadruple system with both pairs being SB1. First orbit determinations are presented for seven systems (HD 50255, HD 82841, HD 106855, HD 147866, HD 190642, HD 199967, and HD 226099).

3 New observations and data reductions

3.1 High-resolution optical spectroscopy

Time-series high-resolution echelle spectroscopy was taken with the 1.2 m STELLA-I telescope between June 2006 and May 2012. Most spectra were exposed just long enough to measure a precise radial velocity and had S/N of between 40–80:1 but several spectra per target were exposed to reach S/N well above 100:1. A total of 6,609 spectra for a total of 60 stars were obtained over the course of approximately six

years. STELLA-I is a fully robotic telescope that, together with STELLA-II, makes up the STELLA observatory at the Izāna ridge on Tenerife in the Canary islands (Strassmeier et al. 2004, 2010). The fiber-fed STELLA Echelle Spectrograph (SES) is the telescope’s only instrument. It is a white-pupil design with an R2 grating with two off-axis collimators, a prism cross disperser and a folded Schmidt camera with an E2V 2k \times 2k CCD as the detector. All spectra have a fixed format on the CCD and cover the wavelength range from 388–882 nm with increasing inter-order gaps near the red end starting at 734 nm towards 882 nm. The resolving power is $R=55,000$ corresponding to a spectral resolution of 0.12 Å at 650 nm (3-pixel sampling). An example spectrum is shown in Fig. 1. We note that the SES received a major upgrade in summer 2012 with a new cross disperser, a new optical camera, and a new CCD. A bit earlier, the SES fiber was moved to the prime focus of the second STELLA telescope in 2011. Further details of the performance of the system were reported by Weber et al. (2012) and Granzer et al. (2010).

SES spectra are automatically reduced using the IRAF¹-based STELLA data-reduction pipeline (Weber et al. 2011). The images were corrected for bad pixels and cosmic-ray impacts. Bias levels were removed by subtracting the average overscan from each image followed by the subtraction of the mean of the (already overscan subtracted) master

¹ The Image Reduction and Analysis Facility is hosted by the National Optical Astronomy Observatories in Tucson, Arizona at URL iraf.noao.edu.

Table 1 Summary of program stars and name aliases. Listed are the *Tycho* V brightness and the $B - V$ color in magnitudes, the spectral classification if available, the binarity according to this paper (S=single star, SB=spectroscopic binary, SB1=single-lined SB, SB2=double-lined SB, SB3=triple-lined, VB=visual binary), the number of STELLA spectra N_{STELLA} obtained and used for the orbit determination, its time span covered (Δt), and a primary reference if existent.

HD	Var. name	HIP	SAO	V	$B - V$	Sp.type	SB	N_{STELLA}	Δt	Ref.
HD 553	V741 Cas	834	11013	8.17	1.03	K0	SB2	121	1320	s,34
	LN Peg	999	91772	8.59	0.81	K0	SB2+1	135	1302	r
HD 8997	EO Psc	6917	74742	7.74	0.96	K2/K1-K6V	SB2	165	1453	b
HD 9902	BG Psc		74827	8.71	0.63	F5-6V/G9-K0IV	SB2	95	748	a,c
HD 16884			110699	8.94	1.37	K4III	2×SB1	83	1046	a,e
HD 18645	FU Cet	13968	130230	7.86	0.75	G2III-IV	S	70	784	f
HD 18955	IR Eri	14157	148731	8.45	0.82	K0V/K2-3V	SB2	67	1446	g
HD 23551	MM Cam	18012	12924	7.11	0.91	K0III	S	101	836	
HD 24053		17936	111446	7.7	0.8	G0	S	77	803	
	AI Lep		150676	8.97	0.57	G6IV/G0V	S	93	1460	l
	HY CMa		151224	9.33	1.00	K0-3V-IV/K1V-IV	SB2	87	1782	l
HD 40891		28935	13714	8.40	0.85	G5	SB1	85	1380	h
HD 43516		29750	151290	7.37	0.85	G8III	S	57	830	
HD 45762	V723 Mon	30891	133321	8.30	0.87	G0	SB2+1	89	1231	z
HD 50255		32971	152024	7.43	0.68	G4.5V	SB2	66	1471	
HD 61994		38018	6310	7.08	0.67	G0	SB2	105	899	t
HD 62668	BM Lyn	38003	41995	7.73	1.10	K0III	SB1	137	2000	a,f,i
HD 66553		39515	97536	8.48	0.85	G5	SB1	92	2001	h
HD 73512		42418	116990	7.91	0.90	K0V/K4V	SB2	74	892	a
HD 76799		44007	176747	7.11	0.99	K0III	S	75	1442	
		46634	98614	8.76	0.86	G5	VB,S	96	1129	y
HD 82159	GS Leo	46637	98615	8.85	0.92	G9V	VB,SB1	107	1458	u,32
HD 82286	FF UMa	46919	14919	7.89	0.96	G5	SB2	161	1446	i,31,35
HD 82841	OS Hya	46987	136965	8.45	1.08	K2	SB1	61	1447	
	EQ Leo	50072	99011	9.39	1.09	K1III	SB1	62	1169	a
HD 93915		53051	43492	8.07	0.68	G5V/G6V	SB2	85	1169	a
HD 95188	XZ LMi	53747	81610	8.45	0.74	G8V	S	85	891	v,j
HD 95559	GZ Leo	53923	81634	8.83	0.96	K0V/K2V	SB2	113	1162	k,30
HD 95724	YY LMi	54028	62375	8.96	0.94	G5V	S	76	856	v
HD 104067		58451	180353	7.93	0.99	K2V	S	76	887	
HD 105575	QY Hya	59259	180519	9.04	0.93	(K5/M1)/G4	SB3	51	1164	29
HD 106855	UV Crv	59914	180648	9.59	0.81	K1V	SB2,VB	88	1227	
HD 108564		60853		9.45	0.98	K5V	S	70	867	
HD 109011	NO UMa	61100	28414	8.10	0.94	K2V	SB2	184	1629	o
HD 111487	IM Vir		138983	9.69	0.64	G5	SB2	106	1292	p
HD 112099		62942	119652	8.23	0.86	K1V	SB1	80	1142	a
		63322	63275	9.27	0.84	G6V	VB,SB1	104	937	y,32
HD 112859	BQ CVN	63368	44410	8.09	0.92	F5V/K0III-IV	SB2	93	1249	a,w
	CD CVn	63442	44421	9.39	1.19	K0III	SB1	85	1165	a
HD 120205		67344	158174	8.3	0.9	G5	S	93	849	
HD 127068	HK Boo	70826	101044	8.43	0.89	G8V/G5-8IV	SB2	99	1257	a
HD 136655		75132	83780	9.01	0.9	K0	S	122	842	z
HD 138157	OX Ser	75861	101580	7.14	1.02	K0III	SB1	148	1086	u,32
	V381 Ser	77210	121177	9.16	0.83	K2V	SB2	96	1114	33
HD 142680	V383 Ser	77963	101816	8.71	0.95	K0-2V/K7V	SB2	90	781	a,v
HD 143937	V1044 Sco	78708	184077	8.65	0.91	G9V/M0V	SB2	86	1131	l
HD 147866	V894 Her	80302	84343	8.1	1.1	K0	SB1	115	1269	
HD 150202	GI Dra	81284	30015	7.97	0.93	K0III	SB1	179	1112	a
HD 153525	V1089 Her	83006	46403	7.88	1.04	K0V	S	196	1349	x
HD 153751	ϵ UMi	82080	2770	4.22	0.88	G5III	SB1	220	2144	d
HD 155802		84303	141567	8.51	0.89	K3V	S	114	857	
HD 171067		90864	103819	7.19	0.696	G8V	S	143	857	
HD 184591		96280	104991	7.37	0.85	G5	S	155	842	x,z
HD 190642	V4429 Sgr	99042	163264	8.08	0.99	F6-8V/K1III-IV	SB1	196	1274	
HD 197913	OR Del	102490	106466	7.55	0.76	G6V/G8V	SB2	194	1848	m
HD 199967		103454		8.01	0.58	G5	SB2	121	945	

Table 1 (continued)

HD	Var. name	HIP	SAO	V	$B - V$	Sp.type	SB	N_{STELLA}	Δt	Ref.
HD 202109	ζ Cyg	104732	71070	3.20	0.99	G8III	SB1	150	1288	n
HD 218739		114385	52754	7.14	0.61	G5	S	107	791	
HD 226099		97640	68946	8.01	0.783	G5	SB2	209	1334	
HD 237944		53209	27812	9.36	0.71	(G8V+/G8V+)/?	SB3	119	1431	a,q

References. a: Griffin (2009), b: Griffin (1987), c: Cutispoto et al. (2003), d: Climenhaga et al. (1951), e: Favata et al. (1993), f: Fekel (1997), g: Fekel et al. (2004), h: Latham et al. (2002), i: Henry et al. (1995), j: Wright et al. (2004), k: Karatas et al. (2004), l: Cutispoto et al. (1999), m: Griffin (2005), n: Griffin & Keenan (1992), o: Halbwegs et al. (2003), p: Morales et al. (2009), q: Otero & Dubovsky (2004), r: Fekel et al. (1999), s: Duemmler et al. (2002), t: Duquenois & Mayor (1988), u: Gálvez et al. (2006), v: Barnes (2007), w: Montes et al. (2000), x: Strassmeier (1994), y: Gálvez et al. (2005), z: Griffin (2010), 29: Szalai et al. (2007), 30: Gálvez et al. (2009), 31: Gálvez et al. (2007), 32: Griffin & Filiz Ak (2010), 33: Goldberg et al. (2002), 34: Griffin (2003), 35: Griffin (2012).

Table 2 STELLA radial velocities of standard stars. N is the total number of spectra. $\langle v_{\text{STELLA}} \rangle$ is the average radial velocity from STELLA spectra, σ_{STELLA} its standard deviation, and $\langle v_{\text{CORAVEL}} \rangle$ the CORAVEL velocity from Famaey et al. (2005) or, if not in Famaey et al., from Udry et al. (1999). The velocity difference STELLA-minus-CORAVEL is given in the last column. The averaged offsets from all stars weighted by the number of data points is given in the last line. All velocities are in km s^{-1} .

HD	Name	Class.	N	$\langle v_{\text{STELLA}} \rangle$	σ_{STELLA}	$\langle v_{\text{CORAVEL}} \rangle$	$v_{\text{STELLA}} - \text{CORAVEL}$
HD 3712	α Cas	K0 II-III	230	-3.863	0.094	-4.31	+0.447
HD 4128	β Cet	K0 III	143	+13.686	0.107	+13.1	+0.586
HD 12929	α Ari	K2 III	440	-14.138	0.118	-14.64	+0.502
HD 18884	α Cet	M2 III	60	-25.688	0.293	-26.08	+0.392
HD 20902	α Per	F5 Ib	152	-1.800	0.138	-2	+0.200
HD 25025	γ Eri	M0 III	26	+61.159	0.217	+61.1	+0.059
HD 29139	α Tau	K5 III	503	+54.646	0.188	+54.26	+0.386
HD 36673	α Lep	F0 Ib	53	+25.871	0.413	+25.2	+0.671
HD 62509	β Gem	K0 III	442	+3.783	0.076	+3.23	+0.553
HD 81797	α Hya	K3 III	203	-4.033	0.076	-4.7	+0.667
HD 84441	ϵ Leo	G0 II	165	+5.001	0.046	+4.5	+0.501
HD 107328	16 Vir	K0.5 III	332	+37.117	0.160	+36.4	+0.717
HD 109379	β Crv	G5 II	49	-6.947	0.069	-7.6	+0.653
HD 124897	α Boo	K1.5 III	787	-4.871	0.149	-5.3	+0.429
HD 146051	δ Oph	M0.5 IIIab	146	-19.133	0.146	-19.6	+0.467
HD 156014 ^a	α Her	M5Ib-II	303	-31.168	0.694	-32.09	+0.922
HD 161096	β Oph	K2 III	763	-11.844	0.095	-12.53	+0.686
HD 168454	δ Sgr	K2 III	18	-19.798	0.035	-20.4	+0.602
HD 186791	γ Aql	K3 II	538	-2.430	0.261	-2.79	+0.360
HD 204867	β Aqr	G0 Ib	80	+6.808	0.151	+6.3	+0.508
HD 206778	ϵ Peg	K2 Ib	572	+3.588	0.262	+3.39	+0.198
HD 212943	35 Peg	K0 III	402	+54.740	0.111	+54.16	+0.580
Weighted average							+0.503

^aDouble star with the A component being a “semiregular pulsating variable”.

bias frame. The target spectra were flattened by dividing by a nightly master flat which has been normalized to unity. The nightly master flat itself is constructed from around 50 individual flats observed during dusk, dawn, and around midnight. After removal of the scattered light, the one-dimensional spectra were extracted with the standard IRAF optimal extraction routine (Horne 1986). The blaze function was then removed from the target spectra, followed by a wavelength calibration using consecutively recorded Th-Ar spectra. Finally, the extracted spectral orders were continuum normalized by dividing them with a flux-normalized

synthetic spectrum of the same spectral classification as the target in question.

3.2 VI and by photometry

Johnson-Cousins $V(I)_C$ and/or Strömgren *by* photometry of 56 of the targets were obtained with the *Amadeus* (T7) and/or the *Wolfgang* (T6) automatic photoelectric telescope (APT) at Fairborn Observatory in southern Arizona, respectively. These 56 stars are listed in Table 6 along with the analysis results. A total of 16,591 observations in either

$V(I)_C$ or *by* pairs were obtained. Typically, one APT observation consists of three ten-second (30 s for Strömgren) integrations on the variable, four integrations on the comparison star, two integrations on the check star, and two integrations on the sky. A 30'' diaphragm was used for all targets. The standard error of a nightly mean for *Amadeus* from the overall seasonal mean changed over the past decade but was typically 4–6 mmag in V and 6–8 mmag in I_C for the brightness range of stars in this paper. The observing seasons between 2007–2009 showed increasing scatter due to a slowly but systematic malfunction of the acquisition CCD camera. By late 2009 it got so bad that we had to exchange the entire camera plus its CCD and after that, starting with HJD 2,455,143, the scatter was back to the original values quoted above. The standard error of a nightly mean for *Wolfgang* was between 1.2–3 mmag, depending on system brightness. For further details we refer to Strassmeier et al. (1997) and Granzer et al. (2001).

From concurrent observations of Johnson standards in $V(I)_C$, we also deduce an all-sky solution and apply it to the differential values whenever feasible. Its accuracy never significantly exceeds 0^m01 in V though. In case B data were taken, $B - V$ can be determined only relative to the comparison star because our all-sky standards were not observed in the B band due to time constraints. Absolute errors are typically around 0^m01 for $\Delta(V - I_C)$ except for the time period 2007–2009, as mentioned above, and was then likely 0^m02 .

4 Data products

4.1 Radial velocity precision and zeropoint

Radial velocities were determined from an order-by-order cross correlation with a synthetic template spectrum from an ATLAS9 atmosphere (Kurucz 1993) that roughly matches the target spectral classification. A two-dimensional cross correlation is performed in case the target is double lined. Each of 19 selected echelle orders gives one relative radial velocity. These velocities are then weighted according to the spectral region depending on the amount of available spectral lines and are then averaged. The true internal error is likely close to the rms of these relative velocities. Numerical simulations of the cross correlation errors from synthetic spectra and various two-Gaussian fits to its peaks are discussed in the paper by Weber & Strassmeier (2011). Note that the external rms values were significantly larger during the initial year of STELLA operation in 2006/07 ($\approx 120 \text{ m s}^{-1}$), compared to thereafter ($\approx 30 \text{ m s}^{-1}$). The final radial velocities of our program stars are barycentric and corrected for Earth rotation. No gravitational redshift corrections are applied.

Table 2 lists our standard-star measurements. A total of 22 radial-velocity standards were monitored since mid 2006. Their velocities were derived similarly from cross correlations with a synthetic template spectrum that fitted the star's classification. Among these standards are often

Table 3 Average radial velocities for the single stars. Δt is the time span of STELLA observations in days from Table 1. $\langle v_r \rangle$ is the average radial velocity and its standard deviation. Radial-velocity variations are detected for some of the stars due to stellar rotation and an asymmetrically spotted surface. Rotation periods, P , if existent, are given in days.

Name	Δt (days)	$\langle v_r \rangle$ (km s^{-1})	Note
HD 18645	784	-2.151 ± 0.052	$P=21.5\text{d}$
HD 23551	836	-6.925 ± 0.043	$P=81.7\text{d}$
HD 24053	803	$+4.852 \pm 0.040$	
SAO150676	1460	$+25.69 \pm 0.53$	$P=1.79\text{d}$
HD 43516	830	$+21.846 \pm 0.059$	
HD 76799	1442	-31.015 ± 0.187	$P=50.13\text{d}$
HIP 46634	1129	$+27.927 \pm 0.047$	Var. but no P
HD 95188	891	$+6.439 \pm 0.051$	$P=7.00\text{d}$
HD 95724	856	$+3.365 \pm 0.055$	$P=11.49\text{d}$
HD 104067	887	$+15.355 \pm 0.066$	
HD 108564	867	$+111.363 \pm 0.009$	
HD 120205	849	-28.870 ± 0.048	
HD 136655 ^a	842	-31.921 ± 0.035	
HD 153525	1349	-6.844 ± 0.039	$P=15.4\text{d}$
HD 155802	857	-32.711 ± 0.033	
HD 171067 ^a	857	-45.771 ± 0.042	
HD 184591 ^a	842	-37.635 ± 0.044	$P=48.9\text{d}::$
HD 218739	791	-5.201 ± 0.040	

^aWithout Ca II H&K emission according to our paper I and thus not an active star.

observed bright giant stars like β Oph, α Ari, β Gem, α Tau, 16 Vir, a.o., which are all IAU radial-velocity standards (see Scarfe et al. 1990). These spectra are also used to identify two epochs in our data when all stars on the observing menu showed a constant offset in velocity. These epochs are identified with two of our hardware maintenance episodes where the fiber injection unit had been readjusted. The average offsets determined from above standard stars were -0.244 km s^{-1} and -0.366 km s^{-1} for the epochs 2,453,902–4,085 and 2,454,192–435, respectively. These corrections were applied to all data in this paper.

The preliminary zero point determination in Strassmeier et al. (2010) from four standard stars (β Oph, α Cas, β Gem, β Cet) showed an offset of the STELLA spectra by $+0.46 \text{ km s}^{-1}$ with respect to the CORAVEL system defined by Udry et al. (1999). In the present paper, we revise this value to $+0.503 \text{ km s}^{-1}$ from 22 standard stars. The weights applied for this average shift are the total number of spectra per radial-velocity standard. Note that an absolute heliocentric zero point for STELLA has not been determined yet, e.g. by using asteroids. All velocities in the present paper are on the STELLA system.

Table 3 lists the stars in our sample that were found to exhibit no orbital-induced radial velocity variations, i.e. are presumably single stars. These stars are mostly still very active stars and further investigation with the present

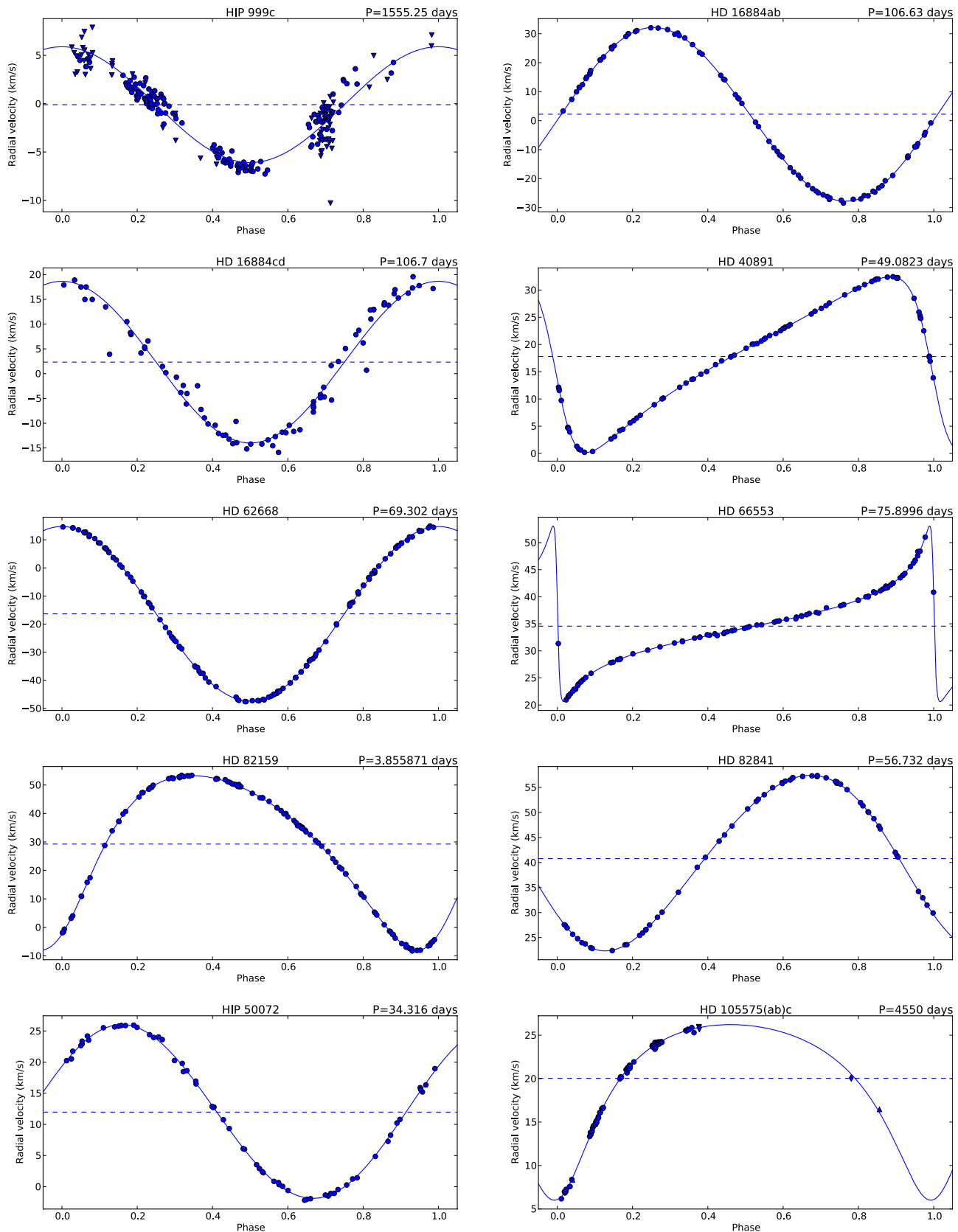


Fig. 2 Velocity curves for the STELLA single-lined orbital solutions. The dots are the observations and the lines are the orbital fits. Velocities are in km s^{-1} and the horizontal axes are in orbital phase. The horizontal dashed line in each plot indicates the systemic velocity. STELLA data are shown as filled dots. For HIP 999, the triangles are from Fekel et al. (1999). For HD 105575, values from paper I are shown as down-ward pointing triangles, the one FEROS point as a diamond, and the two HARPS points as upward-pointing triangles. For the other long-period system, HD 202109, data from Griffin & Keenan (1992) are added and shown as triangles.

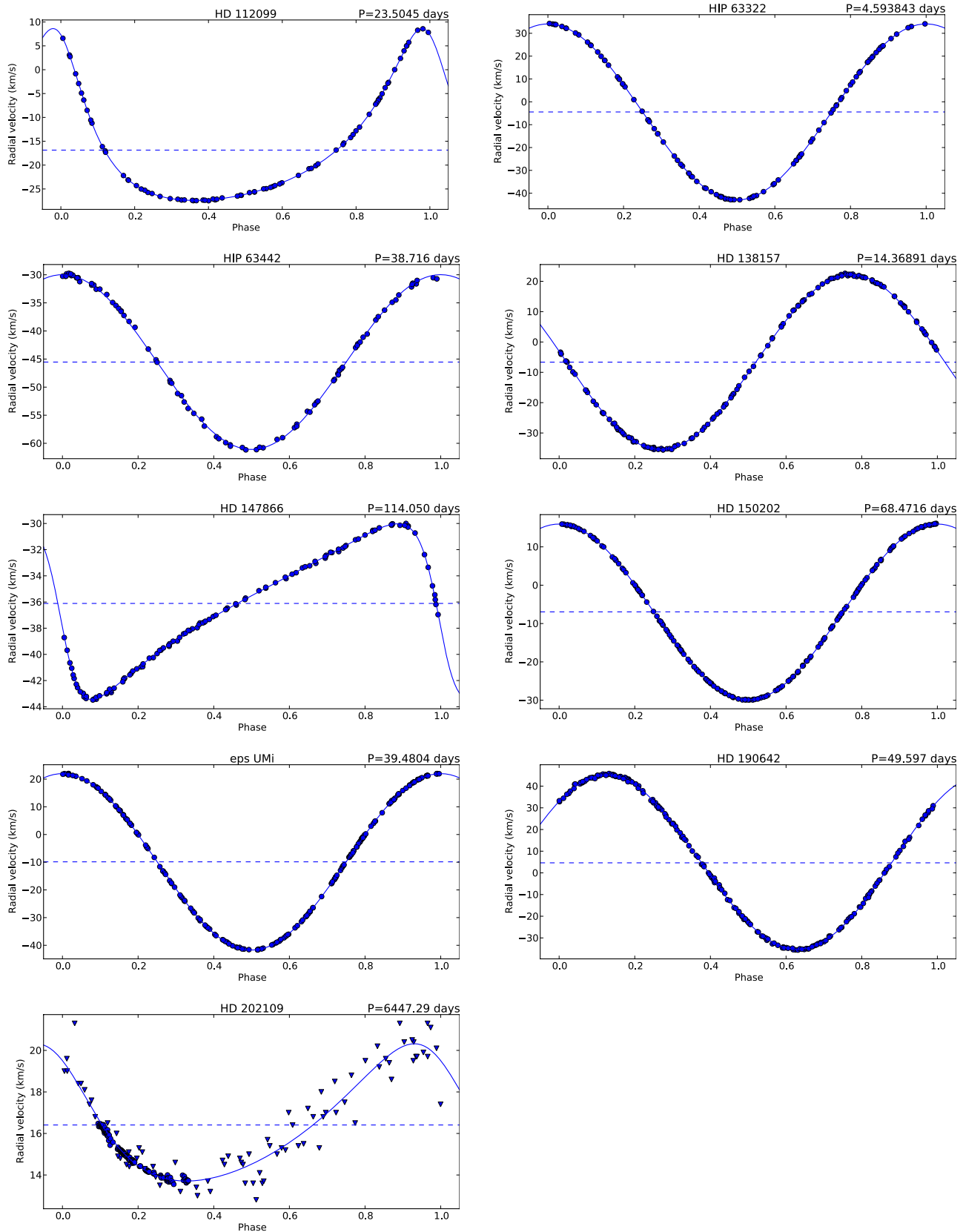


Fig. 2 (continued).

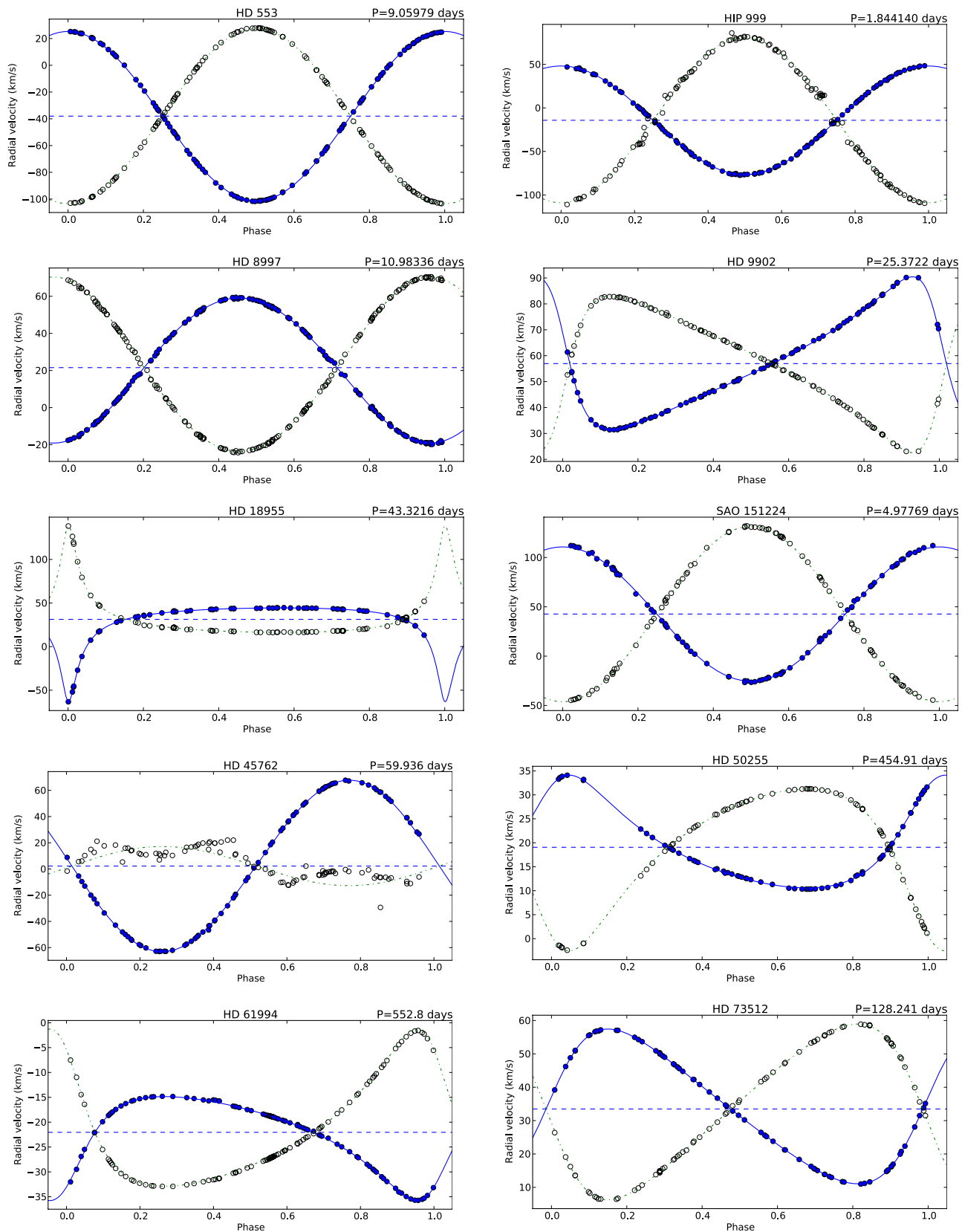


Fig. 3 Velocity curves for the STELLA double-lined orbital solutions. The primary velocities are plotted as filled dots, the secondaries as open circles. Otherwise as in Fig. 2. For HD 237944 the triangles mark the tertiary component.

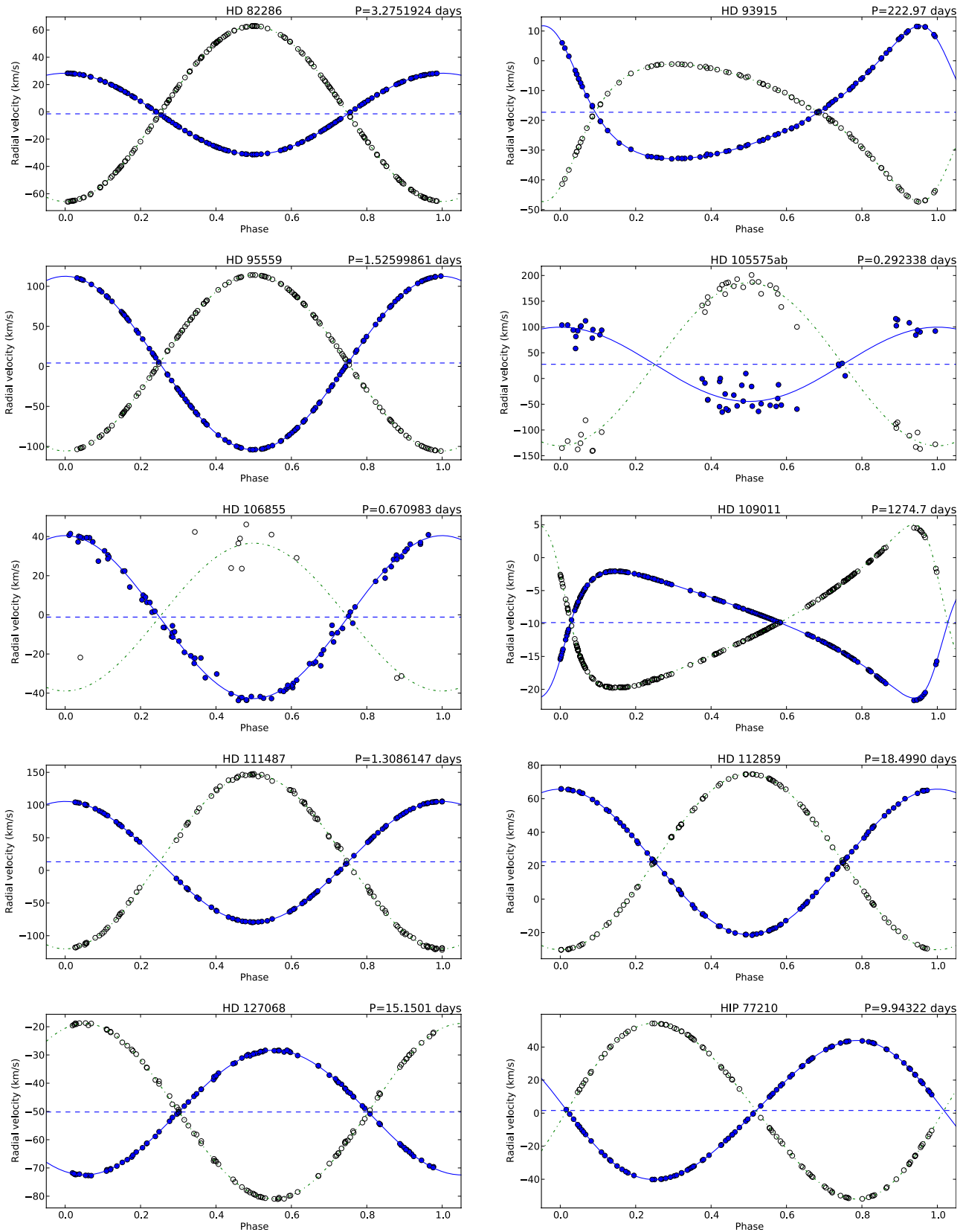


Fig. 3 (continued).

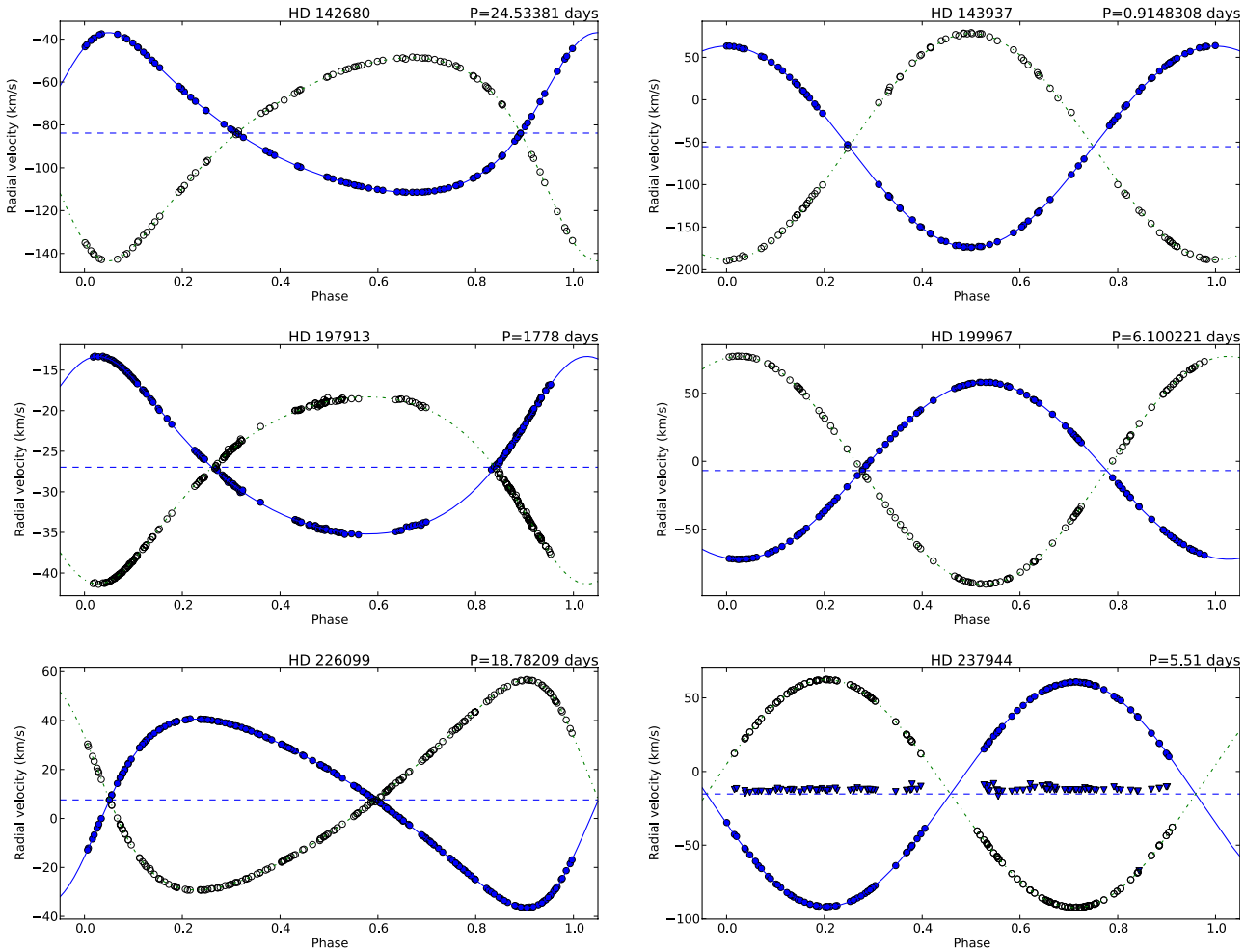


Fig. 3 (continued).

time-series data are forthcoming. Several of them, e.g. SAO 150676 or HD 76799, show periodic radial-velocity variations with amplitudes of the order of 1 km s^{-1} , which we interpret to be due to stellar rotation. Few of our single-star survey targets in paper I were also revisited by Griffin (2010), most notably HD 136655 and HD 184591, for which we recommend to read his “Notes on the six constant-velocity stars” for their observational history.

4.2 Binary orbits

For single-lined (SB1) as well as double-lined (SB2) binaries we solve for the components using the general least-square fitting algorithm *MPFIT* (Markwardt 2009). For solutions with non-zero eccentricity we use the prescription from Danby & Burkardt (1983) to calculate the eccentric anomaly. Usually, we first determine the orbit for both components separately and then combine the two and give rms values for both. Eclipsing binaries were treated slightly separately due to the Rossiter-McLaughlin effect in the radial-velocity curve. Some of the velocities around the two conjunctions were discarded by applying $3\text{-}\sigma$ clipping. Most of the orbits are sampled nearly perfectly due to robotic

scheduling (Granzer et al. 2001) but the unexpected high eccentricity in three systems left some phase gaps during periastron. The STELLA time coverage does not exceed 5.9 years, typical values are around 3.3 years. Although partly compensated for by the high velocity precision and the dense sampling, systems with periods longer than, say, 200 days, have comparably uncertain orbital periods. Whenever there were literature data for the eight systems with orbital periods in excess of $\approx 100 \text{ d}$ that expanded the total time range and improved the orbit, these are included in the period determination. This was the case for HIP 999, HD 105575(ab)c and HD 202109. Otherwise, the orbits are computed from STELLA radial velocities alone. The resulting elements and their errors are summarized in Table 4 and Table 5 for the single-lined and the double-lined systems, respectively. Assuming that the fit is of good quality, we derive the element uncertainties by scaling the formal one-sigma errors from the covariance matrix using the measured χ^2 values. T_{per} is a time of periastron or, if the orbit is circular, a time of maximum positive radial velocity. Note that we give orbital periods as observed and not corrected for the rest frame of the system.

The computed radial-velocity curves are compared with our observed velocities in the series of panels in Fig. 2 and Fig. 3 for the single-lined orbits and the double-lined orbits, respectively. Note that two of the four triple systems, HIP 999 and HD 105575, appear in both figures. The latter system is even triple lined. The third triple system, HD 237944, is also triple lined and consists of an SB2 in a short orbit but with the third component in a wide thousands-of-years orbit around the close pair. The fourth triple system is HD 45762 where the secondary is again an SB1 but with a period exactly 1/3 of the wide SB2 pair. HD 106855 is a close visual double with its primary A-component to appear double lined, its bona-fide more massive Ab component being again an SB1 for itself. HD 16884 appears to be a quadruple system with two SB1 pairs in a bound 106.65-d orbit. More comments to individual systems are collected in Sect. 5. Note that these comments do not intend to give a comprehensive overview of CDS/Simbad-collected literature but are meant to draw attention to some specific system features.

At the time of the start of our monitoring program in 2006, a total of 17 stars were already either known binaries or had even an orbit computed, or at least had an orbital period known. However, we accumulated enough observations for all systems to allow for orbital solutions just using our own data for a certain epoch. This was motivated not only by consistency arguments but also by detections of orbital-period variations in active binaries and particularly in one of our targets (FF UMa; Gálvez et al. 2007)². Orbital-period variations of magnetically active binaries are known for a long time (e.g. Hall & Kreiner 1973; see also Lanza et al. 2006) and were partly explained by mild mass exchange and mass loss due to a stellar wind. However, Aplegate (1992) proposed a connection between the gravitational quadrupole moment and the shape of a magnetically active component in the system as it goes through its magnetic activity cycle. Therefore, it appears rewarding to re-determine the orbits of such binaries from time to time.

4.3 Rotational periods and spot amplitudes from photometry

Table 6 is the summary of the results from our photometric analysis. A total of 56 stars out of the total sample of 60 targets were observed, of which 39 have a detectable period. The time coverage and the sampling are very different from target to target, ranging from a minimum of 20 nights for QY Hya (HD 105575) to 4,160 nights (>11 yrs) for HY CMA (SAO 151224) with a sampling of all-night-long monitoring (QY Hya) to one observation per night as for most targets. This diversity of data wealth makes a coherent spot-modelling analysis not feasible for the present paper and we just focus on the determination of average light-curve parameters. A more detailed analysis per target

is planned for the future whenever feasible (see, e.g. Strassmeier et al. 2011 for the most recent example of HD 123351, excluded from this paper).

Most relevant for this paper is the determination of a precise photometric period, P_{phtm} , that can be interpreted as the stellar rotation period. This allows a superior measurement of rotation with respect to spectroscopic $v \sin i$ measurements because they are independent of the (unknown) inclination of the rotational axis and can be determined much more precisely. To proceed, we first pre-filtered all photometric data by excluding data points with an rms of ≥ 0.02 mag in order to remove data grossly affected by clouds. Periods were then searched for either in Johnson V or in Strömgren y or, for the stars where we have both passbands, in the combined $y + V$ series. For light-curves with a highly harmonic content, the Lomb periodogram (Lomb 1976) in the formulation of Scargle (1982) was applied. In cases where a period could have been affected by the window function, the CLEAN algorithm (Roberts et al. 1987) was employed to verify, but not to alter, the period identification from the Lomb periodogram. For light curves with a highly non-harmonic content, i.e. for eclipsing binaries, a string-length minimization, a variant of a Lafler-Kinman (Lafler & Kinman 1965) statistic described in Dworetzky (1983), was used to determine the final photometric period. Some of the stars had already had a period determined in our paper I but the period in the present paper supersede these values. In Fig. 4, a phased light curve from all data for each of the variable targets is shown. These light curves are phased with the photometric period indicated in the graph and the respective time of periastron listed in Tables 4 or 5, or ascending node for circular orbits. Single-star zero epochs are arbitrary.

Errors for the periods were obtained by using a method sometimes referred to as “refitting to synthetic data sets” (e.g. Ford 2005). This method estimates confidence intervals by synthesizing a large number of data sets (typically 10^5) out from the original data by adding Gaussian random values to the measurements proportional to the actual rms of the data. The respective period-search algorithm is then applied to these synthetic data and the resulting standard deviation assumed to be the standard deviation of the original period. This value is given in Table 6 as the error for P_{phtm} .

Note that Table 6 strictly lists photometric periods. We interpret these usually as stellar rotational periods but emphasize that care must be taken because, e.g., in case the star is a close binary, an ellipticity effect could mimic a spot light curve with a $P_{\text{orb}}/2$ photometric period that is easily misinterpreted as the stellar rotation period. For one system, HD 138157, we interpret the 55-mmagnitude amplitude partly due to the ellipticity effect. Its true rotational period is close to the orbital period. For five of our six eclipsing binaries the rotational modulation appears to have the same period as the orbital motion. For one case, HD 190642, a newly discovered eclipsing pair, the spot wave appears doubled humped and gives half of the true rotation period.

² See our individual notes for this star though.

Table 4 STELLA single-lined orbital solutions. Column “rms” denotes the quality of the orbital fit for a point of unit weight in km s^{-1} .

Name	P_{orb} (days)	T_{Per}^a (HJD 245+)	K (km s^{-1})	γ (km s^{-1})	e	ω (deg)	$a_1 \sin i$ (10^6 km)	$f(M)$	rms
HIP999(ab)c ^b	1555. ±2.6	0885.7 ±5.5	5.99 ±0.14	-0.10 ±0.08	0	128. ±3.1	0.0348 ±0.0025	1.154
HD 16884ab ^c	106.63 ±0.011	4088.3 ±1.6	29.97 ±0.045	2.23 ±0.031	0.0161 ±0.0014	266. ±5.2	43.93 ±0.066	0.2978 ±0.0013	0.261
HD 16884cd ^c	106.7 ±0.17	4115.6 ±0.77	16.3 ±0.38	2.3 ±0.26	0	24.0 ±0.56	0.0482 ±0.0034	2.215
HD 40891	49.0823 ±0.00071	4092.901 ±0.012	16.122 ±0.015	17.791 ±0.0098	0.5105 ±0.00069	100.3 ±0.11	9.357 ±0.0098	0.01358 ±0.000043	0.080
HD 62668	69.3023 ±0.0016	4115.271 ±0.022	31.10 ±0.037	-16.34 ±0.028	0	29.64 ±0.036	0.2165 ±0.00080	0.294
HD 66553	75.89957 ±0.00048	4110.790 ±0.0075	16.2 ±0.19	34.564 ±0.015	0.8719 ±0.0028	80.71 ±0.32	8.30 ±0.13	0.00396 ±0.00018	0.130
HD 82159	3.855871 ±0.000006	4064.9028 ±0.0025	30.68 ±0.036	29.261 ±0.025	0.2640 ±0.0012	215.2 ±0.25	1.569 ±0.0019	0.01038 ±0.00004	0.242
HD 82841	56.7316 ±0.0017	4064.48 ±0.11	17.552 ±0.017	40.782 ±0.013	0.0874 ±0.0010	126.2 ±0.72	13.640 ±0.013	0.03149 ±0.00009	0.092
HIP50072	34.3157 ±0.0027	4220.7 ±1.7	13.95 ±0.060	11.97 ±0.042	0.014 ±0.0043	301. ±18	6.582 ±0.029	0.00967 ±0.00013	0.310
HD105575 ^d	4550. ±52	4061. ±13	10.11 ±0.09	20.03 ±0.075	0.391 ±0.0059	186.8 ±1.2	582. ±8.7	0.381 ±0.012	0.160
HD112099	23.50447 ±0.00013	4082.691 ±0.0051	18.017 ±0.015	-16.858 ±0.0079	0.4466 ±0.00057	21.90 ±0.094	5.2105 ±0.0046	0.01023 ±0.000027	0.067
HIP63322	4.593843 ±0.000005	4078.3032 ±0.00056	38.530 ±0.017	-4.429 ±0.012	0	2.4340 ±0.0011	0.02729 ±0.000036	0.119
HIP63442	38.7156 ±0.0026	4071.693 ±0.031	15.56 ±0.042	-45.538 ±0.030	0	8.282 ±0.023	0.01514 ±0.00012	0.266
HD138157	14.36891 ±0.00010	4150.70 ±0.40	28.83 ±0.047	-6.642 ±0.018	0.0051 ±0.0009	83. ±9.9	5.696 ±0.0093	0.03574 ±0.00018	0.216
HD147866	114.050 ±0.0073	4234.12 ±0.043	6.713 ±0.012	-36.108 ±0.0075	0.5141 ±0.0013	100.5 ±0.22	9.030 ±0.018	0.002261 ±0.000014	0.076
HD150202	68.47160 ±0.00097	4162.339 ±0.0081	22.913 ±0.0090	-6.9620 ±0.0064	0	21.573 ±0.0085	0.08553 ±0.00010	0.083
ϵ UMi	39.48042 ±0.00012	3933.392 ±0.0047	31.849 ±0.013	-9.8623 ±0.0085	0	17.290 ±0.0068	0.1325 ±0.00016	0.121
HD190642	49.5969 ±0.0012	4166.0 ±0.73	40.20 ±0.045	4.631 ±0.033	0.0126 ±0.0011	314. ±5.3	27.42 ±0.031	0.3346 ±0.0011	0.445
HD202109 ^e	6446. ±14	2421363. ±82	3.30 ±0.057	16.41 ±0.043	0.244 ±0.016	40.7 ±3.3	284. ±5.1	0.0220 ±0.0012	0.413

^aTime of periastron, or ascending node for circular orbits.^bTriple system. Orbit (ab) around c is given.^cQuadruple system with two SB1 pairs in a synchronized orbit.^dSB1 orbit of the tertiary component, c, around the close (eclipsing) ab pair.^eSB1 with long period. The orbit given is from a combination of STELLA data and selected published values. T_{Per} is 2421363. See individual notes.

The typical error of the magnitude zero point is around 0.01–0.02 mag, but never higher than 0.05 mag. The wave amplitude, ΔV , in Table 6 is the maximum observed amplitude within our data coverage. For the eclipsing systems, we cut out the data points during eclipse phases and then re-determined the maximum amplitude. The color index, C.I., is the average color index over all observations. In case of T7 observations it is $(V-I)_C$, for T6 it is $b-y$, if available. Variations in the C.I. are present but are in general too noisy for

period analysis. Most of the observations of HD 136655 had to be discarded due to obvious instrumental problems. Its remaining data shows no evidence for photometric variability. Orbital period and T_0 of the eclipsing binary HD 105575 are equally constrainable from photometry than from radial velocities. If $e=0$ is adopted, we obtain $T_0=2,454,160.772$ and $P_{\text{orb}}=0.29238\pm 0.00009$ d just from our 20-day long time series. However, because the photometry was obtained around JD2,451,250, i.e. almost 10,000 eclipses prior to the

Table 5 STELLA double-lined orbital solutions. Suffices 1 and 2 denote the primary and the secondary star, respectively.

Name	Period	T_{Per}^a	K_1 K_2	γ	e	ω	$a_1 \sin i$ $a_2 \sin i$	$M_1 \sin^3 i$ $M_2 \sin^3 i$	rms ₁ rms ₂
	(days)	(HJD245+)	(km s ⁻¹)	(km s ⁻¹)		(deg)	(10 ⁶ km)	(M _⊙)	(km s ⁻¹)
HD 553	9.059792	4087.1233	63.312	-38.014	0	...	7.8874	1.019	0.411
	±0.000032	±0.0019	±0.037	±0.027	±0.0047	±0.0073	
			65.46				8.155	0.9854	0.390
HIP 999 ^b	1.8441405	4063.6374	62.40	-14.24	0	...	1.582	0.447	0.519
	±1.6 10 ⁻⁶	±0.00055	±0.063	±0.041	±0.0016	±0.0071	
			94.77				2.403	0.2945	3.292
HD 8997	10.98336	4072.091	39.124	21.546	0.0412	195.2	5.9040	0.3956	0.365
	±0.00004	±0.029	±0.027	±0.021	±0.0007	±0.93	±0.0041	±0.0011	
			47.00				7.092	0.3294	0.400
HD 9902	25.3722	4079.516	29.46	56.956	0.5068	74.33	8.861	0.1813	0.201
	±0.00026	±0.0060	±0.035	±0.014	±0.00074	±0.11	±0.012	±0.00066	
			30.22				9.089	0.1767	0.154
HD 18955	43.32161	4086.710	53.83	31.273	0.75874	174.84	20.89	0.9982	0.237
	±0.00022	±0.0045	±0.090	±0.024	±0.00050	±0.080	±0.039	±0.0052	
			61.02				23.68	0.8807	0.480
SAO151224	4.977691	4069.9382	68.07	42.67	0	...	4.659	1.130	1.130
	±0.000012	±0.0021	±0.085	±0.057	±0.0058	±0.0041	
			88.92				6.087	0.8652	0.869
HD 45762 ^c	59.9363	4110.40	65.447	2.23	0.0150	84.6	53.935	0.599	0.533
	±0.0016	±0.61	±0.064	±0.048	±0.0009	±3.7	±0.053	±0.058	
			14.9				12.3	2.63	6.4
HD 50255	454.910	4152.91	11.77	19.059	0.3440	324.42	69.11	0.5414	0.150
	±0.038	±0.28	±0.023	±0.011	±0.0011	±0.23	±0.14	±0.0045	
			16.89				99.23	0.3771	0.176
HD 61994	552.82	4397.45	10.46	-22.038	0.4230	222.3	72.07	0.465	0.118
	±0.25	±0.26	±0.018	±0.0088	±0.0012	±0.18	±0.013	±0.0044	
			15.81				108.9	0.3120	0.117
HD 73512	128.241	4145.44	23.200	33.478	0.26240	277.27	39.478	0.7722	0.087
	±0.0046	±0.045	±0.014	±0.0086	±0.00045	±0.13	±0.025	±0.0016	
			26.349				44.836	0.6799	0.170
HD 82286	3.2751924	4066.0088	29.775	-1.473	0	...	1.3410	0.19296	0.025
	±4 10 ⁻⁷	±0.00012	±0.0043	±0.0026	±0.00019	±0.00010	
			64.282				2.8951	0.089378	0.174
HD 93915	222.965	4182.78	22.35	-17.288	0.3795	37.80	63.40	0.8732	0.180
	±0.022	±0.086	±0.033	±0.015	±0.00088	±0.16	±0.097	±0.0032	
			23.10				65.54	0.8447	0.196
HD 95559	1.5259986	4076.8100	108.369	4.212	0	...	2.27402	0.8282	0.106
	±7.5 10 ⁻⁸	±0.00003	±0.011	±0.0064	±0.00022	±0.0004	
			109.93				2.3068	0.81644	0.165
HD105575 ^d	0.2923378	4160.768	87.4	27.4	0	...	0.351	0.288	8.6
	±1.7 10 ⁻⁶	±0.0044	±4.5	±2.3	±0.018	±0.027	
			158.				0.635	0.16	13
		±6				±0.024	±0.016		

Table 5 (continued)

Name	Period (days)	T_{Per}^a (HJD245+)	K_1 K_2 (km s ⁻¹)	γ (km s ⁻¹)	e	ω (deg)	$a_1 \sin i$ $a_2 \sin i$ (10 ⁶ km)	$M_1 \sin^3 i$ $M_2 \sin^3 i$ (M _⊙)	rms ₁ rms ₂ (km s ⁻¹)
HD106855	0.6709843 ±0.0000026	4097.2944 ±0.0031	41.8 ±0.65 37.7 ±1.4	-1.1 ±0.42	0	0.385 ±0.006 0.348 ±0.013	0.0166 ±0.0012 0.0183 ±0.0009	1.811 9.92
HD109011	1274.7 ±0.86	5213.63 ±0.23	9.582 ±0.014 12.47 ±0.021	-9.8616 ±0.0044	0.5071 ±0.00060	247.36 ±0.13	144.8 ±0.24 188.4 ±0.35	0.5130 ±0.0021 0.3941 ±0.0014	0.094 0.147
HD111487	1.3086147 ±0.0000002	4072.3403 ±0.00014	92.350 ±0.027 133.4 ±0.19	13.17 ±0.021	0	1.6618 ±0.0005 2.401 ±0.0033	0.9217 ±0.0028 0.6381 ±0.0011	0.268 1.776
HD112859	18.49896 ±0.00014	4072.681 ±0.0038	43.466 ±0.031 52.57 ±0.07	22.267 ±0.020	0	11.057 ±0.0078 13.37 ±0.018	0.9293 ±0.0027 0.7683 ±0.0015	0.300 0.265
HD127068	15.15011 ±0.00011	4108.69 ±0.23	22.09 ±0.026 31.06 ±0.071	-50.188 ±0.014	0.0098 ±0.00087	161. ±5.5	4.601 ±0.0055 6.471 ±0.015	0.1377 ±0.00069 0.09790 ±0.00034	0.190 0.364
HIP77210	9.943224 ±0.000011	4106.9724 ±0.0041	42.096 ±0.007 53.262 ±0.030	1.609 ±0.0047	0.06069 ±0.00015	83.32 ±0.15	5.7451 ±0.001 7.2691 ±0.0041	0.4962 ±0.00060 0.39213 ±0.00028	0.052 0.203
HD142680	24.53381 ±0.00006	4169.6573 ±0.0022	37.257 ±0.006 47.398 ±0.031	-83.830 ±0.0041	0.3158 ±0.00015	324.81 ±0.031	11.926 ±0.0021 15.172 ±0.010	0.7375 ±0.0010 0.5797 ±0.00047	0.042 0.205
HD143937	0.91483076 ±0.0000002	4150.5197 ±0.0001	118.56 ±0.04 133.5 ±0.16	-55.307 ±0.030	0	1.4914 ±0.0005 1.679 ±0.0020	0.8036 ±0.0019 0.7137 ±0.0010	0.285 1.258
HD197913	1778.5 ±1.3	6285.5 ±2.0	10.941 ±0.010 11.52 ±0.013	-26.969 ±0.0060	0.2600 ±0.00072	342.57 ±0.24	258.4 ±0.30 272.1 ±0.37	0.9649 ±0.0026 0.9161 ±0.0021	0.100 0.161
HD199967	6.1002208 ±0.000005	4169.06 ±0.06	65.12 ±0.076 83.89 ±0.10	-6.830 ±0.007	0.00244 ±0.00015	170. ±3.5	5.463 ±0.0064 7.037 ±0.0085	1.177 ±0.0032 0.9139 ±0.0024	0.102 0.149
HD226099	18.78209 ±0.000019	4162.0653 ±0.0016	38.528 ±0.0068 42.968 ±0.013	7.5772 ±0.0042	0.30961 ±0.00014	242.63 ±0.031	9.4618 ±0.0017 10.552 ±0.0033	0.47739 ±0.00032 0.42807 ±0.00021	0.086 0.182
HD237944 ^c	5.5076262 ±0.0000047	4070.103 ±0.019	76.237 ±0.048 77.410 ±0.048	-15.25 ±0.017	0.0141 ±0.0003	105. ±1.3	5.7733 ±0.0036 5.8621 ±0.0036	1.042 ±0.0015 1.027 ±0.0014	0.264 0.223

^aTime of periastron, or ascending node for circular orbits.

^bSB2, but with a third component determined from the γ -residuals. The third-component orbit is given in the SB1 list in Table 4. See also the individual notes.

^cHierarchical triple system with lines from components a and c . The orbit ab is SB1 with $P=19.933$ d. See individual notes.

^dSB3 with a third component in the spectrum denoted c . Its orbit around the (eclipsing) ab pair is given in Table 4.

^eSB3. The third component, c , has a median velocity of $-12.25 \pm 1.3(\text{stdev})$ km s⁻¹ for the time of our observations.

Table 6 Summary of photometric data and results. Listed are the comparison (“cmp”) star used for the differential observations, the start date of observations (“HJD start”), the time span of observations (Δt) in days, the telescope and photometric bandpasses used (Johnson-Cousins VI for the T7 APT and Strömgren by for the T6 APT), and the number of actual data points N , each the mean of three individual readings. The results are summarized in the subsequent columns and list V_{\max} , the maximum, i.e. least spotted, brightness during our observations; ΔV , the largest observed amplitude due to spots and, if eclipsing, due to primary eclipse; $\langle C.I. \rangle$, the average color index $(V-I)_C$ for T7 observations and/or $(b-y)$ for T6; P_{phtm} , the photometric period and its likely error obtained from a refitting to synthetic data; and a note if applicable.

HD/name	HD/cmp star	HJD start (2,4+)	Δt	Tel.	N	V_{\max} (mag)	ΔV_{\max} (mag)	$\langle C.I. \rangle$ (mag)	P_{phtm} (days)	Note
HD 553	443	51107	253	T6+7	217	8.15	0.10	...	$\approx P_{\text{orb}}$	rotation
HD 553							0.28		9.061 ± 0.002	eclipsing
HIP 999	977	50395	700	T6	134	8.53	0.08	0.56	1.84475 ± 0.00008	
HD 8997	9472	51098	95	T6	69	7.75	0.02	...	10.54 ± 0.11	
HD 9902	HIP7910	51098	112	T6	122	8.68	0.05	...	7.445 ± 0.02	
HD 16884	17030	51434	3327	T6+7	286	8.87	0.16	1.58	65.44 ± 0.05	
HD 18645	18668	51098	727	T6	241	7.85	0.04	0.55	21.5 ± 0.1	
HD 18955	19223	51099	50	T6	29	8.46	var at 2.3σ
HD 23551	24513	51447	3729	T6+7	242	7.08	0.035	0.94	81.69 ± 0.03	P from T6
HD 24053	23570	55570	74	T7	130	7.72	0.06	0.55	...	
SAO 150676	37792	51434	745	T6+7	389	9.09	0.08	0.79	1.7889 ± 0.0003	
HD 40891	42756	55570	60	T7	71	8.42	0.06	0.76	...	
SAO 151224	43306	51079	4160	T7	1352	9.27	0.39	1.27	$\approx P_{\text{orb}}$	rotation
SAO 151224							0.68		4.98242 ± 0.00003	eclipsing
HD 43516	44396	55576	67	T7	82	7.40	<0.03	0.85	...	
HD 45762	45168	55576	49	T7	61	8.35	0.15	0.98	62.0 ± 1.6	+ellipticity
HD 50255	50674	55576	49	T7	38	7.48	0.05	0.62	...	
HD 61994	63748	55576	49	T7	43	7.05	0.03	0.64	...	
HD 62668	64106	51457	3782	T7	568	7.46	0.40	1.18	67.470 ± 0.007	
HD 66553	65257	55576	29	T7	6	8.52	<0.02	0.72	...	
HD 73512	73764	55572	92	T7	131	7.92	<0.02	0.80	...	
HD 76799	77361	55572	92	T7	133	7.25	0.06	0.92	...	
HD 82159	82410	51242	89	T6	52	7.97	0.05	...	3.055 ± 0.003	polluted
HD 82286	82719	51459	3780	T7	609	7.84	0.16	1.12	3.27629 ± 0.00003	
HD 82841	83046	51476	3763	T7	914	8.22	0.07	1.15	56.58 ± 0.04	
HIP 50072	88853	51242	96	T6	58	9.44	0.12	...	33.782 ± 0.009	
HD 93915	95379	55572	138	T7	156	8.10	0.20	0.65	...	
HD 95188	94996	51249	102	T6	77	8.51	0.025	...	7.00 ± 0.06	
HD 95559	95242	51551	3686	T6+7	1061	8.83	0.08	0.93	$1.517000 \pm 4 \cdot 10^{-6}$	
HD 95724	96778	51239	112	T6	78	8.97	0.05	...	11.49 ± 0.02	
HD 104067	104414	55572	168	T7	158	7.98	0.05	0.92	...	
HD 105575	105814	51239	20	T6	101	8.98	...	0.62	$\approx P_{\text{orb}}$	rotation
HD 105575							0.36		0.29238 ± 0.00009	eclipsing
HD 106855	106991	51551	3685	T7	992	9.35	0.11	1.27	$0.6705258 \pm 6 \cdot 10^{-7}$	
HD 108564	108599	55572	168	T7	203	9.50	0.06	1.02	...	
HD 109011	109894	51225	135	T6	60	8.10	0.02	...	8.4 ± 0.2	
HD 111487	111276	51142	4116	T7	1571	9.62	0.15	0.86	$\approx P_{\text{orb}}$	rotation
HD 111487							0.76		1.30859 ± 0.000007	eclipsing
HIP 63322	113168	51240	65	T6	35	8.89	0.08	...	2.227 ± 0.003	FAP 20%
HD 112099	111733	55569	171	T7	171	8.22	0.04	0.70	...	
HD 112859	112220	51225	135	T6	76	8.23	0.06	...	18.34 ± 0.05	
HIP 63442	113828	51240	120	T6	80	9.39	0.12	...	40.29 ± 0.08	
HD 120205	120969	55572	168	T7	199	8.35	0.06	0.75	14.3 ± 0.7	
HD 127068	126583	51537	3700	T7	972	8.47	0.18	1.05	18.187 ± 0.0001	
HD 136655	136643	50492	355	T7	465	8.81	<0.02	1.00	...	constant
HD 138157	138085	51540	3697	T6+7	1159	7.11	0.14	1.10	7.18357 ± 0.00005	$P/2 + \text{ell.}$
HIP 77210	140750	51260	100	T6	49	9.14	0.02	...	13.7 ± 0.1	
HD 142680	142245	51260	100	T6	64	8.70	0.03	...	33.4 ± 1.5	
HD 143937	143438	51559	48	T7	57	8.67	0.10	1.16	$\approx P_{\text{orb}}$	rotation
HD 143937							0.41		0.91479 ± 0.00003	eclipsing
HD 147866	147266	51447	728	T6+7	92	8.08	0.03	1.14	80.3 ± 2.2	

Table 6 (continued)

HD/name	HD/cmp star	HJD start (2,4+)	Δt	Tel.	N	V_{\max} (mag)	ΔV_{\max} (mag)	<C.I.> (mag)	P_{phtm} (days)	Note
HD 150202	149843	55572	168	T7	210	7.94	0.05	0.73	36.4±0.5	1/2 P_{rot}
HD 153525	153286	51260	100	T6	53	7.94	0.02	...	15.4±0.1	
HD 155802	156227	55580	160	T7	149	8.50	0.03	0.85	...	
HD 171067	170651	55602	138	T7	194	7.17	0.02	0.55	...	
HD 184591	183849	51099		T6	263	7.34	<0.01	0.62	(48.9±2.2)	uncertain
HD 226099	188149	55634	106	T7	210	7.98	0.05	0.65	...	
HD 190642	189893	51434	3668	T7	791	8.15	0.32	1.26	$\approx P_{\text{orb}}$	rotation
HD 190642							0.43		24.8339±0.0009	eclipsing
HD 197913	198109	51098	51	T6	33	7.13	0.02	...	6.556±0.07	
HD 199967	199354	55652	88	T7	160	7.65	0.03	0.40	...	
HD 237944	93470	55569	169	T7	675	9.27	0.07	0.50	5.41±0.013	rotation
HD 237944							0.25		5.5075±0.0003	eclipsing

spectroscopic data, the combination of the two data sets still results in a loss of the cycle count and could not be combined. Table 5 gives the orbit computed only with the radial velocities.

4.4 Rotational velocities

Selected spectra of our program stars were subjected to a de-noising procedure based on a principal component analysis developed for Doppler imaging (Carroll et al. 2007, 2009). This procedure employs typically a total of around 1100 spectral lines in the wavelength range 480–850 nm to determine the noise spectrum. This noise spectrum can then be used to de-noise an arbitrary wavelength section. The only free parameter is the number of principal components. No strict rule can be given for the choice of this value but we followed the prescription laid out in Martínez González et al. (2008). It suggests 15 components for our typical late spectral types and wavelength coverage. It is then used to de-noise a well-known and unblended spectral line from which we measure $v \sin i$ under the assumption of a temperature and gravity dependent macroturbulence. For this paper, we have chosen the well-known and unblended Fe I 549.7516 nm line with an excitation energy of 1.011 eV, a transition probability of $\log gf = -2.849$, and a typical microturbulence of 2.0 km s^{-1} . The radial-tangential macroturbulences, ζ_{RT} , are taken from Gray (2005), as listed in Fekel (1997). This macroturbulence is then subtracted from the measured total line broadening. At this point, we note that Gray (2005) gave most probable macroturbulent velocities, which are 1.414 times greater than the rms values given here. The total line broadening is measured independently from fits with synthetic spectra over a large range of wavelengths (see next section) and the resulting $v \sin i$ measures were then compared and found to agree within their estimated errors. The final values of $v \sin i$ and ζ_{RT} for all our program stars are tabulated in Table 7 for further reference.

Up to three nightly (and two daily) Th-Ar calibration frames are used to monitor the spectrograph focus throughout the year. The line widths of Th-Ar emission lines are

determined automatically and an unweighted average stored in the STELLA data base. No focus drifts were evident during the time in question. However, manual refocusing was done after every maintenance run. The telescope focus is being controlled and adjusted daily by inserting a focus pyramid into the telescope beam. It splits a stellar image into four equally distant images if the telescope is in focus (see Granzer et al. 2010). The STELLA control system issues a message to the operator in Potsdam if this had to be corrected.

4.5 Stellar atmospheric parameters

Five selected spectral orders (#28, 29, 33, 37, 39) from the STELLA/SES spectra are used to determine the stellar effective temperature, the gravity and the metallicity. These orders cover the wavelength ranges 549–556, 560–567, 583–591, 608–616, and 615–623 nm. Our numerical tool PARSES (“PARAMeters from SES”; Allende-Prieto 2004) is implemented as a suite of Fortran programs in the STELLA data analysis pipeline. It is based on the synthetic spectrum fitting procedure described in Allende-Prieto et al. (2006). Model atmospheres and synthetic spectra were taken from the ATLAS9 CD (Kurucz 1993). Synthetic spectra are pre-tabulated with metallicities between -2.5 dex and $+0.5$ dex in steps of 0.5 dex, logarithmic gravities between 1.5 and 5 in steps of 0.5, and temperatures between 3500 K and 7,250 K in steps of 250 K for a wavelength range of 380–920 nm. All calculations were done with a microturbulence of 2 km s^{-1} . This grid is then used to compare with the five selected echelle orders of each spectrum. Free parameters are T_{eff} , $\log g$, $[\text{Fe}/\text{H}]$, and line broadening $\sqrt{(v \sin i)^2 + \zeta_{\text{RT}}^2}$, where ζ_{RT} is the radial-tangential macroturbulence, again adopted from Gray (2005) and was fixed during the fit. Internal errors are estimated from the rms of the solutions to the five echelle orders and were for T_{eff} typically 20–30 K, for $\log g$ typically 0.06 dex, and for $[\text{Fe}/\text{H}]$ typically 0.03 dex.

Double-lined spectra can not be run automatically through the PARSES routines. We first apply a similar dis-

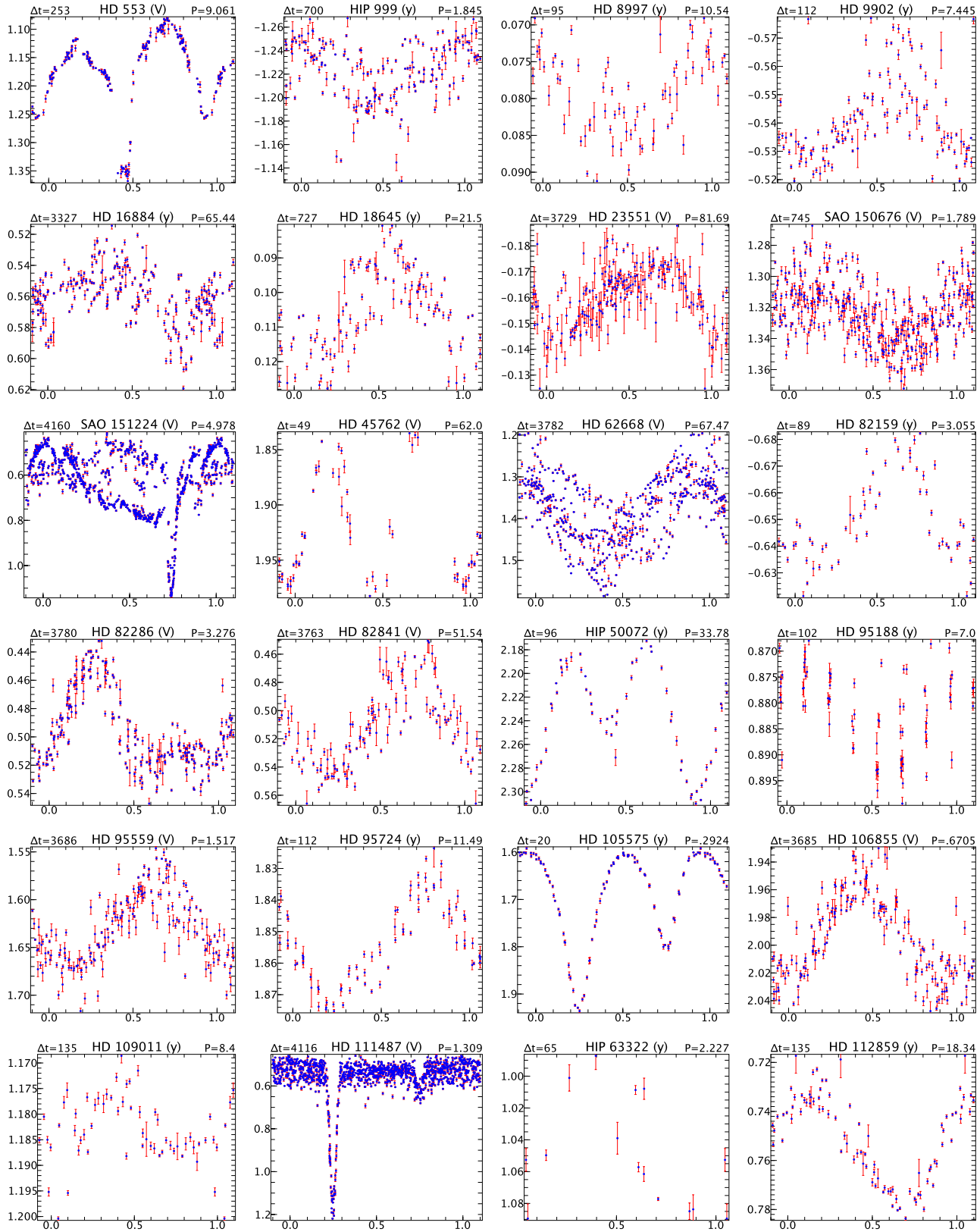


Fig. 4 Light curves for the stars in Table 6. The time coverage of the observations, Δt , and the photometric period, P , are indicated on the top of each panel, both in days. The dots are the V or y observations from the full epochs given in Table 6. Error bars indicate the standard deviation from three individual measurements. Photometric phase has been computed with the photometric period and the respective time of periastron or ascending node for circular orbits. Single star light curves are plotted with an arbitrary starting time. Note that most of the scatter is due to intrinsic spot changes and not due to instrumental origin. The standard error of a mean was 4–6 mmag for the V data and 1.2–3 mmag for the y data.

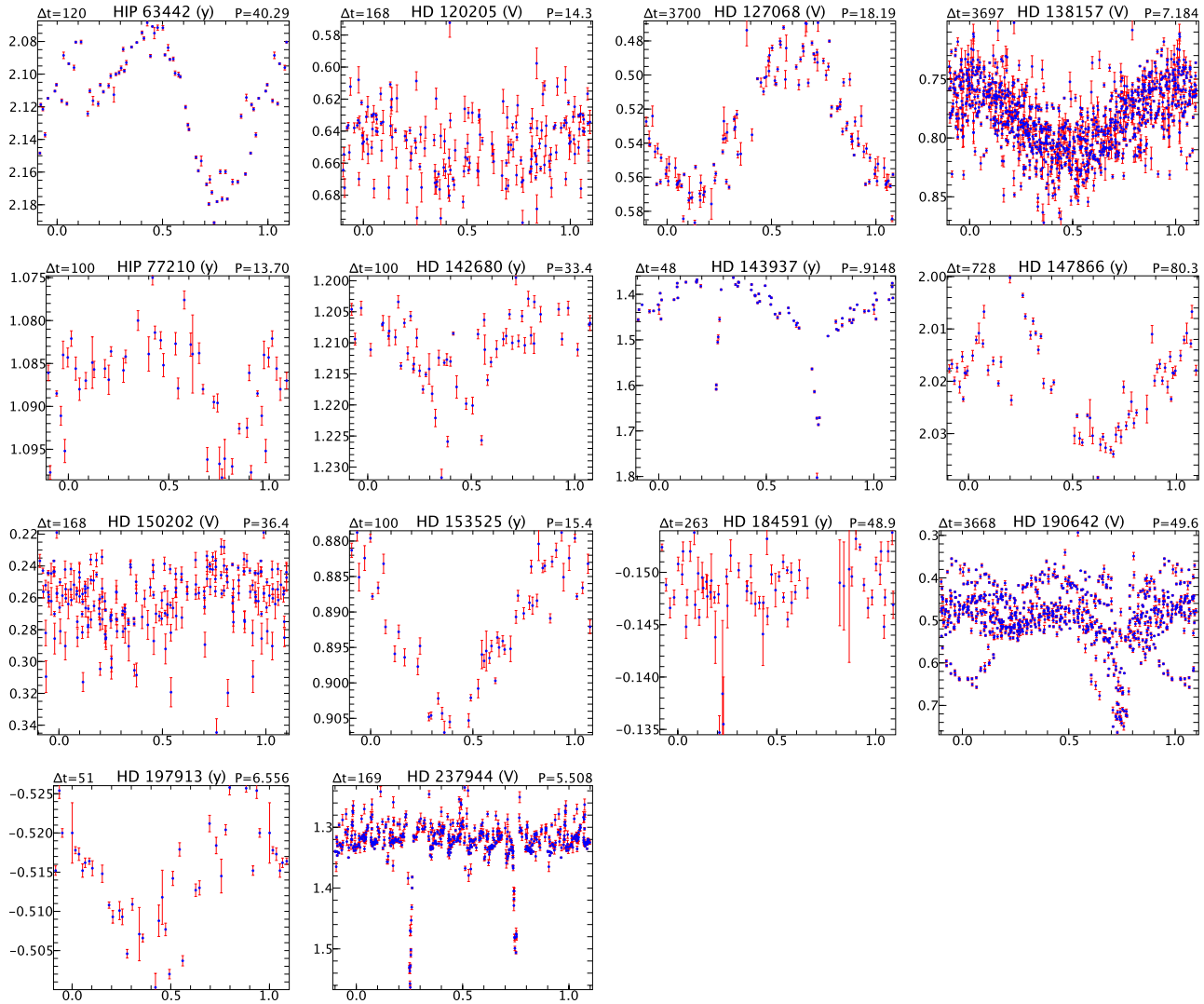


Fig. 4 (continued)

entangling technique as for the automatic radial-velocity measurement of triple-lined spectra, i.e. we remove once the primary and once the secondary component from the combined spectrum at well-separated phases in order to create a single-star spectrum for each component. The resulting spectra were then subjected to the PARSES synthetic-spectrum fitting. This was done only for the five echelle orders that are employed for the PARSES fit (see above) and not for the entire 80 orders. Errors are generally larger for SB2s than for SB1 and single systems due to continuum cross talk. External errors are again estimated from the rms of the solutions to the five echelle orders and were for T_{eff} typically 100 K, for $\log g$ typically 0.3 dex, and for $[\text{Fe}/\text{H}]$ typically 0.3 dex. However, the range of errors is systematically larger for the SB2 systems than for the SB1 and single stars because of the large range of brightness differences between the components in our sample (ranging from $\approx 1:1$, i.e. nearly equal components, to 12:1 for HIP 999).

Lithium abundances are determined for all individual spectra that had sufficient S/N in the respective echelle or-

der. The time averaged results are listed in Table 7 with respect to the $\log n(\text{H}) = 12.00$ scale for hydrogen. A double Gaussian fit to Li I 6707.8 Å and the nearby Fe I 6707.4-Å line yields an individual equivalent width for the lithium line. Despite that these values are still the combined equivalent width for the close blend from the ^6Li and the ^7Li isotopes, it effectively removes the Fe I blend. Weaker CN features are neglected in this study because of limited S/N and spectral resolution. The listed equivalent widths are the averages of the individual measures with unit weight. The errors in Table 7 are still the O-C error from an individual Gaussian fit but again averaged over all measures in time. Because the rms values of the equivalent widths of an entire time series per star were never larger than 3σ of above O-C error, we do not explicitly list them in Table 7. However, these rms are useful to judge eventual long-term variability. SB2's are measured only at phases of quadrature, where blending is minimized. The curves of growth from Pavlenko & Magazzú (1996) are then used to convert the equivalent width to a logarithmic lithium abundance using the non-LTE

Table 7 Determination of astrophysical properties. Column SB denotes the binary component in case the system is SB2 or even SB3 (S means single star, *a* means primary component, *b* secondary component, *c* tertiary component). The parallaxes are from the revised *Hipparcos* catalog (van Leeuwen 2007). Effective temperatures, gravities and metallicities are from the STELLA PARSES analysis. Note that errors are mean internal errors from the fits to five spectral orders. The Li abundance is from equivalent-width measures of the Li I 670.8nm line converted with the NLTE calibration of Pavlenko & Magazzú (1996) and the temperatures listed here. ζ_{RT} is the radial-tangential macroturbulence adopted.

Name	SB	π (mas)	T_{eff} (K)	$\log g$ (m s^{-2})	[Fe/H]	W_{Li} (mÅ)	$\log n(\text{Li})$ ($H = 12.00$)	ζ_{RT}	$v \sin i$ (km s^{-1})
HD 18645	S	8.71	5445±30	3.53±0.04	-0.19±0.03	14±4	1.47±0.15	3	11.0±0.2
HD 23551	S	5.00	5045±25	3.04±0.05	-0.11±0.02	12±4	1.03±0.16	3	6.4±0.2
HD 24053	S	30.74	5600±25	4.09±0.03	-0.01±0.02	49±8	2.26±0.12	3	<3
SAO150676	S	...	5750±50	4.54±0.11	-0.16±0.07	97±10	2.71±0.10	3	23.6±0.7
HD 43516	S	4.10	5120±50	2.86±0.07	-0.15±0.04	39±6	1.72±0.15	3	<3
HD 76799	S	6.13	4915±25	3.26±0.07	-0.12±0.03	12±4	0.86±0.18	3	7.8±0.3
HIP46634	S	27.46	5140±35	4.44±0.04	-0.01±0.03	33±6	1.59±0.14	2	<3
HD 95188	S	27.63	5330±40	4.39±0.06	-0.18±0.03	13±6	1.29±0.24	3	6.9±0.7
HD 95724	S	28.37	4960±20	4.45±0.06	+0.06±0.02	15±5	0.97±0.16	2	<3
HD 104067	S	48.04	4820±20	4.37±0.04	-0.03±0.02	16±4	0.83±0.15	2	8.1±0.3
HD 108564	S	35.30	4560±25	4.40±0.06	-0.90±0.03	21±7	0.66±0.20	2	14.8±1.4
HD 120205	S	31.78	5260±30	4.36±0.05	+0.03±0.03	10±5	1.13±0.18	2	<3
HD 136655	S	24.87	5010±25	4.27±0.03	+0.09±0.04	11±5	0.92±0.20	3	<3
HD 153525	S	57.13	4775±25	4.47±0.05	-0.12±0.03	12±5	0.66±0.20	2	<3
HD 155802	S	34.27	5010±15	4.46±0.04	-0.15±0.02	13±4	0.96±0.13	2	5±1
HD 171067	S	39.73	5520±35	4.03±0.04	-0.15±0.03	12±4	1.43±0.16	3	<3
HD 184591	S	4.58	4800±40	2.82±0.07	-0.18±0.03	14±6	0.80±0.24	3	4.7±0.8
HD 218739	S	34.06	5670±20	4.19±0.05	-0.07±0.02	135±6	2.80±0.05	3	7.6±0.2
HD 40891	<i>a</i>	32.95	5140±25	4.37±0.05	-0.10±0.02	11±4	1.03±0.16	3	...
HD 62668	<i>a</i>	4.97	4660±40	2.92±0.10	-0.30±0.04	82±8	1.60±0.10	3	21±1
HD 66553	<i>a</i>	28.03	5275±40	4.33±0.04	+0.09±0.02	12±7	1.20±0.27	2	...
HD 82159	<i>a</i>	21.11	5150±65	4.62±0.08	-0.13±0.03	109±7	2.22±0.10	2	12.5±0.5
HD 82841	<i>a</i>	4.09	4620±30	2.94±0.07	-0.30±0.03	19±6	0.74±0.19	3	8.1±0.3
HIP 50072	<i>a</i>	3.15	4615±39	3.08±0.08	-0.33±0.04	22±6	0.80±0.21	3	20.8±0.8
HD 112099	<i>a</i>	38.12	5095±20	4.37±0.04	-0.14±0.02	11±4	1.00±0.16	2	4.1±0.2
HIP 63322	<i>a</i>	26.24	4995±27	4.48±0.07	-0.23±0.04	142±8	2.19±0.07	2	6±1
HIP 63442	<i>a</i>	3.31	4530±30	2.85±0.08	-0.35±0.04	41±6	1.07±0.13	3	22.3±0.6
HD 138157	<i>a</i>	5.07	4845±82	3.24±0.12	-0.36±0.06	20±5	1.03±0.22	3	40±1
HD 147866	<i>a</i>	5.18	4580±15	2.71±0.05	-0.24±0.02	13±4	0.49±0.14	3	5±1
HD 150202	<i>a</i>	3.75	5010±25	3.06±0.07	-0.12±0.03	25±5	1.32±0.16	3	7.8±0.2
ϵ UMi	<i>a</i>	9.41	5215±50	3.21±0.08	-0.25±0.04	38±6	1.80±0.16	3	25.6±0.2
HD 190642	<i>a</i>	4.48	4760±65	2.96±0.11	-0.47±0.05	19±6	0.90±0.23	3	19.6±1.0
HD 202109	<i>a</i>	21.62	4910±15	2.14±0.04	-0.08±0.02	21±5	1.13±0.15	3	...
HD 553	<i>a</i>	4.74	4645±90	3.38±0.36	-0.23±0.08	22±4	0.85±0.22	3	41±2
	<i>b</i>		5940±150	4.40±0.77	-0.41±0.26	21±6	2.07±0.26	2	27±
HIP 999	<i>a</i>	24.69	5280±70	4.40±0.30	-0.31±0.04	20±4	1.44±0.19	2	27±1
	<i>b</i>		4840±150	3.6±1.2	+0.3±0.3	15±8	0.83±0.42	3	50±2
HD 8997	<i>a</i>	43.16	5060±65	4.53±0.25	-0.12±0.04	10±6	0.91±0.27	2	3.0±0.5
	<i>b</i>		4525±50	4.74±0.26	+0.02±0.18	11±4	0.34±0.21	3	8±1
HD 9902	<i>a</i>	...	5130±80	4.0±0.4	-0.50±0.16	52±7	1.85±0.16	2	12±1
	<i>b</i>		5715±150	3.37±0.20	-0.38±0.15	26±8	1.97±0.31	5	2.0±0.5
HD 16884	<i>a</i>	...	4500±50	2.4±0.4	+0.29±0.11	31±7	0.85±0.20	3	6±1
	<i>c</i>		4535±70	3.4±0.5	-0.26±0.15	10±9	0.36±0.38	3	44±2
HD 18955	<i>a</i>	20.56	5410±80	4.84±0.10	+0.03±0.06	9±2	1.25±0.13	2	9±1
	<i>b</i>		5095±150	4.8±0.3	+0.22±0.17	8±2	0.90±0.23	2	5±1
SAO151224	<i>a</i>	...	4595±110	3.7±0.4	-0.18±0.14	45±7	1.20±0.23	3	45±2
	<i>b</i>		5420±105	4.8±0.3	-0.09±0.12	22±6	1.67±0.25	2	6±2
HD 45762	<i>a</i>	3.45	4630±100	3.0±0.7	-0.48±0.24	31±5	1.02±0.22	3	60±2
	<i>c</i>		6015±150	3.5±1.0	-0.19±0.18	5	16±2
HD 50255	<i>a</i>	30.26	5580±100	4.07±0.12	-0.18±0.11	45±6	2.19±0.18	2	3.0±1.0
	<i>b</i>		4980±150	3.7±1.0	-1.0±0.8	9±4	0.81±0.30	3	5±1

Table 7 (continued)

Name	SB	π (mas)	T_{eff} (K)	$\log g$ (m s^{-2})	[Fe/H]	W_{Li} (mÅ)	$\log n(Li)$	ζ_{RT}	$v \sin i$ (km s^{-1})
HD 61994	<i>a</i>	35.13	5630±150	4.13±0.11	+0.03±0.12	17±4	1.69±0.23	2	4±1
	<i>b</i>		4775±150	4.6±0.6	-0.27±0.33	9±4	0.56±0.33	3	9±1
HD 73512	<i>a</i>	39.28	5110±115	4.58±0.12	-0.25±0.04	11±5	1.00±0.17	2	5±1
	<i>b</i>		4600±130	4.4±0.5	-0.37±0.17	11±3	0.41±0.27	3	5±1
HD 82286	<i>a</i>	9.57	4800±40	3.73±0.31	-0.05±0.09	21±5	1.00±0.17	3	37.5±1.5
	<i>b</i>		4785±150	3.92±0.35	-0.42±0.20	24±6	1.04±0.32	3	40.5±2
HD 93915	<i>a</i>	22.78	5520±105	4.28±0.24	-0.29±0.09	12±4	1.43±0.22	2	5±1
	<i>b</i>		5315±120	4.25±0.24	-0.22±0.09	9±3	1.17±0.22	2	3±1
HD 95559	<i>a</i>	18.43	5090±110	4.47±0.27	-0.10±0.12	16±6	1.14±0.28	2	33±2
	<i>b</i>		5065±150	4.56±0.33	+0.07±0.12	20±6	1.23±0.32	2	33±2
HD 105575	<i>a</i>	19.77	5650±150	4.73±0.11	-0.46±0.08	14±2	1.61±0.17	2	42±15
HD 106855	<i>a</i>	22.88	4750±110	4.48±0.33	-0.87±0.19	22±4	0.91±0.24	2	30±2
	<i>b</i>		4950±150	4.0±0.8	-0.5±0.4	11±4	0.85±0.30	3	5±2
HD 109011	<i>a</i>	42.13	5030±75	4.59±0.27	-0.17±0.10	30±5	1.42±0.19	2	5±1
	<i>b</i>		4900±150	3.7±1.0	+0.2±0.3	13±5	0.84±0.33	3	6±1
HD 111487	<i>a</i>	...	5500±150	4.47±0.28	-0.36±0.11	13±4	1.45±0.26	2	42±2
	<i>b</i>		4700±150	4.6±0.5	-0.1±0.5	14±6	0.64±0.38	3	28±2
HD 112859	<i>a</i>	5.24	4780±120	3.41±0.38	-0.24±0.15	47±7	1.45±0.23	3	20±1
	<i>b</i>		6150±150	2.5±0.5	+0.05±0.3	5	5±1
HD 127068	<i>a</i>	9.75	4850±135	3.61±0.27	-0.48±0.07	76±5	1.79±0.19	3	6±1
	<i>b</i>		5560±150	3.9±0.8	-0.39±0.14	10±5	1.46±0.31	3	8±2
HIP 77210	<i>a</i>	20.73	5190±120	4.41±0.26	-0.43±0.10	14±4	1.18±0.25	2	3±1
	<i>b</i>		4720±150	4.74±0.31	+0.08±0.11	16±5	0.73±0.33	3	5±1
HD 142680	<i>a</i>	28.23	4885±110	4.35±0.26	-0.22±0.05	5±3	0.54±0.24	3	3±1
	<i>b</i>		4500±150	4.6±0.6	-0.51±0.36	8±3	0.21±0.29	3	5±1
HD 143937	<i>a</i>	23.73	5160±140	4.48±0.16	-0.30±0.13	12±6	1.11±0.33	2	55±2
	<i>b</i>		4730±150	4.72±0.17	-0.01±0.13	13±6	0.65±0.35	3	45±2
HD 197913	<i>a</i>	17±6 ^a	5520±100	4.18±0.32	-0.06±0.11	35±4	2.00±0.17	2	5±1
	<i>b</i>		5340±120	4.20±0.45	-0.08±0.10	19±6	1.47±0.28	2	6±1
HD 199967	<i>a</i>	13.57	5850±100	4.26±0.22	-0.24±0.17	28±7	2.13±0.22	2	11±1
	<i>b</i>		5835±150	4.4±0.4	-0.25±0.13	19±8	1.91±0.33	2	9±1
HD 226099	<i>a</i>	35.46	5200±80	4.45±0.34	-0.92±0.23	12±4	1.12±0.21	2	2±1
	<i>b</i>		4560±80	4.20±0.36	-1.1±0.1	9±4	0.30±0.25	3	4±1
HD 237944	<i>a</i>	10.62	(5630) ^b	3	11±2
	<i>b</i>		(5560) ^b	3	9±2
	<i>c</i>		(4900) ^b	3	11±3

^afrom Jenkins (1952),^bassumed from spectral classification.

transformation and the effective temperatures and gravities from Table 7.

4.6 H α -core flux

We measure the central 1-Å portion of the H α line from our continuum-normalized spectra and relate it to the absolute continuum flux, \mathcal{F}_c , expected at H α . The latter is obtained from the relations provided by Hall (1996) for various Morgan-Keenan (MK) classes and color ranges, i.e.

$$\log \mathcal{F}_c = 7.538 - 1.081 (B - V) \quad (1)$$

for MK I – V and $0 < (B - V) < 1.4$,

$$\log \mathcal{F}_c = 7.518 - 1.236 (V - R) \quad (2)$$

for MK V and $0 < (V - R) < 1.4$,

$$\log \mathcal{F}_c = 7.576 - 1.447 (V - R) \quad (3)$$

for MK I – IV and $0 < (V - R) < 1.8$.

The stellar surface H α -core flux in $\text{erg cm}^{-2} \text{s}^{-1}$ is then computed from the measured 1-Å equivalent width, W_{core} , under the spectrum and zero intensity,

$$\mathcal{F}_{\text{H}\alpha} = W_{\text{core}} \mathcal{F}_c. \quad (4)$$

In this way the equivalent width increases with increased line-core filling due to chromospheric emission while the continuum flux reflects the dependency on stellar radius and T_{eff} . Rotational line broadening is accounted for by applying a similar correction to W_{core} as done by Pasquini & Pallavicini (1991). We obtain these corrections by artificially broadening the spectrum of HD 153525, a K0 dwarf with an otherwise unresolved $v \sin i$, in steps of 5 km s^{-1}

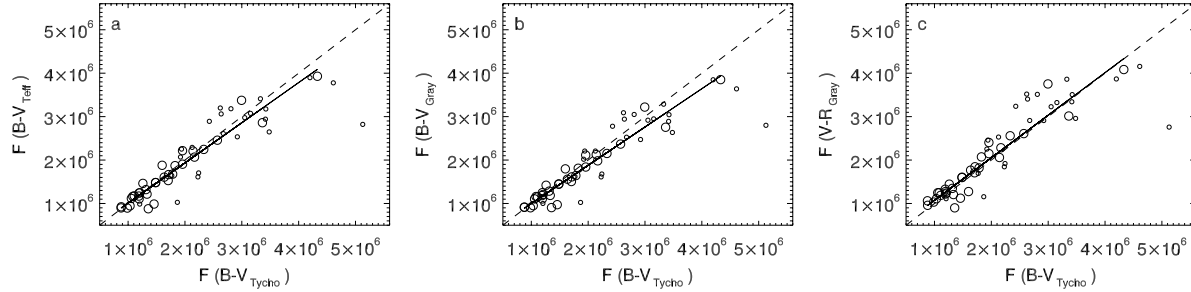


Fig. 5 A comparison of absolute continuum flux at $H\alpha$ from different calibrations. Only our single and SB1 stars are plotted. **a** Fluxes based on the effective temperatures from Table 7 converted to $B - V$ with the T_{eff} vs. $B - V$ calibration of Flower (1996) versus the flux based on the $B - V$ listed in the Tycho-2 catalog. **b** Again our effective temperatures converted to $B - V$ but with the T_{eff} calibration of Gray (2005) versus the $B - V$ listed in the Tycho-2 catalog. **c** Our effective temperatures converted to $V - R$ with the T_{eff} calibration of Gray (2005) versus the $B - V$ -based fluxes listed in the Tycho-2 catalog. Minimized rms errors of the flux residuals are achieved in panel **a**. The dashed line is just a 45-degree line. The solid lines are non-weighted regression fits.

up to 60 km s^{-1} and then measure the $H\alpha$ line as done previously. The correction factor, Δ , for each stellar measurement is obtained from the fit to these simulations by inserting the stellar values for $v \sin i$ from Table 7;

$$\Delta = A + B v \sin i + C v \sin i^2 + D v \sin i^3. \quad (5)$$

The coefficients are $A = -0.00068990582$, $B = 0.00029478396$, $C = 0.00011360807$, $D = -9.4974126e-07$. Note that the corrections are negligible for $v \sin i < 10 \text{ km s}^{-1}$ but reach a maximum for HD 45762 ($v \sin i = 60 \text{ km s}^{-1}$) of 30%. Table 8 lists the corrected fluxes.

The line-core fluxes from Eq. 4 are not corrected for photospheric light. Such a correction for the $H\alpha$ line core is not without problems because several line-formation processes are at work at the same time and significant star-to-star differences are expected (see Cram & Mullan 1985). There is no readily available photospheric $H\alpha$ -core flux tabulated for standard model atmospheres. Therefore, previous attempts relied on empirical methods, e.g., the subtraction of an observed profile of a bona-fide inactive star of otherwise similar quantities (e.g. Soderblom et al. 1993b) or the subtraction of an empirically predetermined minimum flux from a large sample of stars (e.g. Cincunegui et al. 2007). However, as was shown nicely in the work by Cincunegui et al. (2007), this photospheric correction significantly worsened the relationship with Ca II H&K flux. The conclusion is that empirical photospheric corrections may not be fully photospheric in origin. In the present paper, we refrained from any photospheric correction and give combined photospheric+chromospheric fluxes as observed.

The largest contribution to the flux error is due to the continuum-flux calibration and comes from systematic differences in the T_{eff} -color relations and the error in T_{eff} . We compared fluxes based on four different relations. Our two prime choices for \mathcal{F}_c are based, firstly, on the $B - V$ from the Tycho-2 catalog (Høg et al. 2000) and, secondly, on the $B - V$ from the conversion of our measured T_{eff} in Table 7

with the color transformation from Flower (1996). Two secondary choices were fluxes from our T_{eff} values but converted to $B - V$ and $V - R$ using the tables in Gray (2005). The inter comparison in Fig. 5 shows minimized rms errors of the flux residuals for the two prime choices, i.e. the Tycho-2 $B - V$ -based fluxes vs. the fluxes from measured T_{eff} 's with the color conversion from Flower. It gave an rms of 0.45 in units of $10^5 \text{ erg cm}^{-2} \text{ s}^{-1}$. Comparable rms is obtained for the Tycho-2 $B - V$ -based fluxes vs. Gray's $B - V$ based fluxes but significantly larger (0.75) if Gray's $V - R$ based fluxes are used instead. The calibration rms errors per star are listed in Table 8 along with the line-core fluxes based on the Tycho-2 $B - V$ color for the single and SB1 stars, and on the Flower (1996) T_{eff} -($B - V$) transformation for the SB2s using the conversion in Eq. 1. These rms values are useful when judging the reality of time variations, if present. An exceptionally large rms value indicates most likely that the calibration assumptions in Eq. 1–3 were not fully appropriate, e.g. for SAO150676, which is likely a pre-main sequence star where the applicability of the T_{eff} -($B - V$) conversion is questionable.

The number of spectra used for the $H\alpha$ analysis is smaller than for the radial-velocity curves because we use only the ones with the best S/N and, in case of the SB2 binaries, when the line separation is large enough. We measure single-lined spectra just like single stars, which have continua presumably unaffected by the companion. The few systems where we see a $H\alpha$ line from the secondary component, but not its photospheric lines, were also treated like single stars. The regular SB2 spectra, on the other hand, were first multiplied by the respective photospheric light ratio, $R(\text{Fe I})$. It is obtained from line pairs near $H\alpha$ (with highest weight given to the unblended Fe I 654.6 nm line) before measuring the $H\alpha$ flux for each component. These fluxes are generally less precise because the available S/N ratio in the continuum is distributed among the two components. Table 8 lists the measurements for all single stars

and single-lined binary stars as well as for all individual stars in the double-lined binaries. The triple-lined system HD 105575 was too uncertain to be measured reliably and only the primary is included in Table 8.

5 Notes to individual systems

HD 553 = V741 Cas. The system was discovered to be an eclipsing binary by the *Hipparcos* satellite. In paper I, we had verified its eclipsing nature and shown that the system is double lined. A first orbit was published shortly thereafter by Duemmler et al. (2002) followed by an independent orbit by Griffin (2003). Both their orbits were circular with a period of 9.0599 d and a solution rms residual of 0.56 and 1.36 km s⁻¹, respectively. The component's rms in the Duemmler et al. orbit were 0.59 and 0.97 km s⁻¹. Our new orbit is also assumed to be circular. The forced $e=0$ solution gives residuals of 0.41 and 0.39 km s⁻¹ for the two components, respectively. There is no conclusive period in the H α -core flux but a peak at 4.5 d could be interpreted to be $\approx P_{\text{orb}}/2$. The out-of-eclipse light variations have a V amplitude of 0.10 mag and suggest a photometric period of 9.061 d (eclipse depth is 0.28 mag in V).

HIP 999 = LN Peg. An initial SB1 orbit was determined by Latham et al. (1988) while Fekel et al. (1999) presented a SB2 orbit and found the star to be at least a triple system. Our radial-velocity residuals indicate a long-term period of around 4.2 years with a full amplitude of 12 km s⁻¹ zero eccentricity (see Fig. 2). This verifies the preference put forward by Fekel et al. (1999) that the long-period orbit is rather 4 years with zero eccentricity than 8 years with 0.5 eccentricity. The long orbit of 1555 d is listed in Table 4 and was obtained by including the Fekel et al. data with a shift of +0.50 km s⁻¹. The total time span of data was then 9430 d with 213 velocities. The STELLA data alone would give elements of $K_3=5.654\pm0.085$ km s⁻¹, $T_0=2,454,117.4\pm8.5$, $P=1310\pm16$ d. The H α line from the secondary star in the close pair appears in emission. The third component c is not directly seen in the spectra but is recognized only due to the systematic radial velocity zero-point variations of the ab pair. The ab -pair orbit is given in Table 5 and shown in Fig. 3.

HD 8997 = EO Psc. Griffin's (1987) SB2-orbit is basically confirmed but now considerably more precise. Our low rms of ≈ 0.4 km s⁻¹ for the a and b component radial velocities allowed to search for residual variations and a period of 88.3 ± 0.5 d is found for the primary with a full amplitude of 0.20 km s⁻¹. No period is seen in the secondary-star residuals. If above period would be interpreted to be the rotational period of the primary, and combined with our $v \sin i$ measures of 3 km s⁻¹, the minimum radius would be 5.2 R $_{\odot}$. This value is clearly in disagreement with the distance of 23 pc and a system brightness of 7.74 mag and $B-V=0.96$. This period must be of other origin or is even spurious. The photometry yields a period of 10.54 ± 0.11 d, with a small amplitude of 0.02 mag in y . This period suggests $R \sin i$

of ≈ 0.6 R $_{\odot}$, in good agreement with the distance and the spectrum synthesis that indicates $T_{\text{eff}}=5060\pm 65$ K, a $\log g$ of 4.5, and a metallicity of -0.12 ± 0.04 , suggesting a K2 dwarf star.

HD 9902 = BG Psc. This system contains two almost equally massive stars with a mass ratio of 0.9750 ± 0.0026 in a 25.3722-d orbit with $e=0.5068$. We refer to the slightly more massive and more rapidly rotating star as the primary. Note that the rms for the orbit for the secondary (154 m s⁻¹) is lower than for the primary due to its sharper lines. Our photometry of the combined system reveals a period of 7.44 ± 0.02 d that we interpret to be the rotation period of the primary ($v \sin i=12$ km s⁻¹) rather than that of the secondary ($v \sin i=2$ km s⁻¹). Also note that the V amplitude of 0^m.05 in Table 6 is for the combined light and not for, say, the primary. The expected pseudo-synchronized rotation periods are ≈ 8.9 d according to Hut (1981). The primary is thus likely rotating faster than synchronous.

HD 16884. The star is double lined from the cross-correlation functions but its spectral lines do not appear to originate from a single physical pair. Most likely HD 16884 is a quadruple system and we see lines from the two primaries a and c , with each system being single lined, i.e., SB1+SB1. The orbital periods for the two pairs (each 106.63 d) appear to be identical within its errors, and so does the systemic velocity (+2.2 km s⁻¹). The K -amplitude of the a and c components are 30.0 km s⁻¹ and 16.3 km s⁻¹, respectively, while their $v \sin i$'s are 6 km s⁻¹ and ≈ 44 km s⁻¹, respectively, which means that the radial velocity attributed to the c component can not be caused by rotationally modulated line-profile variations of the a component, its $v \sin i$ is too small. Not much can be said about the orbital period $ab-cd$ but the two nodal lines appear co-aligned and did not change recognizably during our observations, its orbital period must be very long. Griffin (2009) obtained a sparsely sampled single-lined orbit from 14 of his own velocities, an orbit which is superseded in the present paper. We also note that the stronger-lined a star's H α line profile appears as a broad and asymmetric emission line (full width at continuum of up to 400 km s⁻¹) with a deep central absorption that follows the radial velocities of the a component (Fig. 6). Our photometry reveals a period of 65.44 ± 0.05 d and an amplitude of 0.16 mag in V for the combined stars. It is likely that this is the rotation period of the brighter a component, a K4 giant according to Griffin (2009). His classification is in rough agreement with our T_{eff} of 4500 K and $\log g$ of 2.4 ± 0.4 from the spectrum synthesis. With a $v \sin i$ of 6 km s⁻¹ its minimum radius, $R \sin i$, would be 7.8 ± 1.3 R $_{\odot}$. However, a K4 giant is expected to have a nominal radius of approximately 25 R $_{\odot}$. Thus, if indeed a K4 giant, i would be only $\approx 18^\circ$ and together with an assumed mass of 2.3 M $_{\odot}$ for the primary, this contradicts the large mass function of 0.2972 ± 0.0013 , which would otherwise imply an unreasonable secondary mass of order 7.5 M $_{\odot}$. Doubling the photometric period to get the true rotation period would lead to an inclination

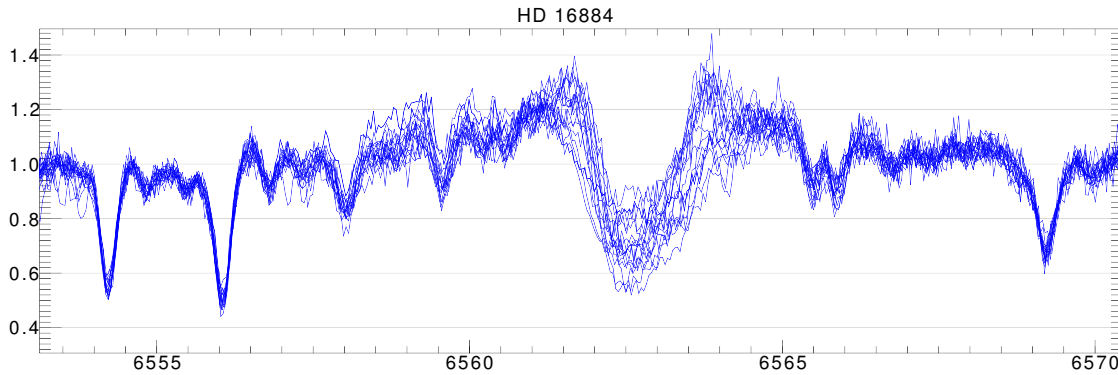


Fig. 6 $H\alpha$ profile variations of HD 16884 in 2007/08. Spectra are corrected for orbital radial velocity of the primary. The photospheric absorption lines belong to the primary of the ab system, a K giant, and agree with the radial velocities from $H\alpha$. It is safe to conclude that the majority of the $H\alpha$ profile originates from this K giant. The signature from the primary component of the cd system, i.e. the secondary in this composite spectrum, is lost in this representation. See text.

much closer to 90° and, lowering the assumed primary mass to $2.0 M_\odot$ the secondary mass gets closer to a minimum mass of $\approx 1.6 M_\odot$, still rather high for an “unseen” star. Certainly, this system warrants further investigation.

HD 18645 = FU Cet. Single star. Our photometry suggests a period of 21.5 d that we interpret to be its rotation period. A residual period of 3.069 d is seen from the radial velocities but with a very weak amplitude of 0.1 km s^{-1} . Additionally, the $H\alpha$ -core emission shows a seasonal trend and, after its removal, a period of ≈ 17 d. Although this period is badly determined and inconclusive it may suggest that the photometric period of 21.5 d is to be preferred against the 3-d period. Our $v \sin i$ measure of $12.0 \pm 0.2 \text{ km s}^{-1}$ converts then to a minimum stellar radius of $5.1 R_\odot$, appropriate for its mid G giant classification.

HD 18955 = IR Eri. This system consists of two dwarf stars of mass ratio 0.88 in a 43-day orbit with a high eccentricity of 0.7587 ± 0.0005 . The expected pseudo-synchronization period would be a mere 11% of the orbital period, i.e. ≈ 5 d. Unfortunately, our photometry did not allow to obtain a period despite that the data indicate variability at the 2.3σ level. Both components show a weak residual radial-velocity variation with a period of 25–26 d and an amplitude of 0.5 km s^{-1} . This could be the stellar rotation period but the data are too noisy to be conclusive. It appears that the secondary is cooler than the primary by ≈ 300 K, and also slower rotating ($v \sin i = 5 \text{ km s}^{-1}$ vs. 9, respectively).

HD 23551 = MM Cam. The star appears to be single. A radial velocity of $-7.5 \pm 0.3 \text{ km s}^{-1}$ was reported in the Pulkova survey by Gontcharov (2006) in good agreement with the average -7.38 ± 0.22 by Famaey et al. (2005). Our two velocities from KPNO in paper I were -9.5 from the blue spectrum and -7.4 ± 0.2 from the red spectrum, also in reasonable agreement. A peak with a period of ≈ 80 d is existent in the $H\alpha$ flux and the photometry suggests a clear period of 81.69 ± 0.03 d that we interpret to be the rotation period of the star. Note that we observed the star with both

APTs (T6 and T7) and that the independent photometric period from T7 data is 81.2 ± 0.5 d, in good agreement with the more precise T6 period. Its $v \sin i$ of $6.4 \pm 0.2 \text{ km s}^{-1}$ converts then to a minimum radius of $10.3 R_\odot$ in agreement with $\log g = 3.0$ from our spectrum synthesis. We also note its significant metal deficiency of -0.11 ± 0.02 . No Li I 6707.8-Å absorption feature is seen above our detection threshold of $\approx 10 \text{ mÅ}$ (Fig. 7).

HD 24053. This star first appeared in the literature in the *uvby* calibration for FGK stars by Olsen, e.g., Olsen (1994). Its effective temperature was determined spectroscopically from spectral line ratios by Kovtyukh et al. (2003) to 5723 K. The revised Geneva-Copenhagen catalog (Holmberg et al. 2007) lists it with a metallicity of -0.04 and 5640 K and suggests an age of 0.2 Gyr. From 2-MASS colors Masana et al. (2006) derived 5711 K and the N2K-consortium (Robinson et al. 2007) derived 5699 K, a metallicity of $+0.09$, and $\log g = 4.45 \text{ cm s}^{-2}$. Earlier velocities were given in our paper I ($5.3 \pm 1.4 \text{ km s}^{-1}$ from a blue spectrum and $2.9 \pm 0.6 \text{ km s}^{-1}$ from a red spectrum two days apart) while the catalog by Gontcharov (2006) lists $4.1 \pm 0.2 \text{ km s}^{-1}$. Two spectra are given in the Elodie archive. We have 77 STELLA spectra and all of them appear to be constant. The average values from our spectrum synthesis yields 5600 ± 25 K, $\log g = 4.09 \pm 0.03$, and a metallicity of -0.01 ± 0.02 . No significant variations are seen in $H\alpha$.

SAO 150676 = AI Lep. Cutispoto et al. (1999) listed the star in their ROSAT follow-up observations. They noted a spectral classification of G2V but added “(PMS?)” indicating possibly pre main sequence. In the same study a photometric variability of 0^m02 in V with a period of 1.78 d was reported. The authors also measured a $v \sin i$ of $28 \pm 2 \text{ km s}^{-1}$ in reasonable agreement with $25.6 \pm 2 \text{ km s}^{-1}$ from our paper I. Their two radial velocity measures agreed to within their errors and were averaged to $+25.8 \pm 1.6 \text{ km s}^{-1}$. In paper I we had given velocities of $+26.1 \pm 1.6 \text{ km s}^{-1}$ from a single red-wavelength spec-

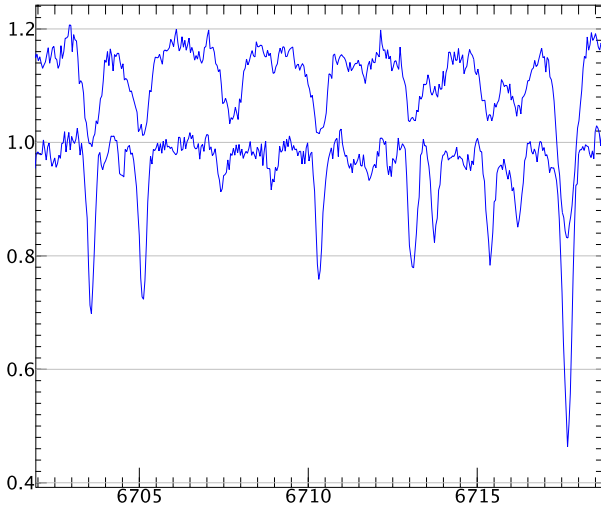


Fig. 7 Li I 6707.8-Å line region for the K0III component of the SB-1 binary HD 62668 (top spectrum; shifted by +0.2) and for the single K0III star HD 23551 (bottom spectrum). Notice the broad Li I absorption line in HD 62668 and its absence in HD 23551.

trum and $+21.5 \pm 5.3 \text{ km s}^{-1}$ and $-18.5 \pm 2.1 \text{ km s}^{-1}$ for two components from a single Ca II H& K emission-line spectrum. The latter must have been an erroneous measurement because it is not verified in the present paper. In paper I, we also measured the large equivalent width of 195 mÅ from the Li I 670.8-nm line, in agreement with the suggestion of being a pre-main sequence star. Our 93 STELLA radial velocities have an unreasonable high scatter of 0.53 km s^{-1} which is likely due to rotational modulation of a spotted surface. A Lomb periodogram shows two equal peaks at periods of 0.64 d and 1.79 d. Unfortunately, the H α fluxes do not show the same peaks but favor a (poorly determined) 1.2-day period. However, our photometry shows a clear 1.79-d period, in good agreement with Cutispoto et al. (1999) and one of the two radial-velocity periods. We interpret it to be the rotation period of the star.

SAO 151224 = HY CMa. The star is an eclipsing SB2 binary in a circular 4.977691-d orbit. Photometry from late 1993 (Cutispoto et al. 1995, 1999) revealed the eclipsing nature while follow-up photometry in 1994 by Cutispoto et al. (2003) failed to confirm the eclipses and the author's stated to the contrary that "No primary eclipses are apparent." Our photometry verifies the eclipsing nature of the light variations with a period of 4.98 d and an eclipse depth of 0.68 mag in *V*. The residual radial velocities of the primary star indicate a period of 5.25 d, likely due to rotation of its spotted surface which partly explains the unexpected high rms of its orbital fit of 1.13 km s^{-1} . The $v \sin i$ of the primary of 45 km s^{-1} converts directly into a radius of $4.4 R_{\odot}$.

HD 40891. We see no traces of Ca II H&K emission in our echelle spectra. Therefore, its emission can be classified at best "very weak". Note that in paper I, we listed the

star in the table for stars with emission, but did not show a plot of the spectrum. This might indicate a logistics error in our paper I. The star is an SB1 in an eccentric orbit with $e=0.5105 \pm 0.0007$ and a period of 49.0823 d. The expected pseudo-synchronization period would be ≈ 17 d.

HD 45762. Griffin (2010) noted in his Table 1 "Binary, $P \sim 60$ days" but otherwise gave no information. We find the star to be a double-lined triple system with the more massive component being an SB1 with a period of $\approx 1/3$ that of the wider *c* component. The (*ab*) – *c* orbit has a period of 59.9363 ± 0.0016 d and a small but non-zero eccentricity of 0.0150 ± 0.0009 . Its rms of the residuals is 0.533 km s^{-1} which increases to 0.88 km s^{-1} if an $e=0$ solution is enforced. The mass ratio $c/(a+b)$ is 0.23 from an averaged *ac* solution (shown as a dotted line in the respective panel in Fig. 3). The close SB1 orbit has only a small amplitude and we find the following preliminary elements ($e=0$ assumed); $K=7.78 \pm 0.77 \text{ km s}^{-1}$, $T_0=2,454,116.84 \pm 0.49$, and $P(ab)=19.933 \pm 0.014$ d. Note that this star's $v \sin i$ is 60 km s^{-1} , as compared to the *c*-component's 16 km s^{-1} , and is likely an asynchronous rotator because a $P_{\text{rot}}=19.933$ d would suggest a large minimum radius of $23.6 R_{\odot}$. Our photometry shows a double-humped light curve with a clear 62-day periodicity but must be partly due to an ellipticity effect because of its phase coherence with the orbit. The *c* component has an expected minimum radius of $19.6 R_{\odot}$ if $P_{\text{rot}}=62$ d. Obviously, both stars are cool giants, as already indicated by the small Hipparcos parallax and the $V=8.3$ -mag brightness.

HD 50255. The star is a SB2 in an eccentric 455-d orbit. The scatter of the residual radial velocities of the secondary component (0.167 km s^{-1}) is larger than expected for a star with $v \sin i=5 \text{ km s}^{-1}$. A Lomb periodogram shows significant excess power at 485 d with an amplitude of 0.65 km s^{-1} , close to the orbital period of 455 d, but given the comparable short coverage of 1471 d of the entire data set it could be also a sampling effect and remains to be confirmed. Tentatively, we interpret it to be the rotation period of the secondary. Note that our photometry did not reveal any clear light variations above, say, 0.05 mag.

HD 61994. There are 102 secondary-star velocities detected from the STELLA cross-correlation functions and an eccentric SB2 orbit is given ($P=552.8$ d, $e=0.423$). Duquennoy & Mayor (1988) had discovered its binarity and also presented a (marginal) SB2 orbit based on 9 CORAVEL measurements. The visual brightness difference between the two components of 2.6 mag is close to its detection limit. The average line ratio in our spectra is 8.5. The expected pseudo-synchronized rotation period is ≈ 250 d, but neither the velocity residuals nor the H α -core flux show traces of any significant period.

HD 62668 = BM Lyn. Our orbit is assumed circular with a period of 69.3023 d. A formal eccentricity of 0.0043 ± 0.0011 is judged too uncertain. The photometry is best fit with a period of 67.470 ± 0.007 d, close but not identical to the orbital period. The H α absorption line also

Table 8 $H\alpha$ absolute emission-line fluxes. Column SB denotes the binary component in case the system is SB2 or even SB3 (S means single star, a means primary component, b secondary component, c tertiary component). (B-V) and (V-R)_C are the expected Johnson-Cousins indices from our T_{eff} and the transformation from Flower (1996) and Gray (2005), respectively, that we adopted for the flux calibration. N is the number of spectra used. W_{core} is the equivalent width in mÅ in the central 1-Å bandpass and its internal measuring error. $\langle \mathcal{F}(H\alpha) \rangle$ is the average 1-Å $H\alpha$ -core flux in $10^5 \text{ erg cm}^{-2} \text{ s}^{-1}$ and its propagated error from the equivalent width measure plus the flux calibration. “rms” is its standard deviation from the four different flux calibrations for comparison. $\delta \mathcal{F}$ is the rms residual of $\mathcal{F}(H\alpha)$ over the time span of our entire observations. $R(\text{Fe I})$ is the photospheric line ratio secondary/primary from Fe I 654.6 nm that is used to weight the components’ $H\alpha$ equivalent widths for SB2 systems.

Name	SB	N	B-V	V-R	W_{core}	$\langle \mathcal{F}(H\alpha) \rangle$	rms	$\delta \mathcal{F}(H\alpha)$	$R(\text{Fe I})$
			(mag)	(mag)	(mÅ)	($\times 10^5 \text{ erg cm}^{-2} \text{ s}^{-1}$)	($\times 10^5 \text{ erg cm}^{-2} \text{ s}^{-1}$)	($\times 10^5 \text{ erg cm}^{-2} \text{ s}^{-1}$)	(–)
HD 18645	S	64	0.75	0.60	421±19	21.4±2.7	0.6	1.0	...
HD 23551	S	98	0.91	0.70	345±12	12.1±1.4	0.2	0.5	...
HD 24053	S	71	0.70	0.55	349±10	19.6±2.1	1.7	0.6	...
SAO 150676	S	78	0.65	0.53	617±25	43.3±5.4	1.9	1.9	...
HD 43516	S	52	0.88	0.67	334±13	13.1±1.6	0.3	0.6	...
HD 76799	S	69	0.97	0.73	385±17	10.8±1.4	0.6	0.5	...
HIP 46634	S	88	0.87	0.70	461±10	18.3±1.9	1.1	0.4	...
HD 95188	S	82	0.80	0.62	460±11	23.3±2.5	1.6	0.6	...
HD 95724	S	69	0.95	0.78	446±11	14.8±1.6	0.6	0.4	...
HD 104067	S	74	1.02	0.87	444±9	13.3±1.4	0.6	0.3	...
HD 108564	S	69	1.15	0.99	482±11	13.6±1.4	2.0	0.4	...
HD 120205	S	88	0.82	0.65	414±11	19.6±2.1	1.2	0.5	...
HD 136655	S	103	0.93	0.76	424±12	14.8±1.6	0.6	0.5	...
HD 153525	S	185	1.04	0.90	480±12	11.9±1.3	0.3	0.3	...
HD 155802	S	111	0.93	0.76	483±13	17.8±1.9	0.8	0.5	...
HD 171067	S	135	0.73	0.57	351±8	21.7±2.2	1.2	0.5	...
HD 184591	S	145	1.03	0.75	366±8	14.6±1.5	2.0	0.4	...
HD 218739	S	96	0.68	0.54	376±12	25.7±2.9	1.0	0.9	...
HD 40891	a	82	0.87	0.70	410±10	17.1±1.8	0.9	0.4	...
HD 62668	a	99	1.10	0.81	571±34	11.9±1.8	0.7	0.8	...
HD 66553	a	69	0.82	0.82	399±15	16.0±1.9	2.4	0.6	...
HD 82159	a	97	0.87	0.69	830±46	30.0±4.1	2.8	1.7	...
HD 82841	a	59	1.12	0.82	430±25	9.9±1.4	0.6	0.6	...
HIP 50072	a	56	1.12	0.82	566±53	11.9±2.2	0.8	1.3	...
HD 112099	a	73	0.89	0.72	419±9	16.4±1.7	0.8	0.4	...
HIP 63322	a	98	0.94	0.77	823±36	33.6±4.2	2.3	1.5	...
HIP 63442	a	79	1.16	0.85	531±57	8.8±1.8	0.8	1.1	...
HD 138157	a	149	1.00	0.74	522±29	10.6±1.7	0.8	0.8	...
HD 147866	a	114	1.14	0.83	471±20	10.3±1.3	0.7	0.5	...
HD 150202	a	176	0.93	0.71	344±10	11.1±1.2	0.3	0.3	...
ϵ UMi	a	110	0.84	0.65	400±14	12.6±1.6	0.9	0.6	...
HD 190642	a	180	1.05	0.77	631±55	17.1±3.0	1.0	1.6	...
HD 202109	a	200	0.97	0.74	299±5	8.8±0.9	0.3	0.2	...
HD 553	a	68	1.10	0.82	590±25	9.9±1.4	0.6	0.6	0.62
	b		0.69	0.50	908±21	41.1±4.9	4.2	1.7	
HIP 999	a	38	0.81	0.64	793±33	34.0±4.3	2.5	1.6	0.21
	b		1.00	0.74	929±16	4.4±0.8	0.3	0.5	
HD 8997	a	100	0.91	0.74	614±12	22.5±2.3	1.1	0.5	0.42
	b		1.16	1.00	844±11	6.4±0.8	0.2	0.2	
HD 9902	a	16	0.88	0.70	883±11	35.1±3.2	2.3	0.5	1.23
	b		0.66	0.54	632±21	53.3±5.6	2.1	1.4	
HD 16884	a	29	1.18	0.87	636±95	11.3±2.6	0.9	1.7	0.19
	c		1.16	0.84	1378±120	4.5±2.6	0.5	2.3	
HD 18955	a	31	0.77	0.60	557±34	29.2±4.1	2.0	1.8	0.67
	b		0.89	0.72	851±30	21.8±2.9	1.3	1.2	
SAO 151224	a	21	1.13	0.83	934±103	16.1±3.5	1.1	2.2	0.98
	b		0.76	0.60	913±43	47.6±6.1	3.2	2.3	
HD 45762	a	26	1.11	0.82	501±29	10.3±1.5	0.7	0.7	0.35
	c		0.56	0.47	775±50	16.4±5.5	0.6	4.2	
HD 50255	a	9	0.71	0.56	498±17	30.8±3.5	1.6	1.0	0.26
	b		0.94	0.71	846±26	7.4±1.5	0.2	0.9	

Table 8 (continued)

Name	SB	N	B-V	V-R	W_{core}	$\langle \mathcal{F}(\text{H}\alpha) \rangle$	rms	$\delta \mathcal{F}(\text{H}\alpha)$	$R(\text{Fe I})$
			(mag)		(mÅ)	($\times 10^5$ erg cm $^{-2}$ s $^{-1}$)			(-)
HD 61994	<i>a</i>	12	0.69	0.55	474±9	30.0±3.0	1.4	0.6	0.27
	<i>b</i>		1.04	0.90	823±23	5.7±1.1	0.1	0.6	
HD 73512	<i>a</i>	12	0.88	0.71	582±20	22.9±2.6	1.4	0.8	0.57
	<i>b</i>		1.13	0.97	805±22	9.5±1.2	0.1	0.5	
HD 82286	<i>a</i>	33	1.03	0.75	1197±73	29.3±4.3	2.1	2.0	0.58
	<i>b</i>		1.03	0.76	1114±66	15.1±3.0	1.0	1.8	
HD 93915	<i>a</i>	31	0.73	0.57	565±45	33.1±5.3	2.1	2.7	0.89
	<i>b</i>		0.80	0.63	801±36	34.5±4.5	2.5	1.8	
HD 95559	<i>a</i>	66	0.89	0.72	928±30	32.0±3.7	1.9	1.2	1.09
	<i>b</i>		0.90	0.73	886±21	32.2±3.4	1.8	0.8	
HD 105575	<i>a</i>	21	0.68	0.55	775±39	41.2±5.8	1.5	2.6	...
HD 106855	<i>a</i>	35	1.05	0.91	1198±64	28.2±3.9	0.3	1.6	0.34
	<i>b</i>		0.95	0.79	1061±23	12.1±1.7	0.4	0.8	
HD 109011	<i>a</i>	23	0.92	0.75	581±17	20.7±2.3	1.0	0.6	0.34
	<i>b</i>		0.98	0.74	926±24	9.7±1.5	0.3	0.8	
HD 111487	<i>a</i>	34	0.74	0.58	799±23	37.8±4.3	2.2	1.3	0.60
	<i>b</i>		1.08	0.93	1005±15	13.2±1.4	0.1	0.4	
HD 112859	<i>a</i>	21	1.04	0.76	684±34	17.0±2.3	1.1	0.9	0.43
	<i>b</i>		0.52	0.44	825±36	32.4±5.8	1.2	3.3	
HD 127068	<i>a</i>	18	1.00	0.74	930±25	26.5±2.8	1.5	0.8	0.12
	<i>b</i>		0.71	0.57	996±66	7.1±4.5	0.2	4.0	
HIP 77210	<i>a</i>	58	0.85	0.68	613±19	26.1±2.9	1.7	0.8	0.33
	<i>b</i>		1.07	0.92	876±13	6.9±0.9	0.1	0.3	
HD 142680	<i>a</i>	24	0.99	0.83	546±11	16.4±1.7	0.4	0.4	0.31
	<i>b</i>		1.18	1.02	883±14	4.9±0.7	0.1	0.3	
HD 143937	<i>a</i>	47	0.87	0.69	937±38	30.6±4.0	2.0	1.6	0.79
	<i>b</i>		1.06	0.92	1016±29	16.7±2.1	0.2	0.8	
HD 197913	<i>a</i>	52	0.73	0.57	543±14	31.8±3.4	2.0	0.9	0.86
	<i>b</i>		0.79	0.62	830±20	35.2±3.8	2.7	1.0	
HD 199967	<i>a</i>	70	0.62	0.52	531±23	39.0±4.8	0.2	1.8	0.57
	<i>b</i>		0.62	0.53	804±19	33.3±4.1	0.2	1.4	
HD 226099	<i>a</i>	94	0.85	0.67	595±19	25.4±2.8	2.0	0.8	0.65
	<i>b</i>		1.15	0.99	759±23	9.4±1.2	0.2	0.5	
HD 237944	<i>a</i>	14	0.69	0.55	721±29	44.8±5.4	2.1	1.9	1.07
	<i>b</i>		0.71	0.56	747±26	47.7±5.3	2.8	1.6	0.61
	<i>c</i>		0.98	0.82	870±26	16.2±2.1	0.4	0.9	

shows a clear time-dependent variability (Fig. 8) but no period. The residual radial velocities indicate a period of 22.35 d, which we believe is an alias of the 69-d period. A weak lithium line at 6707.8 Å is seen (a representative plot is shown in Fig. 7).

HD 66553. There are some secondary-star velocities detected from our cross-correlation functions but close-up inspection of the spectra did not unambiguously show spectral lines from it. Therefore, we refrained from giving an SB2 orbit. This system shows the most eccentric orbit in our sample ($e=0.8719\pm 0.0028$) at a period of 75.8996 d. Latham et al. (2002) discovered the radial-velocity variations and determined an SB1 orbit. “The ninth catalogue of spectroscopic binary orbits” (Pourbaix et al. 2004) lists another independent SB-1 orbit from Imbert (2006), in agreement with the Latham et al. orbit. The expected pseudo-synchronization period would be ≈ 3.4 d, i.e. just $\approx 4\%$ of

the orbital period. No signs of periodic velocity residuals or H α -flux variations are evident. Thus, the rotation period of the star still remains to be determined. Our spectrum synthesis gives $T_{\text{eff}}=5275\pm 41$ K, $\log g=4.33\pm 0.04$, and a higher than usual metallicity of $+0.09\pm 0.02$.

HD 73512. A SB2 orbit with a period of 128.241 d and $e=0.26240\pm 0.00045$ is given. The mass ratio is 0.88 while the component’s line-depth ratio is 2.2 with both stars having the same $v \sin i$ of ≈ 5 km s $^{-1}$. The expected pseudo-synchronized rotation period is ≈ 90 d. The star appears constant in our photometry.

HD 76799. The star shows radial-velocity variations with an amplitude of 0.23 km s $^{-1}$, peak to valley, with an uncertainty of ± 0.04 km s $^{-1}$ if phased with the most-likely period of 50.13 ± 0.15 d from a Lomb-Scargle analysis. A periodogram from four years of H α line fluxes shows two peaks with periods of ≈ 64 d and 55 d. Although not

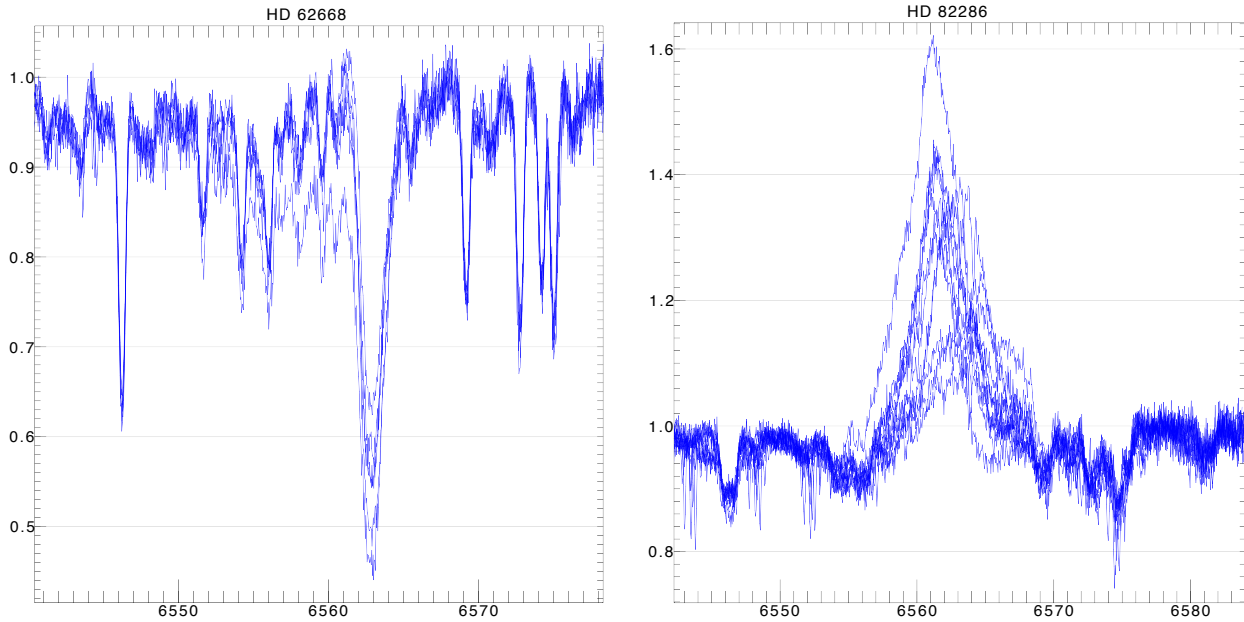


Fig. 8 $H\alpha$ profile variations of, left, HD 62668 (SB1) in 2007 and, right, HD 82286 (SB2) in 2010. Spectra are corrected for orbital radial velocity. Note that the spectral lines from the secondary star in HD 82286 appear as apparently increased scatter around the primary-star lines while the sharp lines are actually water-vapor lines.

quite in agreement with the photospheric radial-velocity period, they are in the same range. We interpret both variations to be due to stellar rotation. The star is otherwise a single star. Our spectrum synthesis gave $T_{\text{eff}}=4915\pm 24$ K, $\log g=3.26\pm 0.07$, and a significantly sub-solar metallicity of -0.12 ± 0.03 . The $v \sin i$ of 7.8 ± 0.3 km s $^{-1}$ suggests a minimum radius of $7.7 R_{\odot}$, in agreement with the low gravity and the small parallax.

HIP 46634 = BD+11 2052 B. This star is the B component of the visual binary ADS 7406, about $14''$ away from the brighter A component. Gálvez et al. (2005) found it to exhibit a constant radial velocity of $+27.07\pm 0.04$ km s $^{-1}$ within their time of observation in 2004. The A component is HD 82159 and was identified in our KPNO H&K survey as an active single-lined spectroscopic binary. Our current STELLA/SES spectra show the B component to have a constant radial velocity of $+27.927\pm 0.047$ km s $^{-1}$. It is apparently single. There are two equally strong peaks of 372 d and 185 d in the radial velocities with an amplitude of 0.2 km s $^{-1}$. The $H\alpha$ -line fluxes show peaks at 120 d and 298 d indicating some long-term variations. None of the periods is conclusive though and the true rotation period remains to be determined.

HD 82159 = GS Leo = BD+11 2052 A. This is the bright component of the double star ADS 7406, denoted component A. Its orbital elements with a period of 4.8122 days and $e=0.176$ were given by Gálvez et al. (2005, 2006) from data taken within nine nights in March/April 2004. Griffin & Filiz Ak (2010) had revised this orbit from 30 new Cambridge CORAVEL measurements from 2008/09. Our SB1 orbit is computed from 107 STELLA measures spread over four years with a period of 3.855871 ± 0.0000066 d and an

eccentricity of 0.2640 ± 0.0012 and supersedes yet the Griffin orbit. The velocity residuals are systematic and indicate a period of 3.50 d, significantly longer than our photometric period of 3.054 d. Note that our photometry is polluted by the B component HIP46634 which, however, should not affect the period determination. The $H\alpha$ -core emission fluxes indicate, besides an annual trend that must be removed, a residual period of 2.97 d, in good agreement with the photometric period. Therefore, we feel confident to interpret the photometric period to be the rotation period of the primary star. Its expected pseudo-synchronization period is ≈ 2.7 d. Obviously, the system did not reach equilibrium yet and the primary is still rotating asynchronously.

HD 82286 = FF UMa. A double-lined binary with a short 3.275-d orbit and a very precise mass ratio of 0.4632 ± 0.0002 is given. Both component's spectral lines are rotationally broadened to nearly the same value (38 km s $^{-1}$)³ and appear variably asymmetric, most likely due to cool surface spots. Our photometry shows an amplitude of 0.16 mag with a clear and precise period of 3.27629 ± 0.00003 d. We attribute it to the brighter primary component (line ratio of 2.9). The spots are the largest contributor to the radial velocity error budget in our orbital solution, in particular for the secondary component. Residual periods of 1.945 d and 8.714 d are evident from its radial velocity. Given the 9.6-mas parallax and the 7.8-mag system brightness, we expect two subgiant stars, already noted by Henry et al. (1995) and in our paper I, while Gálvez et al. (2007) favored the odd K0V+K1IV classification with the

³ In paper I we measured $v \sin i$ for the two components of 35 and 29 km s $^{-1}$, respectively, but Gálvez et al. (2007) quoted us with values of 17 and 16 km s $^{-1}$ which we do not know where they came from.

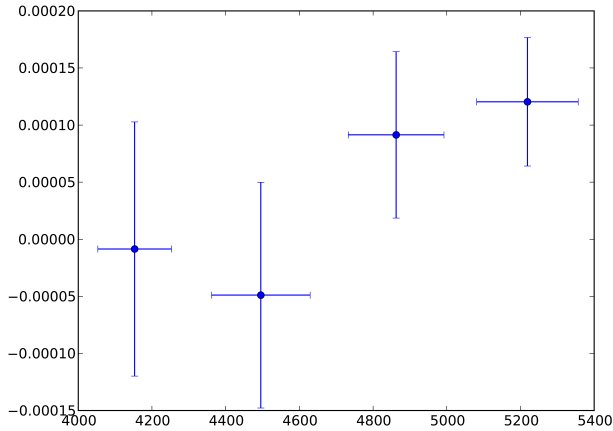


Fig. 9 Seasonal orbital periods for HD 82286 (FF UMa). Shown is the period difference in days versus truncated Julian date for four independent orbital solutions with respect to the period that is obtained from the full data set (i.e. 3.2751924 d; see Table 5).

less-massive component to be the evolved star. Two subgiants are more likely and would favor the 1.945-d period to be the true rotation period of the secondary (suggesting a minimum radius of $1.45 R_{\odot}$). The $H\alpha$ line appears in emission and with a strongly variable profile (Fig. 8).

Gálvez et al. (2007) claimed to have detected an orbital-period variation on the order of $dP/P = 5 \cdot 10^{-4}$, but Griffin (2012) could not confirm this variation from a reanalysis of the same data. Due to this situation our STELLA data received a special treatment of the systematic errors. We followed the procedure outlined by Weber & Strassmeier (2011) for Capella. Briefly, we compute synthetic spectra for both components and combine them according to their real brightness ratio and then extract a radial velocity with the same 2d-cross correlation as for the real data. This enables the removal of the systematic blending effects and converges on rms residuals smaller than the precision of a single data point. With this, our four consecutive years of observations do vaguely hint towards such an orbital-period variation but unfortunately remain still inconclusive (Fig. 9). We computed orbits for all four observing seasons separately as well as for the entire data set and derived upper and lower limits for dP/dt between $2.76 \cdot 10^{-7}$ and $0.2 \cdot 10^{-7}$. In case we take an equal-weight approach for the four solutions the most likely value for dP/P would be $5.5 \cdot 10^{-5}$, with an upper limit of $1.2 \cdot 10^{-4}$ and a lower limit of $8.5 \cdot 10^{-6}$, i.e. close to zero; altogether not quite consistent with above claim by Gálvez et al. (2007). Fig. 9 shows the orbital periods of the four STELLA observing seasons over time.

HD 82841 = OS Hya. Our photometry shows a period of 51.54 ± 0.02 d while the SB1 orbital solution gives a period of 56.7316 d with a slightly eccentric orbit with $e=0.087$. The pseudo-synchronous rotation period would be expected to be near 53.9 d. As the photometric period is even shorter than this, the star is likely an asynchronous rotator. Our

$v \sin i$ measure of 8 km s^{-1} converts to a minimum radius of $8.1 R_{\odot}$ and, together with the temperature and gravity from our spectrum synthesis, suggests a K2 giant. We note that the metallicity of -0.30 ± 0.03 is significantly subsolar.

HIP 50072 = EQ Leo. We give an SB1 orbit with a formally but marginally significant eccentricity of 0.014 ± 0.0043 and a period of 34.3157 d. An $e=0$ solution has an rms of the residuals worse by $\approx 10\%$. The $H\alpha$ -line profile appears as an asymmetric and variable absorption line, indicating chromospheric activity. The $H\alpha$ -core flux shows a period of 34.8 d, very close to the orbital period while the photometry gives a 33.36 d as the best-fit period. The latter is better defined and we interpret it to be closest to the true rotation period of the star. The system is then in or close to dynamical equilibrium.

HD 93915. Our SB2 orbit from STELLA data is in good agreement with the Cambridge orbit from Griffin (2009). As our baseline is more than five times longer and better sampled, our orbit clearly supersedes the Cambridge orbit. The orbital period is near 223 d and $e=0.3795 \pm 0.0009$. The expected pseudo-synchronization period is ≈ 111 d but our photometry does not show any type of periodic behavior despite of having a dispersion of up to $0^m.2$ mag in V over 138 days.

HD 95188 = XZ LMi. We judge this star to be single. The radial velocities possibly show small-amplitude variations of $\pm 0.1 \text{ km s}^{-1}$ but no clear period while the $H\alpha$ -core flux indicates a period of 190 d, most-likely spurious. Our photometry revealed an uncertain period of 7.00 ± 0.06 d but with a small amplitude of just 0.025 mag in V , that we nevertheless interpret to be the rotation period.

HD 95559 = GZ Leo. The star was found to be a double-lined spectroscopic binary by Jeffries et al. (1994) who also predicted its photometric variability. The orbit was later refined and the photometric variability discovered by Fekel & Henry (2000). Our new circular orbit is very well determined despite the rotationally broadened line profiles of $v \sin i$ of 33 km s^{-1} for both components. In our original survey paper (paper I), we noted that the star may be triple-lined based on a single coudé spectrum. We find no evidence for a third component in our new echelle spectra. However, the secondary's residual radial velocities of 0.165 km s^{-1} indicate a period of 0.592 d that appears to be an alias of the 1.517-d period obtained from our photometry. The true rotation period is likely 1.517 d as it also agrees with the orbital period of 1.526 d. Obviously, the system is well synchronized.

HD 95724 = YY LMi. Its light variability was discovered in our paper I and accordingly named YY LMi by Kazarovets et al. (2006). The star has a constant radial velocity from 76 STELLA measurements and is likely single. Our APT photometry shows a period of 11.49 d and confirms that YY LMi is a spotted and active star.

HD 104067. Single star with no obvious periodicity down to the detection limit of $\approx 100 \text{ m s}^{-1}$ for the given $v \sin i$ of 8 km s^{-1} . However, there are two equally signifi-

cant peaks in the periodogram from the $H\alpha$ flux of 34 d and 102 d, one the alias of the other. We had no photometry for this target.

HD 105575 = QY Hya. Szalai et al. (2007) presented a photometric and spectroscopic study of this 0.29-d eclipsing binary and derived a complete system's solution from *BV* light curves and radial velocities. These authors also announced the discovery of a tertiary component in the cross correlation function and listed absolute parameters appropriate for a (K5/M1)/G4 system. We dare to note that they (and the referee) had missed our paper I in A&A from 2000 where we gave radial velocities of the binary plus the tertiary and determined $H\alpha$ emission-line fluxes for all three components. We then noted that the primary had moderately strong and sharp Ca II H& K emission and showed that the resonance lines appeared to be asymmetric due to the resonance lines of a third component. The Ca II emission lines even appeared with sharp and red shifted interstellar absorption. Because our new STELLA data sample only one fourth of the tertiary orbit, we added our earlier paper-I KPNO coudé-feed spectra, two HARPS and one FEROS velocity from the ESO archive. With these, we extend the time coverage to 4489 d and obtain an orbital period for the tertiary around the eclipsing pair of 4550 ± 52 d and give a preliminary orbit with $e=0.391\pm 0.006$ for it. Our close-pair orbit is SB2 and circular with a period of 0.2923378 d. Its mass ratio is 0.457. The secondary's K amplitude is 158 km s^{-1} and both stars have a $v \sin i$ of around 40 km s^{-1} ; and accordingly large are the orbital residuals. The disagreement with the elements given by Szalai et al. (2007) possibly comes from the different ways the cross correlation is determined. Our photometric orbital period is 0.292386 d and agrees with the orbital period within its uncertainties. The eclipse depth is 0.36 mag in *V*. No rotational modulation is detected from the radial velocities.

HD 106855 = UV Crv. The catalogue of composites of double and multiple stars (Dommanget & Nys 1994) identifies HD 106855 as the double star Don 520 = CCDMJ12174-2104AB. The B component is just $1.3''$ away from the A component at a position angle of 38° (both values measured in 1959 by Donner) and appears approximately 1.7 mag fainter in *V* than the A component. Worley (1972) gave a more recent measurement of $1.64''$ and 31.6° in 1972.1. The Hipparcos/Tycho photometry lists $V_T=9.76\pm 0.03$ and $(B - V)_T=0.95$ for the A component (Fabricius & Makarov 2000). The fiber-core diameter of our STELLA/SES projected on the sky is $3.0''$ centered on the brighter A component. Therefore, the B-component is just at the rim of the field of view and could have been within the diaphragm from time to time. Our cross-correlation function shows a broad, sometimes doubled, main peak and a third narrow peak which is sometimes stronger than the main peak.

The orbital period from the main peak, i.e. presumably from the Aa component, is 0.67 d with strong aliasing at ≈ 2 d. There are 11 phases where the main peak is split into

two peaks and possibly represent detections of the Ab component (plotted in Fig. 3). However, these velocities have unreasonable high scatter (9.9 km s^{-1}) and a comparably small *K*-amplitude (37.7 km s^{-1}). Possibly, the Ab component is part of another spectroscopic binary. Its velocities alone would suggest a 0.2-d period. A tentative 0.85-d period is found from the third, narrow peak of the cross correlation function but we can not claim it conclusively. However, it clearly appears sometimes on the one or the other side of the main peak, but not always. One possibility is that the visual B component is only sometimes within the STELLA fiber aperture *and* is itself a spectroscopic binary. It would make HD 106855 a quadruple system.

HD 108564. Single star with a high average radial velocity of $+111.363\pm 0.009\text{ km s}^{-1}$. A periodogram of the radial velocities hint at a period of 9.58 d with a small amplitude of 0.1 km s^{-1} while the $H\alpha$ flux favors a (formally even more uncertain) period of 3.63 d. The $v \sin i$ of 14.8 km s^{-1} would convert to a minimum radius of $\approx 1 R_\odot$ if 3.63 d is interpreted as the rotation period. The 9.58-d period would result in a minimum radius in disagreement with the Hipparcos distance of 28 pc. Our spectrum synthesis clearly indicates a late K dwarf with $T_{\text{eff}}=4560\pm 24\text{ K}$, $\log g=4.40\pm 0.06$ and a significant sub-solar metallicity of -0.90 ± 0.03 which implies a radius of $\approx 0.7 R_\odot$.

HD 109011 = NO UMa. Griffin (2010) noted for this star "Slow changes in velocities, SB2". We verify the system to be a SB2 and find an orbital period of 1274.7 ± 0.9 d. Our photometry indicates variations with a period of 8.4 ± 0.2 d and an amplitude of 0.02 mag in *V*, which we interpret to be due to rotational modulation of the primary component. This period is similar but not completely in agreement with the values of 8.56 and 9.19 d found by Gaidos et al. (2000). But in any case, the system contains at least one very asynchronously rotating component because the expected pseudo-synchronization period would be ≈ 440 d ($e=0.507$). The orbital solution shows radial-velocity residuals of 0.17 and 0.46 km s^{-1} , respectively, which are larger than expected for the $v \sin i$ given. A Lomb-Scargle periodogram of these residual velocities indicate periods of 639 d for the primary and 246 d for the secondary, the former roughly half the orbital period. The large Hipparcos parallax and a $V=8.1$ mag system brightness suggests two dwarfs rather than giants. If interpreted due to rotation, the periods of ≈ 639 and 246 d would indicate minimal radii appropriate for supergiants, totally impossible for a distance of 23.7 pc. If these periods are real at all, they are possibly connected with surface activity, e.g. due to a spot cycle or active longitudes. The adopted rotation period of 8.4 d and the $v \sin i$ of 5 km s^{-1} for the primary suggests a minimum radius of $0.83 R_\odot$.

HD 111487 = IM Vir. An SB2 orbit with a period of 1.3086147 d is given. Our photometry confirms the eclipsing nature of the system with a period of 1.3085900 ± 0.000007 d and an eclipse depth of 0.76 mag in *V*. A rms of the residual velocities of the primary

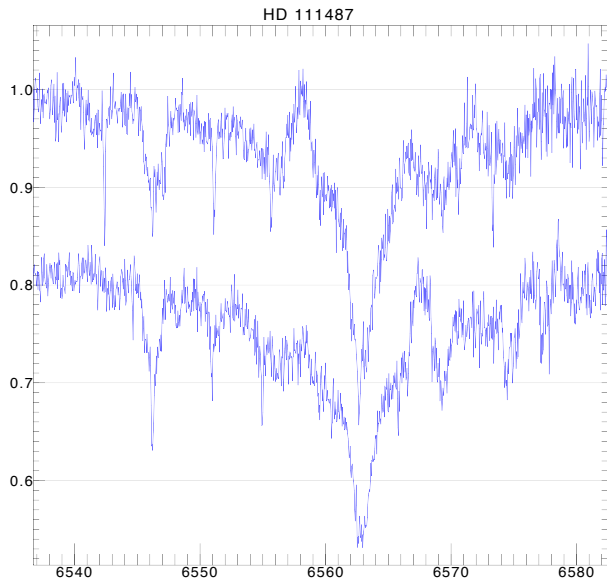


Fig. 10 $H\alpha$ line profile of HD 111487 at two orbital phases 180° apart. Its secondary component is detectable only in $H\alpha$ where it is seen as an emission line (appearing bluewards of the primary's absorption line in the top spectrum, and redwards in the lower spectrum).

of 0.268 km s^{-1} is appropriate for rotationally broadened spectra of $v \sin i = 42 \text{ km s}^{-1}$ but the residuals for the secondary-star velocities are anomalously high (1.8 km s^{-1} ; $v \sin i = 28 \text{ km s}^{-1}$), indicating an asymmetrically spotted star. However, residual periods of 3.45 d or 1.41 d (one the alias of the other) are seen for the primary but none for the secondary. Their amplitude is $\approx 0.6 \text{ km s}^{-1}$. The secondary shows strong $H\alpha$ emission while the primary appears with $H\alpha$ in absorption (see Fig. 10). The photometry reveals a period of 1.309 d from data outside of eclipse and have a full amplitude of 0.15 mag in V that we interpret to be from rotational modulation synchronized to the orbital motion.

HD 112099. A single-lined eccentric orbit with a period of 23.50447 ± 0.00013 d and an rms of 67 m s^{-1} is obtained. The expected pseudo-synchronization period is ≈ 9.6 d ($e=0.447$). A residual period of 4.6 d is seen in a Lomb-Scargle periodogram but is not conclusive. Together with our $v \sin i$ measure of 4.2 km s^{-1} , it would indicate a minimum radius of $0.38 R_\odot$, at least in principle agreement with the Hipparcos parallax. Our spectrum synthesis confines this to a K1V classification, in agreement with its $B - V$ color.

HIP 63322 = BD+39 2587 B. B component of a visual pair with HD 112733 (HIP63317) as the primary. The spectrum appears at almost all wavelengths single lined but shows doubled Ca II H&K lines (Strassmeier et al. 2000). Gálvez et al. (2006) presented an SB2 orbit from data taken during nine nights in March/April 2004. They found an eccentricity of 0.3 and noted that the spectrum is best fit with a G8V primary and an M0V secondary star. An SB1 orbit with zero eccentricity and $P=4.593843$ d is derived from

STELLA data. Our spectra show the secondary with $H\alpha$ in emission and the primary with $H\alpha$ in absorption, similar to HD 111487. The $H\alpha$ -line flux of the primary shows a clear periodicity of 2.30 d, exactly half the orbital period within the uncertainties, which is simply due to the fact that the secondary-star emission is sweeping through the primary-star line. The photometry reveals a period of 2.227 ± 0.003 d, assumed to be from a double-humped light curve, and we adopt twice its value to be the true rotation period of the star.

HD 112859 = BQ CVn. Just recently, Griffin (2009) obtained an orbit very similar to ours and we refer the reader to his discussion on the various stellar properties. Our orbit was determined from 93 velocities for the primary and 87 for the secondary over a time range of 1249 d and achieved rms residuals of 0.30 km s^{-1} and 0.26 km s^{-1} for the primary and secondary, respectively. Our photometry indicates a rotational period that is synchronized to the orbital revolution.

HIP 63442 = CD CVn. A single-lined orbit with $P=38.7156$ d and $e=0$ is given. We see many detections of a second line system in the cross-correlation functions but with such a large scatter (9.9 km s^{-1}) and small amplitude (0.5 km s^{-1}) that we can not be sure of its reality. Its marginally significant period is in agreement with the orbital period of the primary but in phase with all its measurements. It resembles HD 16884, possibly being a pair of SB1 binaries in a bound orbit. The residuals from the primary orbit have an rms of 0.27 km s^{-1} and show a periodicity of 19.14 d, nearly exactly half the orbital period. The $H\alpha$ -core flux varies with a period of 39.2 d and our photometry gives a period of 40.3 d, which we interpret to be the true rotational period of the star. Thus, CD CVn is rotating not quite but close to synchronous.

HD 127068 = HK Boo. We present a new SB2 orbit with a period of 15.15011 ± 0.00011 from 98 velocities for the primary and 99 for the secondary spanning a time range of 1257 days. The residual rms is 0.19 km s^{-1} for the primary and 0.36 km s^{-1} for the secondary. There are periods in the residuals of both stars of 18.6 d and 24.3 d for the primary and secondary, respectively. The primary's value is in agreement with our photometric period of 18.187 d in this paper and suggests that it is likely the rotational period of the star. The secondary's period is maybe spurious as its amplitude is also very low, 0.3 km s^{-1} . From photometry in paper I we found 17.62 d. In any case, this would make the HK Boo primary an asynchronously rotating star. Griffin (2009) gives a discussion of the star's properties and cited a photometric period from Hipparcos data of 6.953 d that we can not verify.

HD 136655. In paper I, we had given two velocities of -29.9 ± 4.1 and $+17.9 \pm 1.7 \text{ km s}^{-1}$ from a single blue-wavelength spectrum for two components. The latter must have been an erroneous measurement because it is not verified in the present paper. Table 3 lists an average STELLA velocity of $-31.921 \pm 0.035 \text{ km s}^{-1}$ from 122 spectra. Its

Ca II H& K emission appears very weak, if detectable at all. Our photometry shows the star to be constant.

HD 138157 = OX Ser. Our SB1 orbit suggests a very small eccentricity of 0.0051 ± 0.0009 from a total of 148 velocities. The rms of the residuals is 0.22 km s^{-1} , an excellent value for the large line broadening of $v \sin i = 40 \text{ km s}^{-1}$, and somewhat better than if a circular orbit is enforced (rms of 0.25 km s^{-1}). A periodogram from the H α -line fluxes gives the strongest peak at a period of 14.38 d, very close to the orbital period. Our photometry shows clear variations but suggests a period of 7.18 d, pretty much half the period of the orbital revolution. Its phase stability indicates that the amplitude is dominated by the ellipticity effect but annual variations indicate that part of it is due to spots. We conclude that the rotation period of the star is very near the orbital period and thus synchronized with the orbital motion.

HIP 77210 = V381 Ser. The star's alternative name is G16-9. An initial SB2 orbit with a period of 9.94319 d was determined by Goldberg et al. (2002). Our SB2 orbit is among our most precise with an rms of the residuals of the primary of 52 m s^{-1} from 96 velocities (but four times larger rms for the secondary). Our photometry shows variations with a period of 13.7 ± 0.1 d that we interpret to be the rotation period of the primary, thus, significantly asynchronous with respect to the orbital period. The secondary's velocity residuals show a systematic rms with a period of 4.79 d, a little less than half the orbital period. The orbital eccentricity of 0.06032 ± 0.00024 suggests a formal pseudo-synchronization period of ≈ 9.7 d, which is close to twice the secondary's residual period. We conclude that 9.58 d is likely the true rotation period of the secondary and thus synchronized to the orbital revolution.

HD 142680 = V383 Ser. The photometric period from data in 1999 in paper I was 33.52 d. Our new photometry principally verifies this period and gives 33.4 ± 1.5 d. The orbital eccentricity is 0.3158 from our new STELLA SB2 orbit and is in agreement with the eccentricity of 0.3139 from Griffin's (2009) SB1 orbit. The pseudo-synchronous rotation period would be around 15.3 d, which is suspiciously close to 1/2 of the photometric period. However, the photometric period can not be halved if it is due to spots rotating in and out of view and we conclude that the system is rotating super synchronously. The systemic velocity is relatively high with -83.83 km s^{-1} , making this system a high-velocity binary.

HD 143937 = V1044 Sco. This is the A component of the visual binary GJ 9539. The B component is $10.3''$ away and approximately 2.7 mag fainter than component A in the Hipparcos bandpass. It is therefore included in our photometry with a $30''$ diaphragm but well separated for the STELLA spectroscopy. Cutispoto et al. (1999) found the A component to be an SB2 binary (it is listed as an eclipsing binary in Malkov et al. 2006 based on a note in Cutispoto et al. 1999). We verify its eclipsing nature and find an orbital period from photometry of 0.91479 ± 0.00003 d, in excellent agreement with the radial-velocity orbit of 0.91483076 d.

The eclipse depth is 0.41 mag in *V* while the spot wave shows an amplitude of 0.10 mag. The rms of our orbital residuals for both stars are comparably high, 0.28 km s^{-1} and 1.26 km s^{-1} , but appropriate for the $v \sin i$ of 55 and 45 km s^{-1} for primary and secondary, respectively. Large residuals are related to the short orbital period of 0.9 d and the corresponding degree of line blending.

HD 147866 = V894 Her. We present an SB1 orbit with a period of 114.050 d and an eccentricity of 0.5141. The *K* amplitude is just 6.71 km s^{-1} and the mass function accordingly small. Our photometry reveals a likely rotation period of 80.3 ± 2.2 d, while pseudo synchronization would be expected at a period of ≈ 40 d. It appears that the system had not had enough time yet to obtain orbital and rotational equilibrium. With our $v \sin i$ measure of $5 \pm 1 \text{ km s}^{-1}$ the minimum radius is $7.93 R_{\odot}$. The Hipparcos parallax places the star at a distance of 193 pc which implies an absolute magnitude of +1.67 mag (for *V*=8.1 mag). Our spectrum synthesis gave $T_{\text{eff}} = 4580 \text{ K}$ and $\log g = 2.7$ with a significant sub-solar metallicity of -0.24 ± 0.02 . The star is most likely a K1III giant.

HD 150202 = GI Dra. We confirm Griffin's (2009) orbital period with a value of 68.47160 ± 0.00097 d. The STELLA orbit's rms of the residuals is just 83 m s^{-1} from 179 velocities over 1112 d. Our spectrum synthesis yielded $T_{\text{eff}} = 5010 \pm 25 \text{ K}$ and a $\log g = 3.06 \pm 0.07$, suggesting more a G8III star than a K0III as put forward by Griffin (2009). The periodogram from our photometry shows the strongest peak at a period of 36.4 ± 0.5 d. This is likely just one-half of the true rotation period (72.8 d) and is then in rough agreement with the period of 76.70 d from Hipparcos photometry. Thus, the star is an asynchronous rotator with $P_{\text{rot}} > P_{\text{orb}}$.

HD 153525 = V1089 Her. From 196 STELLA spectra we obtain a mean radial velocity of $-6.844 \pm 0.039 \text{ km s}^{-1}$. The star is single but at least moderately active judging from its Ca II H&K emission-line strength (c/o paper I). The new photometry shows variations with a period of 15.4 ± 0.1 d that we tentatively interpret to be the rotational period. A distance of just 17.5 pc and our values for $T_{\text{eff}} = 4775 \pm 23 \text{ K}$ and $\log g = 4.47 \pm 0.05$ suggest a K dwarf with a $v \sin i < 3 \text{ km s}^{-1}$, in agreement with our upper limit of 3 km s^{-1} .

HD 153751 = ϵ UMi. The system is a single lined spectroscopic binary and has an orbit determination dating back now 60 yrs (Climenthaga et al. 1951). This is certainly because of the high declination of $+82^{\circ}$ despite that Climenthaga et al. already noted the Ca II H&K emission and thus put the system out for further observation. Its eclipsing nature was discovered by Paul Guthnick in 1946 and later verified by Hinderer (1957) who concluded on a pair of gG1 and dA8-dF0 stars for the primary and secondary, respectively. Today's accepted classification is G5III for the primary (e.g. Keenan & York 1988). Our spectrum synthesis gives $T_{\text{eff}} = 5215 \pm 47 \text{ K}$, $\log g = 3.21 \pm 0.08$ and a metallicity of -0.25 ± 0.04 , i.e. significantly subsolar but altogether in agreement with a G5III classification. Our new SB1 orbit

has a period of 39.48042 ± 0.00012 d and zero eccentricity. Its rms of 121 m s^{-1} from 220 velocities spanning 2144 days is mostly due to the moderately large rotational velocity of 25.6 km s^{-1} and only less from the jitter from starspots because no convincing rotation period is found from the residuals.

HD 155802. In paper I, we had given velocities of -33.5 ± 1.2 and $-33.3 \pm 0.5 \text{ km s}^{-1}$ from a blue-wavelength and a red-wavelength spectrum, respectively, and $+24.7 \pm 2.0 \text{ km s}^{-1}$ for another component from the one blue-wavelength spectrum. The latter must have been an erroneous measurement because it is not seen in the spectra in the present paper. The average velocity from 114 STELLA spectra is $-32.711 \pm 0.033 \text{ km s}^{-1}$. Its rms is practically the precision of the STELLA/SES system and thus the star is constant down to our detection limit of $\approx 30 \text{ m s}^{-1}$. However, its chromospheric activity is verified by the presence of weak Ca II H&K emission lines.

HD 184591. The star is single according to our 155 STELLA velocities. Its mean is $-37.635 \pm 0.044 \text{ km s}^{-1}$. The photometry indicates just a weakly determined period of $P=48.9 \pm 2.2$ d with an amplitude of below 0.01 mag in y . Our spectrum synthesis resulted in $T_{\text{eff}}=4800 \pm 40$ K, $\log g=2.82 \pm 0.07$ and a metallicity of -0.18 ± 0.03 . If the 48.9-d period is real and the true rotational period of the star, the $v \sin i$ of $4.7 \pm 0.8 \text{ km s}^{-1}$ confines the radius to be at least $4.5 R_{\odot}$, in principal agreement with above gravity and the Hipparcos parallax.

HD 190642 = V4429 Sgr. Strohmeier (1967) discovered this star on his Bamberg plates to be variable with an amplitude of 0.25 mag. No other information was given. But based on the Hipparcos satellite data, Kazarovets et al. (2006) assigned a variable star designation. We find the star to be an eclipsing system and detect a photometric period of 24.8339 ± 0.0009 d after excluding the eclipse points which, if doubled, is very close to the orbital period from radial velocities (49.5969 ± 0.0012 d, $e=0.0126 \pm 0.0011$). The eclipse depth is 0.43 mag. The rms (0.445 km s^{-1}) of the velocity residuals is larger than expected for $v \sin i=19.6 \text{ km s}^{-1}$ and a periodogram analysis shows a convincing residual periodicity of 24.72 ± 0.02 d with an amplitude of 1.2 km s^{-1} . The $H\alpha$ -core flux shows also a significant period at 24.9 d. All of these periods must be doubled to obtain the true rotation period and then suggest that the primary's rotation is synchronized to the orbital motion, or at least nearly so. Our spectrum synthesis gives values of $T_{\text{eff}}=4760 \pm 63$ K and $\log g=2.96 \pm 0.11$ with a significant sub-solar metallicity of -0.47 ± 0.05 . The Hipparcos parallax suggests an absolute system magnitude of $+1.34$ mag ($V=8.08$ mag, distance of 223 pc, no extinction). Altogether these values are compatible with a K1III-IV giant. Knowing $i \approx 90^\circ$ gives directly a radius of $19.6 R_{\odot}$ and a rotation period of ≈ 50 d, in good agreement with our various observations. Assuming a mass of two solar masses for the primary, the mass function of 0.330 demands a sec-

ondary mass of $1.22 M_{\odot}$; it suggests a late F main-sequence star, maybe F6-8.

HD 197913 = OR Del. This is the A component of the visual binary ADS 14270. Griffin (2005) gave an overview of its observational history and presented a full SB2 orbit in very good agreement with our present determination. Our rms residuals are very low though, 100 m s^{-1} for the primary and 161 m s^{-1} for the secondary. In paper I, we presented double-lined Li spectra for the A component and a single-lined spectrum for the B component (erroneously identified with lower-case a and b in that paper; *pace* Griffin). The fainter B component appeared with somewhat stronger Ca II H&K emission as the (blended) A components. The 6.56-d photometric period that we derived from our APT time series from 1999 was assigned to HD 197913, without an A nor a B specification. This was because our APT diaphragm was $30''$ and the AB separation roughly $11''$. Consequently, it prompted Kazarovets et al. (2006) to assign the variable star designation OR Del to the AB system but Simbad resolves it for the A component of which, however, it does not give the HD number. Variability from the B component can not be excluded but it is indeed more likely that the photometric variability stems from the 0.8-mag brighter (combined) A components. Our current photometry has a best-fit period of 6.56 ± 0.07 d. The AB period is suggested by Griffin (2005) to be around "thousand years". Our new STELLA orbit gives a period of 1778.5 ± 1.3 d for the A component from basically a single revolution (time span of data is 1848 d) but still better confined than the published value of 1790 ± 13 d.

HD 199967. We find it to be an SB2 in a 6.100213-day orbit with a very low but significant eccentricity of 0.0024 ± 0.0002 . An $e=0$ solution has an rms of the residuals worse by more than 10 % for each component. No photometric period is detectable but such a short orbital period makes it likely a synchronized system. Our $v \sin i$ measures of 11 and 9 km s^{-1} for the primary and the secondary, respectively, then lead to minimum radii of 1.3 and $1.1 R_{\odot}$. The effective line ratio is 3.2 to 1. The Hipparcos parallax gives a distance of 74 pc and an absolute system magnitude of $+3.67$ mag, basically excluding two main-sequence stars. The system's $B - V$ is 0.58 mag and, with a mass ratio of 0.776, does suggest two early G-type dwarf-subgiants.

HD 202109 = ζ Cyg. The primary is a mild barium star with a white-dwarf companion. Griffin & Keenan (1992) discussed its spectral classification in detail and presented an orbit with a period of 6489 ± 31 d, $e=0.22 \pm 0.03$ and an amplitude of $K=3.31 \pm 0.12 \text{ km s}^{-1}$. More recently, Eaton & Williams (2007) listed a mean velocity of $19.55 \pm 0.25 \text{ km s}^{-1}$ from 74 observations but did not give the individual values. Our own radial velocities show a clear non-linear trend with a full range of 2.8 km s^{-1} during the 3.5 yrs of observation. We present a new orbit from the combined values from CORAVEL, the Cambridge spectrometer, STELLA and the literature cited in Griffin & Keenan (1992) in Fig. 2 and list it in Table 4. It covers a time range of 114.8

years! We shifted the Griffin & Keenan (1992) points by $+0.50 \text{ km s}^{-1}$ to bring them from the IAU to the STELLA system. The STELLA data in the panel are the ones between phase 0.1–0.3 and an average rms of 42 m s^{-1} . The refined period is now $6446 \pm 14 \text{ d}$ and $e=0.244 \pm 0.016$, in fair agreement with the Griffin & Keenan orbit.

HD 218739. Visual component to HD 218738 = KZ And, itself a cataloged RS CVn binary $15.6''$ away. HD 218739 appears with a constant radial velocity of $-5.201 \pm 0.040 \text{ km s}^{-1}$.

HD 226099. Duflo et al. (1995) listed six velocities between $+22$ and $+4 \text{ km s}^{-1}$ which were the first measurements that showed the variable velocity. In our paper I, we gave velocities for both stellar components from a single blue-wavelength spectrum but did not find significant Ca II H&K emission lines. In this paper, we present its first orbit (SB2) with a period of 18.78209 d and an eccentricity of 0.3096 (Fig. 3). The two components are of comparable mass with a ratio of 0.897 . The $v \sin i$ for the primary component is below our resolving limit and estimated to be 2 km s^{-1} , but twice as larger for the cool secondary. The rms residuals for the two components are 85 m s^{-1} and 182 m s^{-1} , possible due to the sharp lines. The orbital eccentricity suggests a formal pseudo-synchronization period of $\approx 11.6 \text{ d}$ but no we have no photometry for this star. However, the radial-velocity residuals of the secondary indicate a well-defined period of $3.131 \pm 0.008 \text{ d}$ with a full amplitude of up to 1.6 km s^{-1} , and no power for periods longer than $\approx 4.5 \text{ d}$. We conclude that the 3.1 days is the rotation period of the secondary and that it rotates significantly asynchronous.

HD 237944. The system has a triple-lined spectrum due to Aab and the visual B component and, according to Otero & Dubovsky (2004), is also an eclipsing system (*ab* components). The two stronger lines from component A make up the *ab* SB2 in our Table 5. The third, visual B or spectral *c* component's average radial velocity is $-12.25 \pm 1.3 \text{ km s}^{-1}$, different by 3.0 km s^{-1} from the systemic velocity of *ab*, in accordance with an expected orbital period of ≈ 2500 years noted by Griffin (2009). Our rotational velocities are from a single (well-exposed) spectrum and gave $v \sin i$ of Aa, Ab, and B of 11 km s^{-1} , 9 km s^{-1} , and 11 km s^{-1} , respectively, with errors of at least $\pm 2 \text{ km s}^{-1}$. Note that the SB2 orbital period is just 5.5 d with a very small but significant eccentricity. Our photometry confirms the eclipses of the *ab* pair (Fig. 4) and also shows a sinusoidal light variation with the orbital period indicating that a spotted star is rotating synchronously with the orbit. Therefore, and assuming $i = 90^\circ$, radii are $1.19 R_\odot$ and $0.98 R_\odot$ and masses are $1.042 M_\odot$ and $1.027 M_\odot$, respectively. For our Li abundances in Table 7, we assume effective temperatures based on Gray's 2005 table B.1 and Griffin's (2009) individual absolute magnitudes.

6 Analysis

6.1 Rotational synchronization

Before we try to derive a rotation-activity relation, we inspect our binary sample in the rotational-period versus orbital-period frame and identify its distribution of synchronicity, or the deviation thereof. Asynchronously rotating binaries, or pseudo-synchronously rotating binaries in eccentric orbits, could experience enhanced activity due to stronger shearing forces in their convective envelopes (Schrijver & Zwaan 1991). This may possibly be coupled with enhanced deep convective mixing as in Hertzsprung-gap giants (e.g. Böhm-Vitense 2004). It may thus be rewarding to visualize the $P_{\text{rot}}-P_{\text{orb}}$ plane.

Fig. 11 shows the distribution of synchronism in our active binary sample. The full sample comprises of the entries in the “Chromospherically Active Binary Star (CABS)” catalog (Strassmeier et al. 1988, 1993, Eker et al. 2008), expanded by the stars from the present paper. Of the approximately 410 CABS binaries only 230 are known with both a rotational period and an orbital period (150 have no rotational, 30 have no orbital period). We note that care must be taken when using CABS-III because, e.g., the photometric periods listed are mixed values of rotational periods and $P_{\text{orb}}/2$ -periods due to the ellipticity effect or are simply orbital periods in case the system is eclipsing. Besides, some of the photometric periods are derived from $v \sin i$ measurements and radius estimates (e.g. for HD 37171 of $P_{\text{rot}}=300 \text{ d}$) and are accordingly uncertain. From Fig. 11 we see that the bulk of active binaries is synchronized and in circular orbits but from the 47 systems that have rotational periods considerably shorter than the orbital period 41 are with $e > 0$ and six with $e=0$ (HD 7205, HD 16884ab, see Figs. 2 and 4; HD 72688 HD 90385, HD 108102, and 93 Leo). These six are definitely sub-synchronous rotators and all have orbital periods less than approximately 100 d . Of the 41 systems with $e > 0$, only seven (HD 54563, HD 118981, and HD 133822=HS Lup if its photometric period is exactly doubled, plus the four systems already listed in Hall 1986) are rotating at or near the expected pseudo-synchronized value according to the criteria of Hut (1981), leaving 34 more asynchronous rotators in the sample. Among these, the two most extreme cases are HD 109011 ($P_{\text{rot}}=8.34 \text{ d}$, $P_{\text{orb}}=1275 \text{ d}$, $e=0.508$) and HD 197913 ($P_{\text{rot}}=6.62 \text{ d}$, $P_{\text{orb}}=1790 \text{ d}$, $e=0.265$), rotating 54 times and 190 times faster than pseudo synchronization, respectively. If real – see the individual note for HD 197913 – these systems either had significant mass transfer in the past or are so young that magnetic braking was not effective yet or they experienced a yet unconsidered spin-up mechanism in the past, e.g. the engulfing of Jupiter-sized planets or brown dwarfs (see e.g. Livio & Soker 2002, Carney et al. 2003). We will come back to this thought later in the section on lithium in active stars (Sect. 6.5).

Stars where the rotational period is longer than the orbital period are in any case asynchronous rotators, indepen-

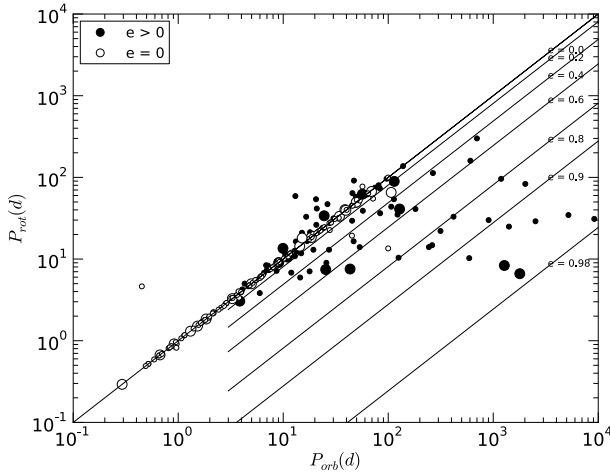


Fig. 11 Rotational period versus orbital period for the binary stars from Table 1 (big dots) and other RS-CVn and BY-Dra binaries from the CABS catalog (small dots). Open symbols indicate circular orbits, a filled symbol indicates an eccentricity larger than zero. The lines depict the (pseudo)-synchronization periods for various values of the orbital eccentricity, e , according to Hut (1981). Our sample mainly consists of synchronized binaries with circular orbits but 26% are asynchronous rotators. See text.

dent of their orbital eccentricity. The early discoveries were summarized in the paper by Hall (1986), e.g. λ And and 39 Cet=AY Cet. Three more systems stick out suspiciously above the 45-degree line in our Fig. 11 though. HD 31738 is a double-lined short-period binary with a recently revised orbital period of just 0.45 d (and $e=0$; Griffin 2009). Its photometric period of 4.55 d was derived from an earlier APT campaign (Strassmeier et al. 1989) which, in the light of the new orbital period, was likely an alias of the true orbital period and needs revision. HD 193216 (a quintuple visual system) is a new entry in CABS-III and its A component a single-lined binary with $P_{\text{orb}}=418.77$ d and $e=0.08$ according to Griffin (2002). In CABS-III it is erroneously listed with the orbital period of 3.62 d of its visual B component, another SB according to Griffin (2002). The rotation period given by Wright et al. (2004) was determined for the brighter A-component indirectly from two measures of its Ca II H&K S -index and an empirical rotation-activity relation, thus, lacks a real observation. The third system is HD 181809 ($P_{\text{rot}}=59.85$ d, $P_{\text{orb}}=13.045$ d, $e=0.04$; Fekel & Henry 2005) and is a well-studied asynchronously rotating K0 giant/subgiant. In total there are 21 rotators with $P_{\text{rot}} > P_{\text{orb}}$ in Fig. 11. The more significant ones are HD 217188 (K0III, $P_{\text{orb}}=47$ d, $e=0.47$), HD 170829 (G8IV, 26 d, 0.18), HD 33363 (K0III, 21 d, 0.07), HD 71071 (K1IV, 16 d, 0.13), and the four stars HD 82841 (K1III, 56 d, 0.09), HD 127068 (G5-8IV, 15 d, 0), HIP 77210 (K2V, 10 d, 0.06) and HD 142680 (K0-2V/K7V, 24 d, 0.31) from this paper (see Tables 4 and 5). Despite that these systems are a mixture of giants and dwarfs, all of them have orbital periods shorter than 60 d with HIP 77210 as short as 9.94 d (and

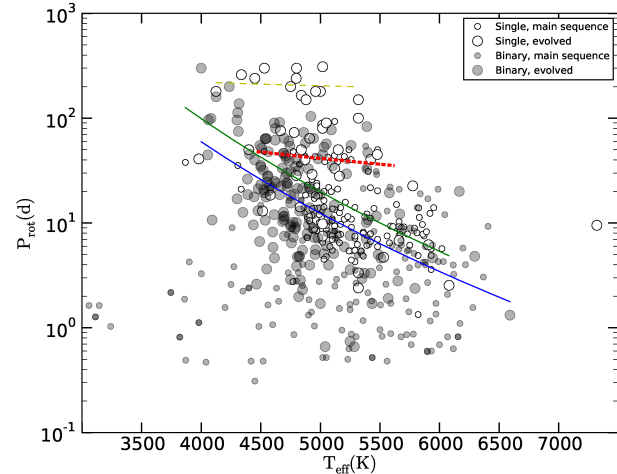


Fig. 12 The relation between rotation period and effective temperature for active single stars (open symbols) and for binaries (filled symbols). Our program stars are now mixed with other stars and are not highlighted. The two symbol sizes indicate a star's luminosity class. Larger symbols are for evolved stars of class III and IV, smaller symbols are for main sequence stars of class V. The short dashed line is the fit to the I-sequence dwarf stars from Böhm-Vitense (2007) while the long dashed line is our fit to the weakly active (single) giant stars. The two full lines indicate the T_{eff}^{-X} fits to the single active stars (upper line) and the evolved binaries (lower line). See text.

$P_{\text{rot}}=13.52$ d). This subclass does not quite follow Middlekoop & Zwaan's (1981) argument that giants in binaries with periods less than 120–200 days will be synchronized, nor Boffin et al.'s (1993) suggestion that they should be generally circularized if the orbital period is shorter than ≈ 50 d. Our active binaries with $P_{\text{rot}} > P_{\text{orb}}$ would need an extra rotational acceleration in order to get synchronized and, at the same time, need to redistribute orbital momentum in order to get circularized (but see Verbunt & Phinney 1995 for the interaction of tidal circularization and orbital eccentricity). Note that the very old (metal poor) binaries with dwarf components in the sample of Latham et al. (2002) appeared to reach circularization at a transition period near 20 d. As rotational synchronization is predicted to occur before orbital circularization (Hut 1981), all of above systems should have $e > 0$, which is actually the case, except for HD 127068 (this paper) and 39 Cet. To summarize, our full sample includes $\approx 26\%$ asynchronous rotators (61 stars) of which about half are rotating slower than in orbital equilibrium and can not be explained by being too young to be synchronized yet or by uncertainties in the measured quantities. We conclude that active binaries must have gone through an extra spin-down besides tidal dissipation and suggest this to be most likely due to a magnetically channeled wind with its subsequent braking torque on the star as described already, e.g., by Mestel (1968).

6.2 The dependency of rotation on effective temperature

Most stars in this paper are within the temperature range 4000–6000 K, i.e. roughly M0 to G0. Such stars undergo the more magnetic braking the stronger their initial magnetic field (c/o Gray 2005 and the abundant literature cited therein). To first order, this should be proportional to the effective temperature. Our first step is thus to extract the relation between rotation period and effective temperature, in particular for the active binary sample where we could expect a qualitatively different behavior due to the spin-orbit coupling. A similar attempt for single main-sequence G and K stars led Böhm-Vitense (2007) to find a strong and systematic increase of P_{rot} with decreasing T_{eff} for “active stars” but at most a very weak increase for the “inactive stars” of form $T_{\text{eff}}^{-1.33}$. Its cause is not so clear but ascribed to an angular momentum transfer from the surface to the interior due to some deep mixing.

Fig. 12 shows the distribution of P_{rot} versus T_{eff} in our full active-star sample. Also shown are the single dwarf stars used by Böhm-Vitense (2007), drawn from the Saar & Brandenburg (1999) sample, and the young solar analogs by Gaidos et al. (2000). We also add the single stars with H&K emission from our paper I where we had a photometric period determined as well as the single giants from Strassmeier et al. (1994). From the latter sample of 12 single giants, only two had a photometric (or S-index) period that we interpreted to be the rotation period (δ CrB, HD 160952), the others were based on $v \sin i$ measures and an estimate of the radius from the revised Hipparcos parallax. Note that we dropped HD 181943 from the sample (single K1V star seen almost pole on) because the photometry likely shows a spot-variability time scale rather than the rotational period (e.g. Fekel & Henry 1995).

In Fig. 12 the four subgroups – single stars on the main sequence, evolved single stars, binary components on the main sequence, and evolved binary components – appear well separated from each other, as expected due to the different radii and the tendency towards synchronization in binaries. The longest rotation periods are found for giants, the shortest periods for dwarfs, while the binary components are generally more rapidly rotating than single stars. For stars with $T_{\text{eff}} < 4000$ K, one has only dwarf stars to work with because M giants exhibit mostly pulsation periods rather than rotational periods. However, the strong increase of P_{rot} with decreasing T_{eff} is obvious in our sample. Two simple functional fits to the single stars and the binaries, respectively, indicate that the steep increase is not only seen in single stars but also in binary components. Their slopes are similar or possibly even identical, as expected if there is a common mechanism. We find

$$P_{\text{rot}} = (27.9 \pm 3.2) T_{\text{eff}}^{-7.2 \pm 0.9} \quad \text{for singles,} \quad (6)$$

$$P_{\text{rot}} = (27.1 \pm 3.5) T_{\text{eff}}^{-7.0 \pm 0.9} \quad \text{for binaries.} \quad (7)$$

This is to be compared with the active (A) sequence stars in Böhm-Vitense (2007).

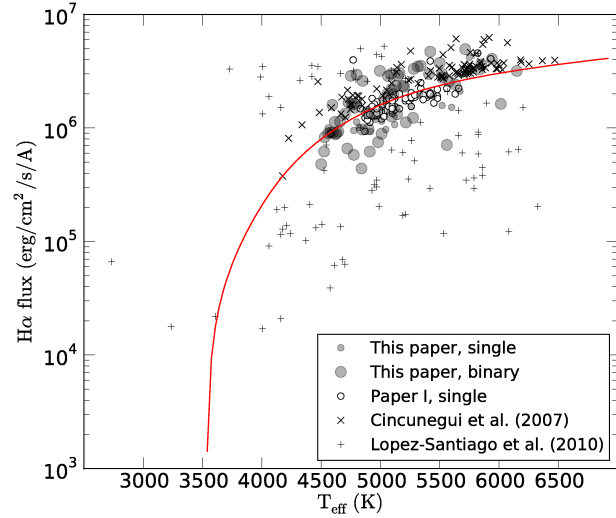


Fig. 13 Average H α -core flux as a function of effective temperature. Our binary sample is shown as large grey dots while the single stars are shown as small grey dots. The single stars from our paper I are shown as open circles. The single-star sample from Cincunegui et al. (2007) is shown as crosses while the stars in the López-Santiago et al. (2010) catalog are shown as pluses. The line is the minimum-flux envelope derived by Cincunegui et al. (2007).

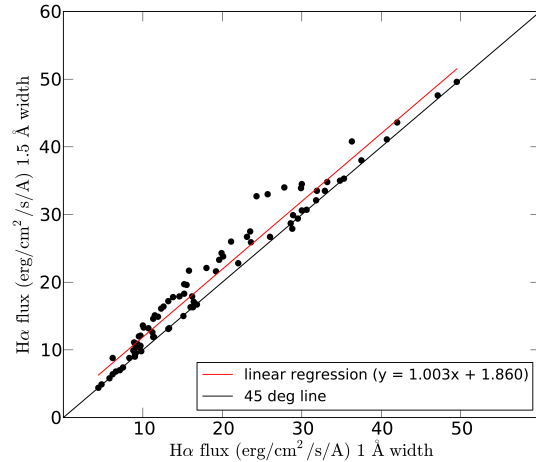


Fig. 14 H α flux measurements of our sample with two different central bandwidths (1 Å and 1.5 Å). The short line is a linear regression fit, the other line is just a 45-deg line to guide the eye. Both slopes are identical but the offset is $2 \cdot 10^5 \text{ erg cm}^{-2} \text{ s}^{-1} \text{ Å}^{-1}$.

A separate fit to the inactive, or only very weakly active, single giants and subgiants with $P_{\text{rot}} > 100$ d yields a slope of $T_{\text{eff}}^{-1.12}$, very similar to the inactive (I) sequence fit for dwarf stars in the Böhm-Vitense (2007) sample, just offset towards longer periods. Note that we plot her fit for inactive dwarfs as a dashed line in Fig. 12 for comparison. Our sample also shows a void of single stars for a period range of ≈ 15 –30 d for $T_{\text{eff}} > 5250$ K, although not overly striking.

6.3 The H α -line core as an activity indicator

The H α -line profile is influenced by a large range of atmospheric optical thicknesses, Doppler widths, and photospheric line strengths, thereby stretching its formation from the photosphere and the chromosphere to the transition region with the corona. In normal FGK stars, H α is dominated by photoionization. Collisions with free electrons are a significant source for the cooler stars and the line becomes particularly sensitive for mass motions and all sorts of (non-thermal) velocity fields (e.g., Cram & Mullan 1985). Moreover, circumstellar hydrogen could add an extra component to the net H α absorption profile. For the average quiet Sun the core of the line forms at about 1500 km and is thus chromospheric in origin. However, extracting just the non-thermal (=activity) contribution from the line core is not unique and neither is its interpretation. Particular contributors are chromospheric inhomogeneities like bright plages, chromospheric network variations, localized in- and outflows associated with flares (nano, micro and macro versions) and, of course, global winds. Cincunegui et al. (2007) pointed out that despite they had found a strong relationship between the mean fluxes in H α and Ca II H&K the relation can break down for individual stars. They suggested that the relationship is the product of the dependence on stellar color rather than on similar activity phenomena.

In Fig. 13 we plot the H α -core flux, obtained as described in Sect. 4.6, versus effective temperature. Our sample is made up of the 71 components of active binaries and 18 single stars from Table 1 with temperatures obtained from spectrum synthesis. These entries are complemented by the stars from paper I, the 109 southern stars in the study by Cincunegui et al. (2007), and the averages for 86 stars from the survey of López-Santiago et al. (2010). Unfortunately, we have no stars in common with Cincunegui et al. and López-Santiago et al. which makes an empirical determination of the zero-point shift between the samples merely impossible. The same is true for the observations of F8-K5 dwarf stars by Pasquini & Pallavicini (1991), also done in the southern hemisphere, while our survey was done in the northern hemisphere. Cincunegui et al. (2007) were able to connect their zero point with that in Pasquini & Pallavicini (1991) for the 24 stars in common and found excellent agreement, suggesting fluxes good to within 20%. Nevertheless, we did not add the Pasquini & Pallavicini (1991) sample in our Fig. 13 because it adds additional uncertainty due to them using a mix of $V - R$ and $B - V$ colors. A zero-point difference between our fluxes and those of Cincunegui et al. (2007) is obvious for the single stars in the sense that our fluxes appear lower by approximately 50%. We note that Cincunegui et al. (2007) and Pasquini & Pallavicini (1991) measured H α -core fluxes from a bandwidth of 1.5 Å and 1.7 Å, respectively, while we used a 1.0-Å bandwidth. It affects how much basal flux is being included in the measurement, which could be significantly different for the cooler stars as well as for the subgiants and giants. To quantify this, we have remeasured our spectra with a 1.5-Å bandwidth and

compared them to the 1.0-Å fluxes (Fig. 14). We found a basically constant offset of $2 \pm 2 \cdot 10^5 \text{ erg cm}^{-2} \text{ s}^{-1} \text{ Å}^{-1}$ (where the error is the rms of the linear fit) and no dependency on color nor on gravity. A correction of this amount was then applied to the Cincunegui et al. fluxes before plotting in Fig. 13.

Quite different is the case for the stars observed by López-Santiago et al. (2010). Their fluxes were obtained after the subtraction of bona-fide inactive standard-star spectra and likely represent only the active part of the chromosphere. This is markedly different to all other fluxes which contain the photospheric flux but also the basal chromospheric flux. We converted the $B - V$ s in their tables to an effective temperature with the calibration of Flower (1996) and plot them as small pluses in Fig. 13 for comparison. The López-Santiago et al. fluxes per temperature bin are on average an order of magnitude lower than the other measures, as expected.

Fig. 13 also shows that the binary components follow basically the same trend as single stars but exhibit twice as much scatter as the single stars. This is expected because the temperature errors for the binary components are typically also twice as large, in particular for the SB2s. The line in Fig. 13 is the minimum H α flux for single stars found by Cincunegui et al. (2007) from a quadratic polynomial. It essentially represents the photospheric contribution. Our measurements have a number of stars with fluxes that fall below this line. These are almost exclusively the weak-lined secondary components in SB2s with comparably uncertain flux measurements.

6.4 An activity-rotation relation for magnetically active binaries

Would a binary component with an equal rotational period of a single star be more active just because it is a component in a tidally interacting binary? Or is rapid rotation in binaries just an unique evolutionary situation because they are speed up to stellar rotations that otherwise would never be reached during regular single-star evolution? Tidal coupling, expressed as the ratio of stellar to Roche radii, was ruled out as a direct factor for increased activity in binaries by Basri (1987) despite that the evolved binary components in his sample were always more active for a given period than a single star (Basri et al. 1985). Yet other authors had claimed such a dependency (e.g. Glebocki & Stawikowski 1988). More recently, Dall et al. (2005) tried to find a relation between binarity, magnetic activity, and chemical surface abundances by comparing observations of two selected cool stars in great detail. What they found was a correlation between the bisector inverse slope and the activity index $\log R_{\text{HK}}$, which both vary in phase with tiny (few m s^{-1}) radial velocity variations. In that paper, Dall et al. (2005) speculated towards the existence of an unseen very-low mass star or even planetary companion as the cause of the low-amplitude velocity variations, but in their follow-up paper of the target in question, Dall et al. (2010) unambiguously

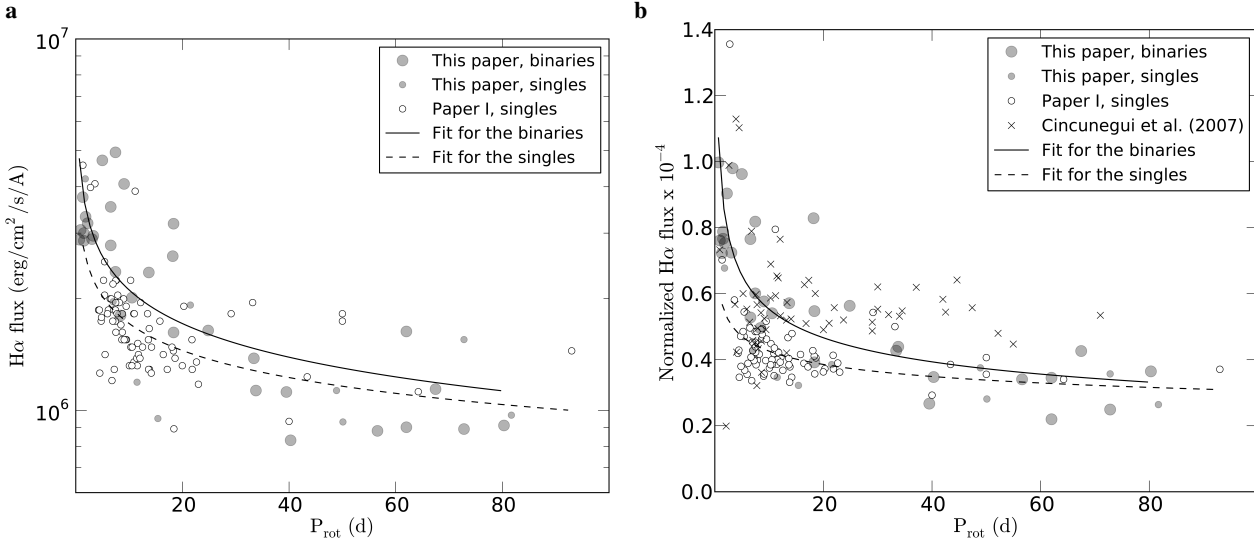


Fig. 15 **a** Average $H\alpha$ -core flux versus rotation period. **b** The same flux but normalized to the bolometric luminosity σT_{eff}^4 . The grey scale dots are the singles and binary components from this paper. The other symbols are single stars from sources as indicated. The lines are power-law fits as described in the text.

verified these to be due to stellar oscillations with an ≈ 50 -min period. We conclude that a straightforward comparison of two well-selected stars, even with (nearly) equal rotation periods, may not be conclusive.

From statistical attempts, weak activity correlations with rotation for binaries were reported in the literature. Simon & Fekel (1987) found a marginally decreasing UV flux with increasing period for evolved binaries. Strassmeier et al. (1990) claimed a slight trend for Ca II H&K, while Dempsey et al. (1993) saw a similar trend for the Ca II infrared triplet. Strassmeier et al. (1994) determined a relation for Ca II H&K flux in giants versus rotational velocity and temperature and emphasized the large range of fluxes for a given rotation rate. Also, the overall consensus was that the flux for evolved binaries with periods longer than 10 d is fairly constant and only increases significantly for stars with periods below ≈ 10 d.

In Fig. 15a, we employ the $H\alpha$ -core flux, $\mathcal{F}_{H\alpha}$, as an activity measure and plot our program stars in the log-normal activity-rotation plane. The sample is expanded by those stars from paper I that had a photometrically determined rotation period. The figure shows that the $H\alpha$ -core flux also levels out with longer periods; for single stars near a period of 10 d, for binaries more near periods of 20 d, comparable to what has been seen from other activity indicators. It also shows that binary components appear generally more active than single stars for a given period bin. Notice that in Fig. 15 only those SB2s are plotted where the photometric rotation period can be assigned unambiguously to the primary star. The secondary stars were not included in the fit for the spectroscopic binaries either because their rotation periods are assumed from $v \sin i$ and a radius instead of observed, as for the primaries. The lines in Fig. 15a are simple power-law fits of form $\mathcal{F} = a P^x$.

Fig. 15b shows the same flux as in panel a but normalized to the bolometric luminosity σT_{eff}^4 ,

$$R_{H\alpha} = \mathcal{F}_{H\alpha} / \sigma T_{\text{eff}}^4. \quad (8)$$

Effective temperatures for the majority of stars were determined spectroscopically from our SES spectra (see Table 7) or, for the single stars from paper I, from the color-temperature calibration from Flower (1996). We also include in the single-star fit the targets from Cincunegui et al. (2007) whenever a rotation period from photometry was known and an effective temperature given. These data are plotted as crosses. Note that the CABS stars have no $H\alpha$ -flux determination as an ensemble but just individual measurements collected from the literature with a variety of calibration issues and are not included here. Again, the lines are power-law fits of the form $R = a P^x$. The results from Fig. 15a and Fig. 15b are

$$\mathcal{F}_{H\alpha} = (4.22_{-0.39}^{+0.43} 10^6) P_{\text{rot}}^{-0.30 \pm 0.05} \text{ binaries}, \quad (9)$$

$$\mathcal{F}_{H\alpha} = (2.99_{-0.22}^{+0.23} 10^6) P_{\text{rot}}^{-0.24 \pm 0.04} \text{ singles}, \quad (10)$$

$$R_{H\alpha} = (9.72_{-0.22}^{+0.67} 10^{-5}) P_{\text{rot}}^{-0.24 \pm 0.03} \text{ binaries}, \quad (11)$$

$$R_{H\alpha} = (5.92_{-0.32}^{+0.34} 10^{-5}) P_{\text{rot}}^{-0.14 \pm 0.03} \text{ singles}. \quad (12)$$

The rms values for the fits in Eq. 9–12 are, from top to bottom, $0.920\text{e}+6$, $0.522\text{e}+6$, $1.353\text{e}-5$, and $1.105\text{e}-5$, respectively. We see that the fluxes are only weakly dependent on the rotation period, in particular when compared to the $P^{-1.33}$ dependency for inactive single stars from Ca II H&K (Böhm-Vitense 2007). This is partly because the magnetic flux seen in the $H\alpha$ core is dispersed over a larger range of optical depths at which a variety of (local) velocities prevail. However, our fit demonstrates the existence of a period-activity relation also for $H\alpha$ and that binary components are stronger dependent on period than single stars.

6.5 An activity-Li abundance relation?

In Fig. 16a and Fig. 16b the lithium abundance relative to hydrogen is shown as a function of effective temperature and as a function of rotational period, respectively. The sample consist of our 18 singles and 42 binaries from Table 7 (the triple systems were omitted), 236 of the 408 CABS binaries that have a Li abundance, plus 75 out of the 109 single stars from paper I. Also included in Fig. 16 are the young solar analogs from Gaidos et al. (2000). Seven stars in the CABS catalog were in common with the more recent Li study by Maldonado et al. (2010) but only one of them had a reasonable lithium equivalent-width measure (HIP 78843), which we converted to a logarithmic abundance of 0.72 with $T_{\text{eff}}=4790\text{K}$ and the NLTE tables in Pavlenko & Magazzú (1996). The same conversion was applied to the averaged equivalent-width measures for 78 single stars and 6 binaries from Lopez-Santiago et al. (2010) and 153 singles and 24 binaries from Maldonado et al. (2010) and added to the sample in Fig. 16a. For these stars, only $B - V$ colors are listed and T_{eff} 's are consequently obtained from the $B - V$ calibration of Flower (1996). Despite that $B - V$ colors are affected by metallicity (see, e.g., Gray 1994), and that at least Maldonado et al. (2010) obtained metallicities from their spectra for most of their targets, the typical metallicity range for our stars is at most ± 0.3 dex with the one or other outlier. This would affect the temperature scale at most by ± 50 K and therefore, we decided not to correct for metallicity simply because metallicities were not known for all stars in our samples.

6.5.1 The lithium-temperature dependency

Figure 16a shows a generally increasing Li abundance for binaries with increasing effective temperature (and therefore likely with increasing mass). Such a result was found earlier for single stars in various open clusters, most noteworthy in the Hyades, Pleiades, Praesepe, M34, and M67 (see, e.g., Jones et al. 1997). Our binary sample shows increasing dispersion of Li abundance with increasing temperature, opposite to what was found for Pleiades stars (e.g. Soderblom et al. 1993a) but in agreement with the Hyades FGK stars (e.g. Thorburn et al. 1993). It reaches up to three orders of magnitude for binaries with $T_{\text{eff}} \approx 5000$ K, i.e. $15\text{--}20\sigma$ of the observational uncertainty, and still two orders of magnitude between 4500–5000 K. The dispersion is still one order of magnitude at the cool end at $T_{\text{eff}} < 4500$ K. For the binaries hotter than 5000 K, the maximum observed Li abundances are primordial (≈ 3.5) and the dispersion decreases due to the generally higher abundances with temperature. Part of the explanation for such a drastic dispersion is certainly that our binary sample is a mix of ages, most likely ranging from ZAMS binaries to maybe 10 Gyr systems. This is evidenced by the fact that our single-star sample in Fig. 16a shows a qualitatively comparable behavior but the dispersion never reaches much above two orders of magnitude.

Binaries have larger systematic errors of the equivalent-width measures than singles, and that certainly also adds to the dispersion. It is particularly due to the double-lined nature for some binaries and their relative continuum uncertainties and associated larger errors for T_{eff} . However, we expect equivalent-width errors never larger than 10% for stars with equivalent widths > 50 mÅ and at most $\approx 30\%$ for equivalent widths < 20 mÅ while effective temperatures are good to within, say, $\pm 50\text{--}70$ K for singles and SB1s, and $\pm 100\text{--}150$ K for SB2s. We also note that we use Li detections and never just upper limits, and use temperatures determined from spectrum synthesis rather than photometry. Our Li abundances are therefore generally good to within ± 0.2 dex. Maybe other – extrinsic – factors may affect the Li abundance to an unknown amount but were deemed unreasonable by Soderblom et al. (1993a); c/o their discussion. We conclude that a significant part of the Li-abundance dispersion in active binaries must be intrinsic.

6.5.2 The lithium-rotation dependency

If the depletion mechanism(s) were dependent on stellar rotation, the expectation is that tidally locked binaries would exhibit lower surface abundances than single stars (of same mass and age). If independent of rotation, one could expect higher Li abundance in binaries because of less depletion. There is evidence in Fig. 16a that binaries exhibit on average less surface lithium than singles. Log-linear fits to the data of the form $\log n(\text{Li}) = aT_{\text{eff}}^b + c$ provide the following average relations;

$$\log n(\text{Li}) = a T_{\text{eff}}^{+0.0010405} - b \quad \text{for binaries,} \quad (13)$$

$$\log n(\text{Li}) = c T_{\text{eff}}^{+0.0076945} - d \quad \text{for singles,} \quad (14)$$

where a, b, c, d are the constants $58.29306 \cdot 10^2$, $58.8000 \cdot 10^2$, $7.66085 \cdot 10^2$, $8.16580 \cdot 10^2$, respectively. The difference between the two fits is significant for our sample and amounts to ≈ 0.25 dex at 5500 K. However, the fits should not to be taken too literally and act just like a guideline.

The general picture is that the Li depletion is related to the star's angular momentum loss, itself related to internal flows and shear instabilities, mixing, as well as external winds (e.g. Pinsonneault et al. 1990). A crystal-clear picture still has to emerge but that magnetic fields and winds play a major role has been accepted widely and new numerical simulations are going in this direction (e.g. Matt et al. 2012). The rotational angular momentum must be thought of being coupled to the orbital angular momentum in binaries where the depletion mechanism(s) can chew on the orbital energy. There is some observational evidence that tidally locked binary systems in the Hyades and M67 have larger lithium abundances than single stars though (see discussion in Barro y Navascues et al. 2001) but, so far, did not amount to a conclusive (quantitative) relation.

In Fig. 16b, we plot Li abundance versus rotational period. Rotation periods range between 0.5 d and 200 d. Because the vast majority of the binaries in our sample cluster

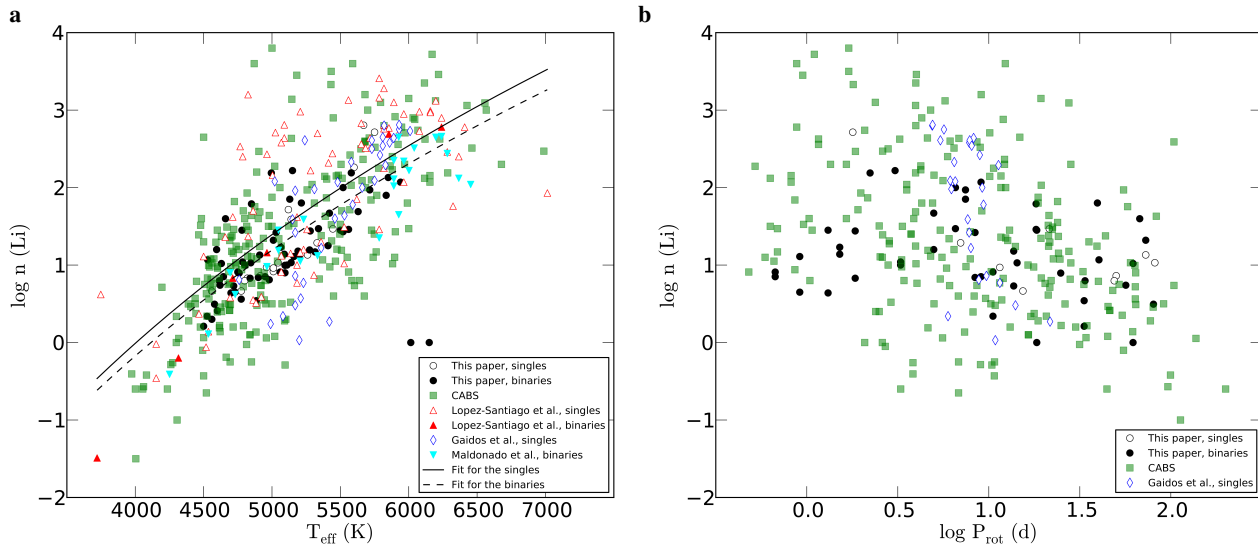


Fig. 16 Average lithium abundances **a** versus effective temperature, **b** versus (logarithmic) rotation period. Filled symbols refer to binaries, open symbols to single stars. The symbols and the sample sources are identified in the inserts. Active binaries show generally lower Li abundances than comparable singles. Our sample of binaries and single (field) stars exhibits a dispersion of up to 2–3 orders of magnitude in the full range 4500–6000 K that peaks at ≈ 5000 K. When plotted versus (logarithmic) rotation period, the dispersion is even 3–4 orders of magnitude.

below or near periods of ≈ 10 d, we had to choose a logarithmic presentation for the period axis as well. Nevertheless, the log-log plot shows a clear trend of higher Li abundance with faster rotation, for binaries as well as for singles, main sequence or evolved. Again, as in the Li- T_{eff} plane, the dispersion is very large, peaking at 3–4 orders of magnitude at around a rotation period of 10 d. This effectively camouflages a clear Li- P_{rot} relation, in particular because we do not know ages for our systems as one does for open clusters. As an averaged guideline, we fit linears to the binary data in the log-log plane and obtain

$$\log n(\text{Li}) = a \log P_{\text{rot}} + b \quad \text{for binaries,} \quad (15)$$

where a , b are the constants -0.60067 and 1.84783 , respectively. No fit is given for the single stars because our sample is not complete due to a general lack of rotation periods. Jones et al. (1997), together with parallel and subsequent work by several other groups, presented clear evidence that the (single) rapid rotators in the Pleiades (age ≈ 100 Myr) have generally also higher Li abundances than their slowly rotating cousins, at least for the temperature range 4400–5400 K. A similar trend appeared in the data for M34 (age ≈ 300 Gyrs) but only for stars of ≈ 4500 K, while the Hyades (625 Myr) shows no rapid rotators anymore and thus no Li relation with rotation.

Several mechanisms were suggested to explain the high Li abundances in rapidly rotating, active stars. Among them the production of Li during coronal flares through spallation reactions, or through an underestimated surface temperature due to large amounts of cool starspots (see, e.g., Pallavicini et al. 1993) or simply through the explanation that active stars are generally being young (Randich et al. 1993). Another interesting explanation for tidally coupled

binary components is through a lack of rotationally induced mixing due to the little magnetic braking compared to single stars (Pinsonneault et al. 1990). Böhm-Vitense (2004) noted that for giants with T_{eff} less than ≈ 6300 K the reduced lithium surface abundance appears related with the decreased surface rotation. She attributes this to effects from deep mixing. Just recently, Takeda et al. (2010) announced evidence for a (positive) correlation of Li abundance with rotational velocity in solar-analog stars. A depletion of two orders of magnitude in Li abundance is seen in the range of $v \sin i$ from 4 km s^{-1} to 1 km s^{-1} according to their Fig. 5. It calls for a *very* efficient envelope mixing process, possibly also related to the exterior angular momentum carried by planets.

Accretion of already a few Earth masses during early main-sequence phase would bring up the ${}^7\text{Li}$ abundance in these stars and a proper amount of mixing may prevent ${}^6\text{Li}$ from destruction (Murray et al. 2001). Such planet engulfing would be in agreement with the observation of increased Li abundance in rapidly-rotating active stars but requires the detection of ${}^6\text{Li}$ in active stars. Such a detection was reported by Israelian et al. (2001) for the planet-hosting solar-type star HD 82943 or the active subgiant binary HD 123531 by Strassmeier et al. (2011) (but see Cayrel et al. 2007 for a warning of such detections).

7 Summary and conclusions

We present and analyzed high-resolution spectra from the STELLA robotic telescope and determined orbital elements for 45 binaries in the period range 0.29–6450 d, many for the first time but all with substantially increased precision

and likely also increased accuracy. Additional photometric monitoring of many of these stars with our APTs allowed the determination of precise rotation periods.

We summarize our findings as follows.

- STELLA/SES achieves a radial-velocity precision for an individual radial-velocity observation of $\approx 30 \text{ m s}^{-1}$ without an iodine cell or a simultaneously recorded comparison spectrum. It enables rms values of as small as $\approx 40 \text{ m s}^{-1}$ for fits of orbital elements. For one of the favorable cases in this paper (the SB2 binary HIP 77210 with $P_{\text{orb}}=9.9 \text{ d}$) the minimum primary mass is precise to 0.12% and the secondary mass to even 0.07%.
- The radial-velocity zero-point difference between STELLA and CORAVEL measurements is $+0.503 \text{ km s}^{-1}$.
- The bulk (74%) of rapidly-rotating active stars in binaries are synchronized and in circular orbits.
- About 26% (61 targets) of the binaries in our full sample are asynchronous rotators. About half of them have $P_{\text{rot}} > P_{\text{orb}}$ and of these, all but two have $e > 0$. As rotational synchronization is predicted to occur before orbital circularization active binaries must have gone through an extra spin-down phase besides tidal dissipation and we suggest this to be due to a magnetically channeled wind with its subsequent braking torque. Such braking depends on the stellar magnetic-field geometry and would result in very different braking efficiencies for stars of otherwise nearly identical physical parameters.
- We find a steep increase of P_{rot} for lower T_{eff} in both single stars and binary components. This verifies earlier claims for active single stars with known cycles and shows that it is also the case in our active binaries. A functional dependence of $P_{\text{rot}} \propto T_{\text{eff}}^{-X}$ is suggested, where $X = 7.2$ for single stars and $X = 7.0$ for binary stars. The difference in X is not significant though.
- A relation between H α -core flux and rotational period is evident for both single stars and binaries. Power-law fits suggest $R_{\text{H}\alpha} \propto P_{\text{rot}}^{-0.24}$ for binary stars and $R_{\text{H}\alpha} \propto P_{\text{rot}}^{-0.14}$ for single stars, where R is H α -core flux normalized to σT_{eff}^4 . The difference of the exponents is only weakly significant on the 3σ level.
- Our data suggest that Li abundances of active binary components also increase with effective temperatures, as known for single stars. However, binaries appear to have on average 0.25 dex lower Li abundances than single stars of same effective temperature, which is what we expect if the depletion mechanism is rotationally enhanced in binary stars. The dispersion for binaries appears to peak around $T_{\text{eff}} \approx 5000 \text{ K}$, amounting to three orders of magnitude. This dispersion decreases towards both ends of the temperature range between 4500 K to 6500 K. Our single-star sample follows this trend as well but with an order of magnitude smaller dispersion. We can not separate age effects in our sample but attribute a significant fraction of the dispersion to it.

- Rotational dependency of Li abundance in binaries is also evident and suggests a law of form $\log n(\text{Li}) \propto -0.6 \log P_{\text{rot}}$ as a guideline. However, a dispersion of up to 3–4 orders of magnitude explains why no quantitative relations were found so far. The dispersion appears largest for binaries with periods shorter than $\approx 10 \text{ d}$ and still amounts to 2–3 orders of magnitude for periods larger than $\approx 10 \text{ d}$.

Acknowledgements. We acknowledge the extremely useful services of ADS/SAO-NASA and CDS/Strasbourg. The STELLA project was funded by the Science and Culture Ministry of the German State of Brandenburg (MWFK) and the German Federal Ministry for Education and Research (BMBF). It's a pleasure to thank Carlos Allende-Prieto and Lars Koesterke for their help implementing PARSES and Janos Bartus for his help with some of the figures. Discussions with Sydney Barnes are also appreciated. We also thank an anonymous referee for the many comments that made this paper a better one.

References

- Allende-Prieto, C. 2004, AN 325, 604
- Allende-Prieto, C., Beers, T. C., Wilhelm, R., Newberg, H. J., Rockosi, C. M., Yanny, B., Sun Lee, Y. 2006, ApJ 636, 804
- Applegate, J. H. 1992, ApJ 385, 621
- Barrado y Navascues, D., Deliyannis, C. P., Stauffer, J. R. 2001, ApJ 549, 452
- Basri, G., Laurent, R., Walter, F. M. 1985, ApJ 298, 761
- Basri, G. 1987, ApJ 316, 377
- Boffin, H. M. J., Cerf, N., Paulus, G. 1993, A&A 271, 125
- Böhm-Vitense, E. 2004, AJ 128, 2435
- Böhm-Vitense, E. 2007, ApJ 657, 486
- Carney, B. W., Latham, D. W., Stefanik, R. P., Laird, J. B., Morse, J. A. 2003, AJ 125, 293
- Carroll, T. A., Kopf, M., Ilyin, I., Strassmeier, K. G. 2007, AN 328, 1043
- Carroll, T. A., Kopf, M., Strassmeier, K. G., Ilyin, I. 2009, in IAU Symp. 259, *Cosmic Magnetic Fields: From Planets, to Stars and Galaxies*, Cambridge University Press, p.633
- Cayrel, R., Steffen, M., Chand, H., Bonifacio, P., Spite, M., Spite, F., Petitjean, P., Ludwig, H.-G., Caffau, E. 2007, A&A 473, L37
- Charbonnel, C., Balachandran, S. C. 2000, A&A 359, 563
- Cincunegui, C., Díaz, R. F., Mauas, P. J. D. 2007, A&A 469, 309
- Climenhaga, J. L., McKellar, A., Petrie, R. M. 1951, Publ. Dominion Astrophys. Obs. 8, 401
- Cram, L. E., Mullan, D. J. 1985, ApJ 294, 626
- Cutispoto, G., Pallavicini, R., Kürster, M., Rdonó, M. 1995, A&A 297, 764
- Cutispoto, G., Pastori, L., Tagliaferri, G., Messina, S., Pallavicini, R. 1999, A&AS 138, 87
- Cutispoto, G., Messina, S., Rodonó, M. 2003, A&A 400, 659
- Dall, T. H., Bruntt, H., Strassmeier, K. G. 2005, A&A 444, 573
- Dall, T. H., Bruntt, H., Stello, D., Strassmeier, K. G. 2010, A&A 514, A25
- Danby, J. M. A., Burkardt, T. M. 1983, Celestial Mechanics 31, 95
- De Laverny, P., do Nascimento, J. D., Lèbre, A., De Medeiros, J. R. 2003, A&A 410, 937
- De Medeiros, J. R., Da Silva, J. R. P., Maia, M. R. G. 2002, ApJ 578, 943
- De Medeiros, J. R., do Nascimento, J. D., Sankaranakutty, S., Costa, J. M., Maia, M. R. G. 2000, A&A 363, 239

- Dempsey, R. C., Bopp, B. W., Henry, G. W., Hall, D. S. 1993, *ApJS* 86, 293
- Dommanget, J., Nys, O. 1994, *Com. de l'Observ. Royal de Belgique* 115, 1
- do Nascimento, J. D., Charbonnel, C., Lébre, A., De Laverny, P., De Medeiros, J. R. 2000, *A&A* 357, 931
- do Nascimento, J. D., Cantos Martins, B. L., Melo, C. H. F., Porto de Mello, G., De Medeiros, J. R. 2003, *A&A* 405, 723
- Duemmler, R., Iliev, I. Kh., Iliev, L. 2002, *A&A* 395, 885
- Duflot, M., Fehrenbach, C., Mannone, C., Burnage, R., Genty, V. 1995, *A&AS* 110, 177
- Duquennoy, A., Mayor, M. 1988, *A&A* 195, 129
- Dworetzky, M. M. 1983, *MNRAS* 203, 917
- Eaton, J. A., Williamson, M. H. 2007, *PASP* 119, 886
- Eker, Z., Ak, N., Filiz, Bilir, S., Dogru, D., Tüysüz, M., Soydugan, E., Bakis, H., Ugras, B., Soydugan, F., Erdem, A., Demircan, O. 2008, *MNRAS* 389, 1722
- ESA 1997, *The Hipparcos and Tycho Catalogues*; ESA SP-1200, Noordwijk ESA
- Fabricius, C., Makarov, V. V. 2000, *A&A* 356, 141
- Famaey, B., Jorissen, A., Luri, X., Mayor, M., Udry, S., Dejonghe, H., Turon, C. 2005, *A&A* 430, 165
- Favata, F., Barbera, M., Micela, G., Sciortino, S. 1993, *A&A* 277, 428
- Fekel, F. C. 1997, *PASP* 109, 514
- Fekel, F. C., Henry, G. W. 1995, *AJ* 109, 2821
- Fekel, F. C., Henry, G. W. 2000, *AJ* 120, 3265
- Fekel, F. C., Henry, G. W. 2005, *AJ* 129, 1669
- Fekel, F. C., Henry, G. W., Alston, F. M. 2004, *AJ* 127, 2303
- Fekel, F. C., Strassmeier, K. G., Washuettl, A., Weber, M. 1999, *A&AS* 137, 369
- Flower, P. J. 1996, *ApJ* 469, 355
- Ford, E. B. 2005, *AJ* 129, 1706
- Gaidos, E. J., Henry, G. W., Henry, S. M. 2000, *AJ* 120, 1006
- Gálvez, M. C., Montes, D., Fernández-Figueroa, M. J., López-Santiago, J. 2005, in Favata, F. et al. (eds.), *13th Cool Stars, Stellar Systems, and the Sun*, ESA SP-560
- Gálvez, M. C., Montes, D., Fernández-Figueroa, M. J., López-Santiago, J. 2006, *Ap&SS* 304, 59
- Gálvez, M. C., Montes, D., Fernández-Figueroa, M. J., De Castro, E., Cornide, M. 2007, *A&A* 472, 587
- Gálvez, M. C., Montes, D., Fernández-Figueroa, M. J., De Castro, E., Cornide, M. 2009, *AJ* 137, 3965
- Gleboki, R., Stawikowski, A. 1988, *A&A* 189, 199
- Goldberg, D., Mazeh, T., Latham, D. W., Stefanik, R. P., Carney, B. W., Laird, J. B. 2002, *AJ* 124, 1132
- Gondoin, P. 2007, *A&A* 464, 1101
- Gontcharov, G. A. 2006, *Astron. Lett.* 32, 759
- Granzer, T., Reegen, P., Strassmeier, K. G. 2001, *AN* 322, 325
- Granzer, T., Weber, M., Strassmeier, K. G. 2010, *Adv. in Astr.* 2010, ID 980182
- Gray, D. F. 1994, *PASP* 106, 1248
- Gray, D. F. 2005, *The observation and analysis of stellar photospheres*, 3rd ed., Cambridge University Press
- Griffin, R. F. 1987, *Observatory* 107, 194
- Griffin, R. F. 2002, *Observatory* 122, 14
- Griffin, R. F. 2003, *Observatory* 123, 129
- Griffin, R. F. 2005, *Observatory* 125, 253
- Griffin, R. F. 2009, *Observatory* 129, 317
- Griffin, R. F. 2010, *Observatory* 130, 60
- Griffin, R. F. 2012, *A&A* 537, A56
- Griffin, R. F., Filiz Ak, N. 2010, *Ap&SS* 330, 47
- Griffin, R. F., Keenan, P. C. 1992, *Observatory* 112, 168
- Halbwachs, J. L., Mayor, M., Udry, S., Arenou, F. 2003, *A&A* 397, 159
- Hall, D. S. 1986, *ApJ* 309, L83
- Hall, D. S., Kreiner, J. M. 1973, *Acta Astr.* 30, 387
- Hall, J. C. 1996, *PASP* 108, 313
- Henry, G. W., Fekel, F. C., Hall, D. S. 1995, *AJ* 110, 2926
- Hinderer, F. 1957, *AN* 284, 1
- Høg, E., Fabricius, C., Makarov, V. V., Urban, S., Corbin, T., Wycoff, G., Bastian, U., Schwekendiek, P., Wicnec, A. 2000, *A&A* 355, L27
- Holmberg, J., Nordstroem, B., Andersen, J. 2007, *A&A* 475, 519
- Horne, K. 1986, *PASP* 98, 609
- Hut, P. 1981, *A&A* 99, 126
- Iben, I. Jr. 1967, *ApJ* 147, 624
- Imbert, M. 2006, *Romanian Astronomical Journal* 16, 3
- Israelian, G., Santos, N. C., Mayor, M., Rebolo, R. 2001, *Nature* 411, 163
- Jeffries, R. D., Bertram, D., Spurgeon, B. R. 1994, *IBVS* 4091
- Jenkins, L. F. 1952, *General Cat. of Trig. Parallaxes*, Yale Univ. Obs.
- Jones, B. F., Fischer, D., Shetrone, M., Soderblom, D. R. 1997, *AJ* 114, 352
- Karatas, Y., Bilir, S., Eker, Z., Demircan, O. 2004, *MNRAS* 349, 1069
- Kazarovets, E. V., Samus, N. N., Durlevich, O. V., Kireeva, N. N., Pastukhova, E. N. 2006, *IBVS* 5721
- Keenan, P. C., York, S. B. 1988, *Bull. d'Inf. CDS* No. 30, 37
- Kovtyukh, V. V., Soubiran, C., Belik, S. I., Gorlova, N. I. 2003, *A&A* 411, 559
- Kurucz, R. L. 1993, *ATLAS-9*, CD-ROM #13
- Lafler, J., Kinman, T. D. 1965, *ApJS* 11, 216
- Lanza, A. F. 2006, *MNRAS* 369, 1773
- Lanza, A. F., Piluso, N., Rodonó, M., Messina, S., Cutispoto, G. 2006, *A&A* 455, 595
- Latham, D. W., Mazeh, T., Carney, B. W., McCrosky, R. E., Stefanik, R., Davis, R. J., 1988, *AJ* 96, 567
- Latham, D. W., Stefanik, R. P., Torres, G., Davis, R. J., Mazeh, T., Carney, B. W., Laird, J. B., Morse, J. A. 2002, *AJ* 124, 1144
- Lébre, A., de Laverny, P., do Nascimento, J. D., De Medeiros, J. R. 2006, *A&A* 450, 1173
- Livio, M., Soker, N. 2002, *ApJ* 571, L161
- Lomb, N. R. 1976, *Ap&SS* 39, 447
- López-Santiago, J., Montes, D., Gálvez-Ortiz, M. C., Crespo-Chacón, I., Martínez-Arnáiz, R. M., Fernández-Figueroa, M. J., de Castro, E., Cornide, M. 2010, *A&A* 514, A97
- Luck, R. E., Heiter, U. 2007, *AJ* 133, 2464
- Maldonado, J., Martínez-Arnáiz, R. M., Eiroa, C., Montes, D., Montesinos, B. 2010, *A&A* 521, A12
- Malkov, O. Yu., Oblak, E., Snegireva, E. A., Torra, J. 2006, *A&A* 446, 785
- Mamajek, E. E., Hillenbrand, L. A. 2008, *ApJ* 687, 1264
- Markwardt, C. B., 2009, in Bohlender, D.A., Durand, D. & Dowler, P. (eds.), *Astronomical Data Analysis Software and Systems XVIII*, ASPC Series, 411, p.251
- Martínez González, M. J., Asensio Ramos, A., Carroll, T. A., Kopf, M., Ramírez Vélez, J. C., Semel, M. 2008, *A&A* 486, 637
- Masana, E., Jordi, C., Ribas, I. 2006, *A&A* 450, 735
- Massarotti, A., Latham, D. W., Stefanik, R. P., Fogel, J. 2008, *AJ* 135, 209
- Matt, S. P., Pinzón, G., Greene, T. P., Pudritz, R. E. 2012, *ApJ* 745, 101

- Mazeh, T., Simon, M., Prato, L., Markus, B., Zucker, S. 2003, *ApJ* 599, 1344
- Mestel, L. 1968, *MNRAS* 138, 359
- Middlekoop, F., Zwaan, C. 1981, *A&A* 101, 26
- Montes, D., Fernández-Figueroa, M. J., De Castro, E., Cornide, M., Latorre, A., Sanz-Forcada, J. 2000, *A&AS* 146, 103
- Morales, J. C., Torres, G., Marschall, L. A., Brehm, W. 2009, *ApJ* 707, 671
- Murray, N., Chaboyer, B., Arras, P., Hansen, B., Noyes, R. W. 2001, *ApJ* 555, 801
- Olsen, E. H. 1994, *A&AS* 106, 257
- Otero, S. A., Dubovsky, P. A. 2004, *IBVS* 5557
- Pace, G., Pasquini, L. 2004, *A&A* 426, 1021
- Pallavicini, R., Cutispoto, G., Randich, S., Gratton, R. 1993, *A&A* 267, 145
- Pasquini, L., Pallavicini, R. 1991, *A&A* 251, 199
- Pavlenko, Ya. V., Magazzú, A. 1996, *A&A* 311, 961
- Pinsonneault, M. H., Kawaler, S. D., Sofia, S., Demarque, P. 1990, *ApJ* 338, 424
- Piskunov, N. A., Valenti, J. A. 2002, *A&A* 385, 1095
- Pizzolato, N., Maggio, A., Micela, G., Sciortino, S., Ventura, P. 2003, *A&A* 397, 147
- Pourbaix, D., Tokovinin, A. A., Batten, A. H., Fekel, F. C., Hartkopf, W. I., Levato, H., Morrell, N. I., Torres, G., Udry, S. 2004, *A&A* 424, 727
- Randich, S., Gratton, R., Pallavicini, R. 1993, *A&A* 273, 194
- Roberts, D. H., Lehár, J., Dreher, J. W. 1987, *AJ* 93, 968
- Robinson, S. E., Ammons, S. M., Kretke, K. A., Strader, J., Wertheimer, J. G., Fischer, D. A., Laughlin, G. 2007, *ApJS* 169, 430
- Saar, S. H., Brandenburg, A. 1999, *ApJ* 524, 295
- Scarfe, C. D., Batten, A. H., Fletcher, J. M. 1990, *Publ. Dominion Astrophys. Obs. Victoria*, 18, 21
- Scargle, J. D. 1982, *ApJ* 263, 835
- Schrijvers, C. J., Zwaan, C. 1991, *A&A* 251, 183
- Skumanich, A. 1972, *ApJ* 171, 565
- Simon, T., Fekel, F. C. 1987, *ApJ* 316, 434
- Soderblom, D. R., Jones, B. F., Balachandran, S., Stauffer, J. R., Duncan, D. K., Fedele, S. B., Hudon, J. D. 1993a, *AJ* 106, 1059
- Soderblom, D. R., Stauffer, J. R., Hudon, J. D., Jones, B. F. 1993b, *ApJS* 85, 315
- Strassmeier, K. G. 1994, *A&AS* 103, 413
- Strassmeier, K. G., Boyd, L. J., Epand, D. H., Granzer, T. 1997, *PASP* 109, 697
- Strassmeier, K. G., Carroll, T., Weber, M., Granzer, T., Bartus, J., Olah, K., Rice, J. B. 2011, *A&A* 535, A98
- Strassmeier, K. G., Fekel, F. C., Bopp, B. W., Henry, G. W., Dempsey, R. C. 1990, *ApJS* 72, 191
- Strassmeier, K. G., Granzer, T., Weber, M., et al. 2004, *AN* 325, 527
- Strassmeier, K. G., Granzer, T., Weber, M. 2010, *Adv. in Astr.* 2010, ID 970306
- Strassmeier, K. G., Hall D. S., Boyd, L. J., Genet, R. M. 1989, *ApJS* 69, 141
- Strassmeier, K. G., Hall D. S., Fekel, F. C., Scheck, M. 1993, *A&AS* 100, 173
- Strassmeier, K. G., Hall D. S., Zeilik, M., Nelson, E. R., Eker, Z., Fekel, F. C. 1988, *A&AS* 72, 291
- Strassmeier, K. G., Handler, G., Paunzen, E., Rauth, M. 1994, *A&A* 281, 855
- Strassmeier, K. G., Weber, M., Granzer, T., Dall, T. H. 2010, *AN* 331, 368
- Strassmeier, K. G., Washuettl, A., Granzer, T., Scheck, M., Weber, M. 2000, *A&AS* 142, 275
- Strohmeier, W. 1967, *IBVS* 178
- Szalai, T., Kiss, L. L., Meszaros, Sz., Vinko, J., Csizmadia, S. 2007, *A&A* 465, 943
- Takeda, Y., Honda, S., Kawanomoto, S., Ando, H., Sakurai, T. 2010, *A&A* 515, A93
- Thorburn, J. A., Hobbs, L. M., Deliyannis, C. P., Pinsonneault, M. H. 1993, *ApJ* 415, 150
- Udry, S., Mayor, M., Maurice, E., Andersen, J., Imbert, M., Lindgren, H., Mermilliod, J.-C., Nordström, B., Prévot, L. 1999, in Hearnshaw, J.B. & Scarfe, C.D. (eds.), *Precise Stellar Radial Velocities*, IAU Colloq. 170, ASPC 185, p.383
- van Leeuwen, F. 2007, *A&A* 474, 653
- Verbunt, F., Phinney, E. S. 1995, *A&A* 296, 709
- Weber, M., Granzer, T., Strassmeier, K. G., Woche, M. 2011, *Proc. SPIE* 7019, 70190L
- Weber, M., Granzer, T., Strassmeier, K. G., Woche, M. 2012, *Proc. SPIE* 8451, 8451-19
- Weber, M., Strassmeier, K. G. 2011, *A&A* 531, A89
- White, R. J., Gabor, J. M., Hillenbrand, L. A. 2007, *AJ* 133, 2524
- Worley, C. E. 1972, *AJ* 77, 878
- Wright, J. T., Marcy, G. W., Butler, R. P., Vogt, S. S. 2004, *ApJS* 152, 261